DISSERTATION

BIOMECHANICAL ANALYSIS OF HYPOPLASTIC LEFT HEART SYNDROME AND CALCIFIC AORTIC STENOSIS: A STATISTICAL AND COMPUTATIONAL STUDY

Submitted by

Banafsheh Zebhi

Department of Mechanical Engineering

In partial fulfillment of the requirements

For the Degree of Doctor of Philosophy

Colorado State University

Fort Collins, Colorado

Fall 2021

Doctoral Committee:

Advisor: David Bark

Xinfeng Gao
Zhijie Wang
Brian Scansen

ABSTRACT

BIOMECHANICAL ANALYSIS OF HYPOPLASTIC LEFT HEART SYNDROME AND CALCIFIC AORTIC STENOSIS: A STATISTICAL AND COMPUTATIONAL STUDY

Cardiovascular diseases are a leading cause of death in the United States. In this dissertation, a congenital heart disease (CHD) and a valvular disease are discussed. CHDs occur in ~5% of live births. Structural CHDs can be complex and difficult to treat, such as hypoplastic left heart syndrome (HLHS) in which the left ventricle is generally underdeveloped, representing ~9% of all congenital heart diseases. Calcific aortic stenosis is one of the most common valvular diseases in which valves thicken and stiffen, and in some cases nodular deposits form, limiting valve function that may result in flow regurgitation and outflow obstruction. The overarching hypothesis of this research is that patient-specific heart geometry and valve characteristics are linked to cardiovascular diseases and may play an important role in regulating hemodynamics within the heart. This hypothesis is studied through three specific aims. In specific aim 1, a computational fluid dynamics study was developed to quantify the hemodynamic characteristics within the right ventricles of healthy fetuses and fetuses with HLHS, using 4D patient-specific ultrasound scans. In these simulations, we find that the HLHS right ventricle exhibits a greater cardiac output than normal; yet, hemodynamics are relatively similar between normal and HLHS right ventricles. Overall, this study provides detailed quantitative flow patterns for HLHS, which has the potential to guide future prevention and therapeutic interventions, while more immediately providing additional functional detail to cardiologists to aid in decision making. The specific aim 2 is a comprehensive review in which we highlight underlying molecular mechanisms of acquired aortic

stenosis calcification in relation to hemodynamics, complications related to the disease, diagnostic methods, and evolving treatment practices for calcific aortic stenosis and, bioprosthetic or native aortic scallop intentional laceration (BASILICA) procedure to free coronary arteries from obstruction. In specific aim 3, we use statistical trends and relationships to identify the role of patient-specific aortic valve characteristics in post-BASILICA coronary obstruction. The findings of this study shows that in addition to direct anatomical measurements of the aortic valve, the aspect ratios of the anatomical features are important in determining the cause of post-BASILICA coronary obstruction. The overall significance of this dissertation is that computational and statistical analysis of patient's specific flow hemodynamics and geometric characteristics can provide more insight into the cardiovascular disease and treatment approaches which can ultimately assist surgeons with procedural planning.

ACKNOWLEDGEMENTS

I would like to express my deepest gratitude to those who supported me in the completion of my dissertation. First and foremost, I would like to acknowledge Dr. David Bark for being an outstanding mentor and for offering me his valuable knowledge and experience throughout my PhD journey. The completion of this journey would not have been possible without his support and guidance. I would like to further extend my sincere gratitude to my committee members, Dr. Xinfeng Gao, Dr. Zhijie Wang, and Dr. Brian Scansen for their presence and their valuable feedback.

I would like to acknowledge Dr. Choon Hwai Yap and Dr. Hadi Wiputra from the National University of Singapore, Dr. Lisa Howley and Dr. Bettina Cuneo and their team from the Children's Hospital Colorado for their collaboration and remarkable contribution to this research. My appreciation extends to Dr. Scansen from the college of Veterinary Medicine and Biomedical sciences for the collaboration that furthered my research and enabled its application in an animal model. I would also like to acknowledge the great opportunity to work with Dr. Mohamad Lazkani in the Medical Center of the Rockies in a collaboration that led to investigating a novel technique.

Additionally, it goes without saying that none of this would have been possible absent the financial support provided by the Mechanical Engineering Department at CSU and NIH.

Special thanks to my peers and fellows in the Bark Lab for bringing their positivity and support to our office every day.

Last but not least, I deeply appreciate my family for inspiring, supporting and encouraging me throughout my journey.

TABLE OF CONTENTS

LIST OF TABLES

LIST OF FIGURES

1. INTRODUCTION

Hypoplastic left heart syndrome (HLHS) represents approximately 9% of all congenital heart defects (CHDs) and is one of the most complex CHDs, with the left side of the heart being generally underdeveloped. Numerous studies demonstrated that intracardiac fluid flow patterns in the embryonic and fetal circulation can impact cardiac structural formation and remodeling. This highlights the importance of quantifying the altered hemodynamic environment in congenital heart defects, like HLHS, relative to a normal heart as it relates to cardiac development. The **overarching hypothesis** of this research is that patient-specific heart geometry and valve characteristics are linked to cardiovascular diseases and may play an important role in regulating hemodynamics within the heart. This hypothesis is studied through three specific aims.

- In **specific aim 1**, a computational fluid dynamics study was developed to quantify the hemodynamic characteristics within the right ventricles of healthy fetuses and fetuses with HLHS, using 4D patient-specific ultrasound scans. In these simulations, we find that the HLHS right ventricle exhibits a greater cardiac output than normal; yet, hemodynamics are relatively similar between normal and HLHS right ventricles. Overall, this study provides detailed quantitative flow patterns for HLHS, which has the potential to guide future prevention and therapeutic interventions, while more immediately providing additional functional detail to cardiologists to aid in decision making.

Calcific aortic stenosis is a progressive disease that has become more prevalent in recent decades. It advances with age, affecting ~0.2% of people 50-59 years of age and increasing to 9.8% for 80-89 years. Despite advances in research to uncover underlying biomechanisms, and development

of new generations of prosthetic valves and replacement techniques, management of calcific aortic stenosis still comes with unresolved complications.

- The **specific aim 2** is a comprehensive review in which we highlight underlying molecular mechanisms of acquired aortic stenosis calcification in relation to hemodynamics, complications related to the disease, diagnostic methods, and evolving treatment practices for calcific aortic stenosis and, bioprosthetic or native aortic scallop intentional laceration (BASILICA) procedure to free coronary arteries from obstruction.

A common treatment for aortic valve stenosis is the transcatheter aortic valve replacement (TAVR) in which expansion of a transcatheter aortic valve (TAV) forces calcified native aortic leaflets to permanently open, and in rare cases, this can obstruct the coronary artery. Coronary obstruction during TAVR is a rare and potentially fatal complication that occurs in <1% of the population. In efforts to prevent coronary obstruction, the bioprosthetic or native aortic scallop intentional laceration (BASILICA) technique has been developed, in which the leaflet facing a coronary artery is typically lacerated from its base to its edge using a catheter and an electrified guidewire. Ideally, the BASILICA procedure is expected to free coronary arteries from obstruction by allowing blood to flow through the lacerated leaflet. However, the lacerated leaflet may not always open properly in front of the ostia to allow coronary perfusion. Leaflet material or calcium deposits may displace toward coronary ostia or TAV-related thrombosis may develop and embolize in the coronary arteries and leave patients with post-procedural coronary obstruction complication.

- In **specific aim 3,** we use statistical comparisons to identify the role of patient-specific aortic valve characteristics in post-BASILICA coronary obstruction. The findings of this study shows that in addition to direct anatomical measurements of the aortic valve, the

aspect ratios of the geometric characteristics are also linked to the post-BASILICA coronary obstruction.

The overall significance of this research is that computational and statistical analysis of patient's specific flow hemodynamics and patients' characteristics can provide more insight into the cardiovascular disease and treatment approaches which can ultimately assist surgeons with procedural planning.

This dissertation is presented in eight chapters. Chapter 1 is an overall introduction to this dissertation. Chapter 2 includes the backgrounds on the anatomy of the heart and the aortic valve, cardiovascular diseases, clinical assessments, and treatments. In chapter 3, 4 and 5, specific aim 1, specific aim 2, and specific aim 3 are discussed in detail. Chapter 6 provides an overall summary and conclusion for this dissertation. Chapter 7 identifies the areas that require further research and the direction for future work; and the last section includes all the references.

2. BACKGROUND

This chapter presents an overview on anatomy and structure of the adult and fetal hearts, heart diseases, clinical assessments, and the possible treatments and complications associated with the treatment options.

2.1 Heart

2.1.1 Anatomy of the Heart

The heart is a pump that is located between the lungs. It has four chambers in adult humans; right atrium (RA), right ventricle (RV), left atrium (LA) and left ventricle (LV). There are four valves in the heart; the tricuspid valve is located between RA and RV, the mitral valve is between LA and LV, pulmonary valve is located between RV and pulmonary artery, and aortic valve is positioned between LV and aorta (Figure 2.1). A healthy valve allows blood to flow in one direction from atriums to ventricles, from RV to pulmonary arteries and lungs (pulmonary circulation), and from LV to aorta and the rest of the body (systemic circulation) while preventing the backflow.

In pulmonary circulation, deoxygenated blood flows into the RA through the superior and inferior vena cava, and goes to the RV. The RV pumps the deoxygenated blood into the pulmonary artery and lungs. The deoxygenated blood receives oxygen and loses its metabolic wastes while passing through the lungs, and returns to the LA. The oxygenated blood flows into the LV and is pumped to the aorta and the systemic circulation. The cardiovascular cycle includes two phases;

diastole and systole. Diastole is when chambers are relaxed and blood flows into the ventricles; and systole is when chambers contract to pump the blood out.

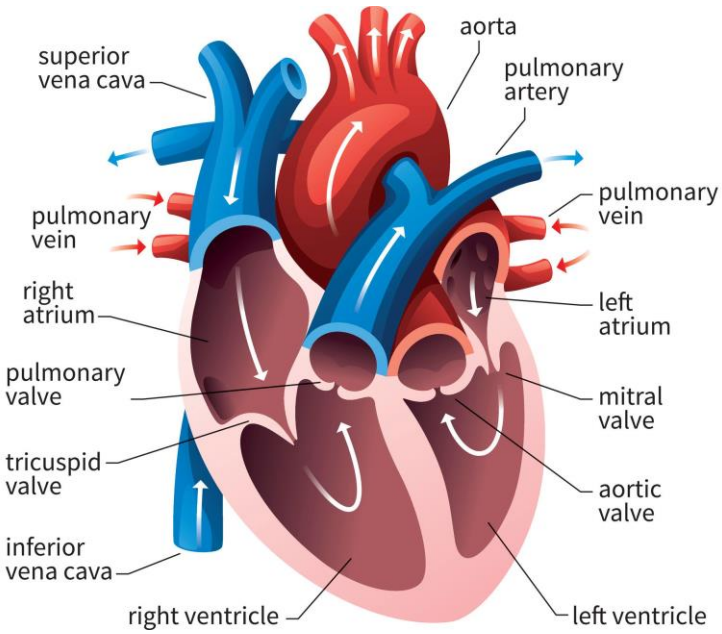

Figure 2.1. The four-chamber view of the adult human heart. Image is adapted from www.thoughtco.com

2.2 Fetal Heart

Human fetal hearts have a similar structure as adult hearts with a few exceptions; (1) in fatal hearts the pulmonary artery and aorta are connected through a vessel called ductus arteriosus, (2) there is an opening in the septal wall between the right and left atriums called foramen ovale that causes oxygenated and deoxygenated blood to mix in the fetal heart.

Blood circulation in fetal hearts is a more complex process. The fetus is dependent on the placenta for oxygen and nutrition. The lungs in the fetus are not used until after birth. The exchange of oxygen and carbon dioxide occurs though the umbilical cord that connects the placenta to the fetus. The oxygenated blood comes back from umbilical cord to the RA. The oxygen rich blood flows from the RA into the LA through the patent foramen ovale, and then into the LV and the

aorta. The deoxygenated blood from the fetal body also goes back to the RA through superior vena cava (Figure 2.2). The blood is then pumped to the pulmonary arteries but because of the high pulmonary resistance most of the blood goes through patent ductus arteriosus[6]. In a normal fetus, the foramen ovale and ductus arteriosus close short after birth to allow a normal heart development.

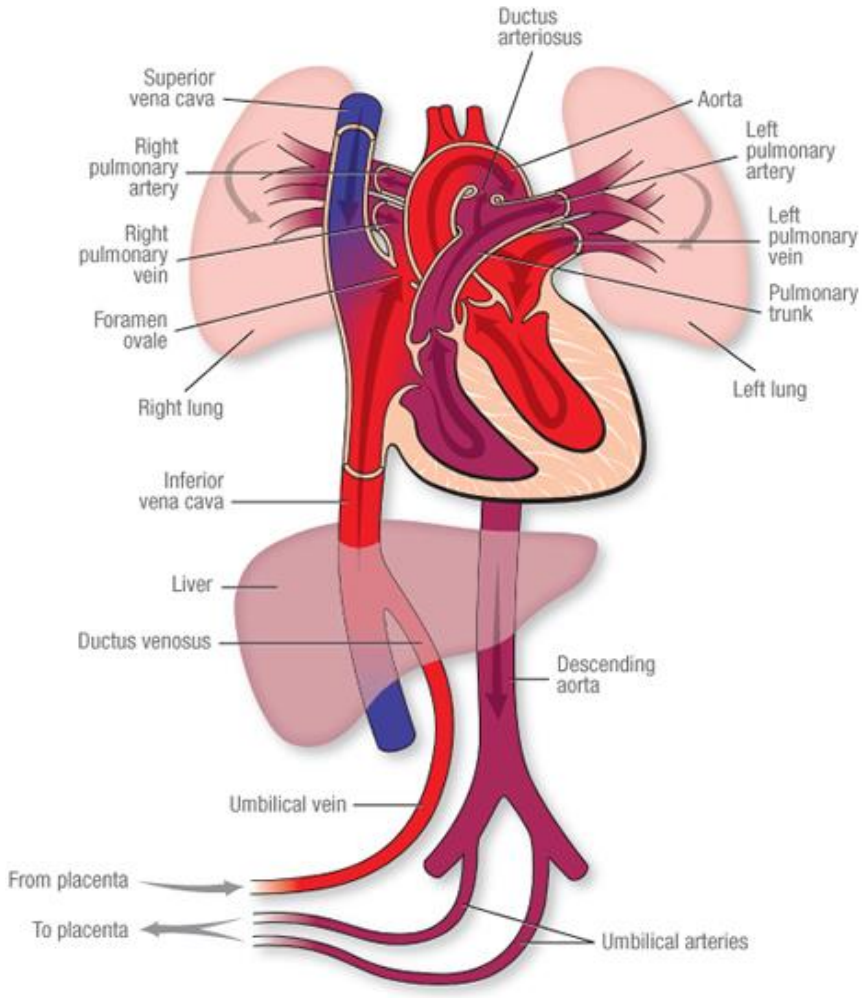

Figure 2.2. Blood circulation in human fetal hearts. Image is adapted from www.heart.org.

2.3 Aortic Valve

A normal aortic valve contains three semilunar cusps and three leaflets; in which cusps are named according to their anatomical positions. The non-coronary cusp is located between the right

and left coronary cusps. The right and left coronary cusps are near the right and left chambers and supply blood into the right and left sides of the heart through coronary arteries. During a cardiac cycle, a healthy aortic valve opens and closes fully to facilitate unidirectional flow between left ventricle and aorta.

2.3.1 Anatomy of the Aortic Valve

Aortic valve anatomy is important in hemodynamics of the left ventricle and aorta. Specific valve configurations and characteristics can be linked to valvular dysfunction and diseases. Aortic valve leaflets are attached to the aortic root at the annulus. The locations where leaflets touch each other is named commissures. The sinus bulges, known as sinuses of valsava are thinner than aortic wall. These sinuses play an important role in supporting coronary flow and reduction of stress on aortic leaflets[7]. The connection of ascending aorta with distal sinuses is called sinotubular junction; this anatomically separates the aortic root from the ascending aorta[3] (Figure 2.3).

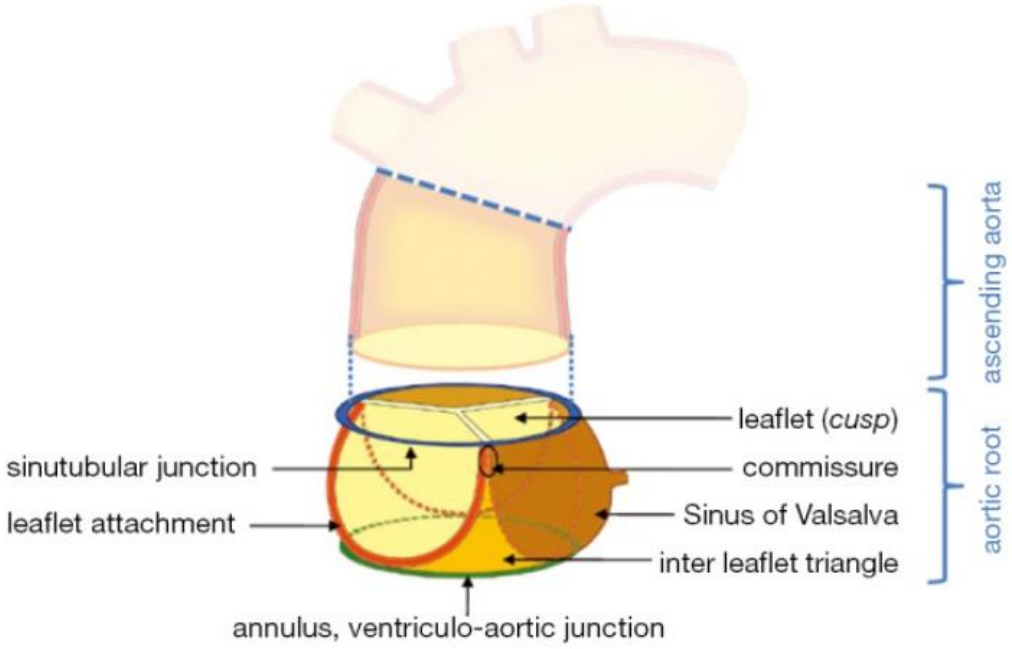

Figure 2.3. Aortic root is characterized by components such as annulus, sinus of valsava, and sinotubular junction. Image is adapted from Charitos et al[3]

2.4 Cardiovascular Diseases

Cardiovascular diseases are a leading cause of death accounted for 17.3 million people annually[8]. Congenital heart diseases (CHDs) are a wide range of various conditions that affect the heart structure and function. These conditions can affect the valve closure and position, and normal development of ventricle and other parts of the heart. In this dissertation, we discuss hypoplastic left heart syndrome (HLHS) and calcific aortic stenosis (one the most common valvular heart diseases).

2.5 Hypoplastic Left Heart Syndrome

Hypoplastic left heart syndrome (HLHS) is a complex congenital heart disease in which the left side of the heart is critically underdeveloped (Figure 2.4). The ductus arteriosus and foreman ovale openings naturally close a few days after birth. This sudden closure of ductus arteriosus cause a serious systemic blood circulation problem in a baby with HLHS[9], as the left ventricle, aortic valve and mitral valve are underdeveloped and left ventricle cannot pump out the oxygenated blood to the body[9].

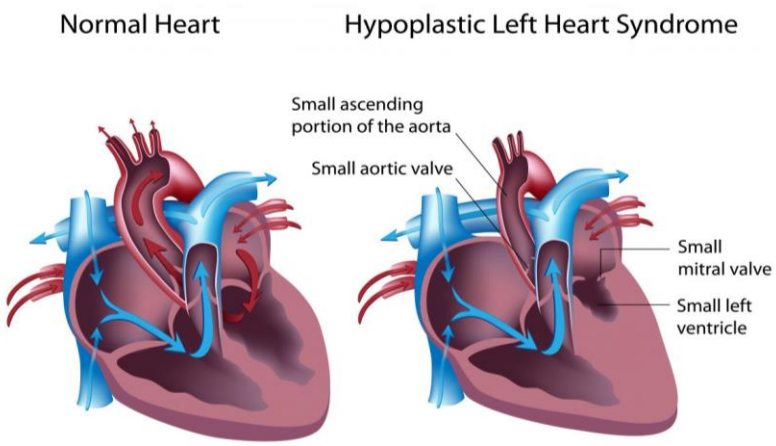

Figure 2.4. A normal heart on the left, a HLHS heart on the right. Image is adapted from www.fetalhealthfoundation.org.

2.5.1 Clinical Assessment of Hypoplastic Left Heart Syndrome

HLHS can be diagnosed during routine pregnancy screenings using ultrasound medical imaging. Ultrasound provides a non-invasive visualization for the tissue structure; it uses high-frequency sound waves generated by piezoelectric crystals that can propagate through the medium. The ultrasound transducer can convert electricity to sound and vice versa. The ultrasound wave entering the body is transmitted from one tissue to another; when an ultrasound wave encounters the interface between two tissues, a part of the wave is being transmitted through the next tissue, a small part of the wave is being scattered, and a part of the wave is being reflected back to the probe and converted into images. The propagation of the ultrasound wave depends on the density and stiffness of the tissue.

In recent years with advances in technology, 4D ultrasound spatial-temporal image correlation (STIC) technique has introduced a new era in fetal cardiovascular imaging. The 4D

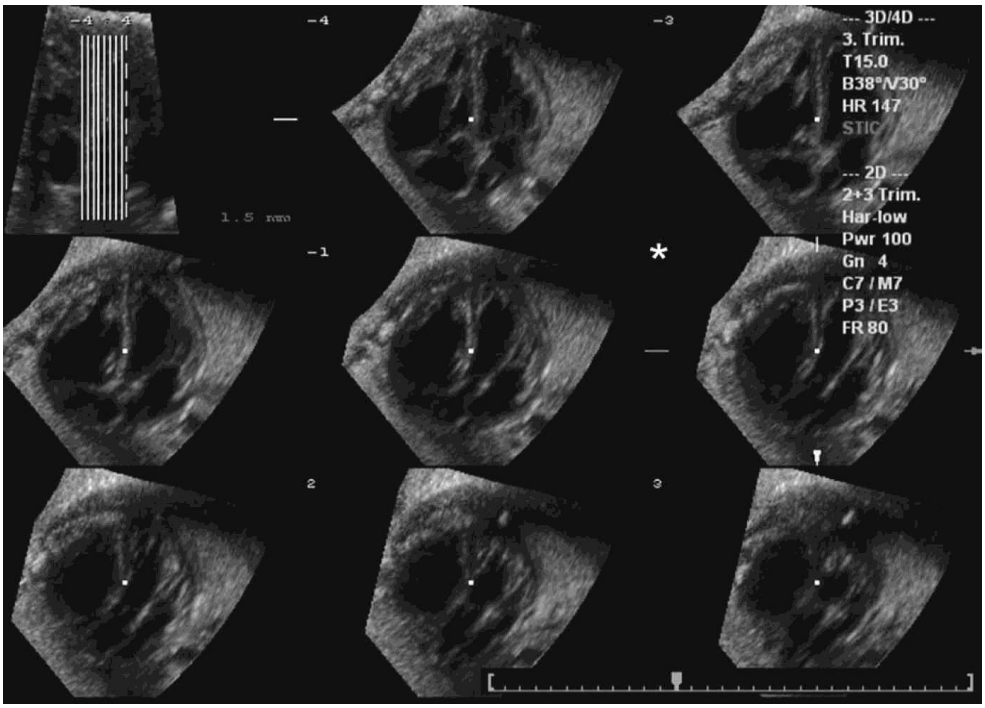

Figure 2.6. Tomographic ultrasound imaging (TUI) view of fetal heart. Image is adapted from Yagel et al.[5]

STIC ultrasound technique provides a high-resolution visualization for the small structures in the fetal heart. Furthermore, tomographic ultrasound imaging (TUI) mode in the 4D STIC ultrasound technique provide spatial and temporal information of the fetal heart, by displaying the volumetric image of the heart in sequential parallel planes (Figure 2.5).

2.5.2 Hypoplastic Left Heart Syndrome Treatment

The common treatment for HLHS is a three-step surgical intervention known as Norwood, Glenn and Fontan operations. The Norwood procedure is performed a few days after birth with the aim of providing a systemic circulation in the fetal body. In this procedure, the left and right atriums are connected to allow blood flow from the left side to the right atrium and right ventricle. The right ventricle and pulmonary artery are connected to the aorta to supply both the systemic and pulmonary circulations (Figure 2.6). Because the pulmonary resistance in newborn babies is high, most of the blood flows to the body through aorta. At this stage oxygenated and deoxygenated blood are mixed[10].

The Glenn procedure is performed within 3 to 6 months after birth, with the aim of decreasing the mixing of the oxygenated and the deoxygenated blood. In this procedure, the aorta and pulmonary artery are no longer connected. The left atrium is connected to the right atrium allowing the oxygenated blood to come to the right side. The right ventricle is connected to the aorta to provide blood for the systemic circulation. The superior vena cava (SVC) is connected to the pulmonary artery, while inferior vena cava (IVC) is still connected to the right atrium (Figure 2.6). Since the baby is older at this stage the pulmonary resistance is lower; this allows low-pressure blood flow to enter lungs from SVC[10].

The Fontan procedure is performed at 18 months to 4 years with the aim of separating the oxygenated and the deoxygenated blood. In this procedure, SVC and IVC are connected to the pulmonary artery. At this stage, the underdeveloped left side and the right side of the heart work as one chamber to pump the blood to the body (Figure 2.6).

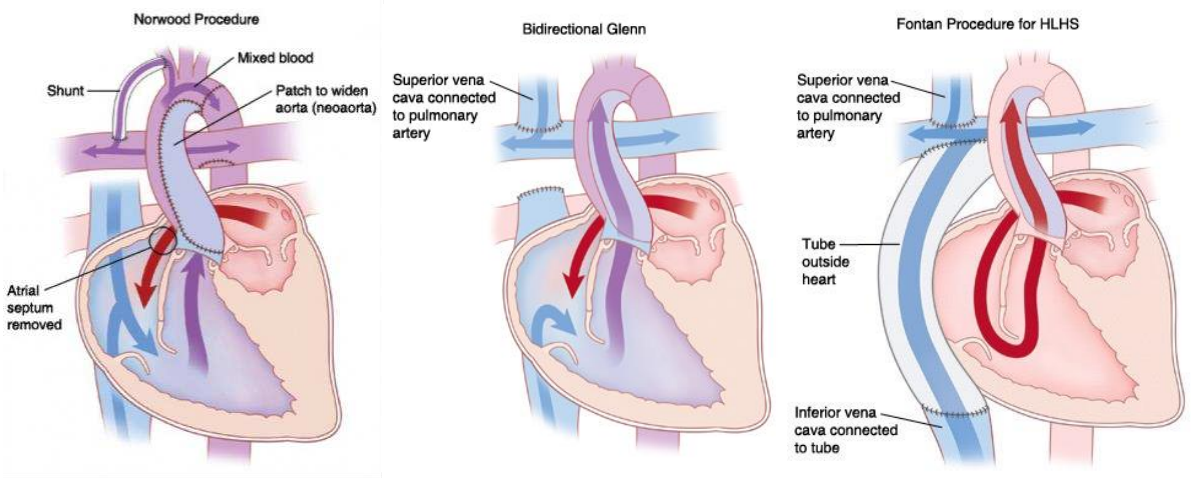

Figure 2.8. (left) Norwood procedure, (middle) Glenn procedure, (right) Fontan procedure. Image is adapted from pedclerk.bsd.uchicago.edu.

2.6 Calcific Aortic Stenosis

Calcific aortic stenosis (AS) is the most common valve disease in which leaflets thickens and stiffens due to formation of calcium nodules; this affects the dynamics of the valve and limits its opening during systole which can ultimately lead to left ventricle outflow obstruction[11]. Calcification is a complex process involving mechanobiology, molecular signaling, tissue remodeling, and inflammation. Endothelial cells can sense mechanical forces in the environment and initiate activation of inflammatory responses and a molecular pathway leading to mineralization and calcification[12] (discussed in detail in chapter 4).

2.6.1 Clinical Assessment of Calcific Aortic Stenosis

The diagnosis of AS occurs when patients experience symptoms, e.g. heart murmur, chest pain, shortness of breath and fatigue, and are referred to care providers for physical examination. Early-stage development of calcification can be detected by novel molecular imaging techniques, while conventional echocardiography and computed tomography (CT) can only visualize the late-stage calcification, when patients are symptomatic[13].

various imaging and diagnostic modalities are used to ensure the accuracy of AS diagnosis[14]. The initial diagnostic modality is transthoracic echocardiography, which is followed by Doppler echocardiography, cardiac catheterization, CT, and magnetic resonance imaging (MRI), depend on indicators from the initial examination[14]. Transthoracic echocardiography is a tool to evaluate AV morphology, left ventricle function, valvular abnormalities and regurgitation.

Table 2.1. Various hemodynamic metrics used for assessment of AS and the cutoff values for severe AS. Table is from Saikrishnan et al.

Metric	Units	Method	Severe AS Cutoff
AS jet velocity*	m/s	Direct measure	> 4.0
Mean pressure gradient*	mm Hg	Direct measure (Cath)Bernoulli equation (Echo)	> 40
EOA*	cm^2	Gorlin equation (Cath)Continuity equation (Echo)	< 1.0
Indexed EOA*	cm^2/m^2	EOA normalized by BSA	< 0.6
Dimensionless index (DI)*	None	Ratio of LVOT velocity and VC velocity	< 0.25
Energy loss index	cm^2/m^2	Indexed EOA accounting for ascending aorta size	< 0.5–0.6
Valvuloarterial impedance	$mm\,Hg \cdot m^{-1} \cdot m^2$	Global systolic LV load, including arterial pressure	4.5–5
AV resistance	$dynes \cdot s \cdot cm^{-5}$	Resistance of AV to flow	> 280
Projected valve area at normal flow	cm^2	Estimated EOA at normal flow	< 1.0
Calcium score	AU	Measured from CT data	> 1651

AS: aortic stenosis, AU: agatston Units, BSA: body surface area, Cath: catheterization; Echo: echocardiography, VC: vena contracta. EOA: effective orifice area.
*Metricss without an asterisk still need validation.

Doppler Echocardiography — is a non-invasive imaging modality used to assess the severity of AS. Doppler echocardiography does not provide direct pressure measurements, but it can use velocity to calculate the pressure gradient across the AV using Bernoulli equation (discussed in detail in chapter 4). A review by Saikrishnan et al.[14] provides a summary of metrics, units, methods of measurement and the cut-off points for severe AS, shown in Table 2.1.

Cardiac Catheterization — In mid 1900s, invasive catheterization was used for understanding physiology, in late 1900s and recent years, the use of cardiac catheterization expanded to diagnosis, treatment and studying coronary and valvular diseases[14]. Nowadays cardiac catheterization is not recommended and is only used if there is discrepancies with clinical data[15]. This approach does not provide information about valve anatomy, but it can directly measure accurate flow rate (Q)

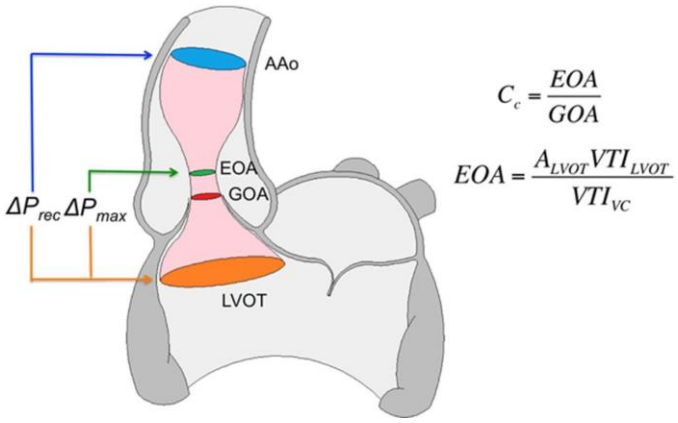

Figure 2.10. Schematic of flow through stenotic aortic valve. AAo: ascending aorta; EOA: effective orifice area; GOA, geometric orifice area; LVOT: left ventricular outflow tract; VC: vena contracta; and VTI: velocity time integral. Image is from Saikrishnan et al.

and pressure gradient (ΔP) from artery, this can also resolve the inconsistency of echocardiography diagnosis. This technique uses Gorlin's equation to relate ΔP to Q. $GOA = \frac{Q}{C_c C_v \sqrt{2g\Delta P}}$, where GOA is the geometric orifice area, Q is the flow rate through the AV, g is the gravitational constant, ΔP is the transvalvular pressure difference, C_c is the contraction coefficient and is equal to $\frac{EOA}{GOA}$, C_v is

the viscous loss coefficient (Figure 2.7). The GOA the area formed by free edges of the leaflets when valves are fully opened. Thus, catheterization measurements are performed at peak systole, while Doppler echocardiography calculates the average of parameters over multiple cycles. Clinical studies states that EOA is more used in practices as it represent a more accurate relationship between LV workload and flow resistance, while GOA is less favorable as it doesn't accurately represent the workload, and its inaccuracies become more significant when valve area is less than 1.5 cm^2 [14,16] or when patient is experiencing low flow condition[17]. Downstream in the distal aorta some kinetic energy is converted back to potential energy which results in pressure increase in that area, known as pressure recovery[18]. This is identified as the source of discrepancy in pressure difference between LVOT and ascending aorta that is reported by Doppler echocardiography and catheterization modalities.

Computed Tomography — CT is a non-invasive method that provides high resolution assessment of calcification in calcific aortic stenosis, and enables accurate measurement of anatomy of leaflets, annulus and other small cardiac features. Calcific deposits have higher density in compared with surrounding soft tissues (Figure 2.8). CT imaging uses attenuation coefficient expressed by Hounsfield unit (HU). High density calcific deposits have a high attenuation value (>130 HU) which makes the calcific area appear bright in the image. Calcium score is quantified by multiplying calcified area by Hounsfield unit, and is known as Agatston score[19]. Agatston score >2000 for men and >1200 for women is used to diagnose severe stenosis[20]. Even though a CT scan offers high spatial resolution data, it is not the first recommended modality to assess calcific AS, because it does not provide hemodynamic information like pressure gradient and velocity, it only shows GOA and quantifies calcium score, which is very helpful for specific applications[14].

Magnetic Resonance Imaging — The big advantage of using MRI is that it can provide accurate measurement of both hemodynamic and geometrical data, without any radiation exposure to

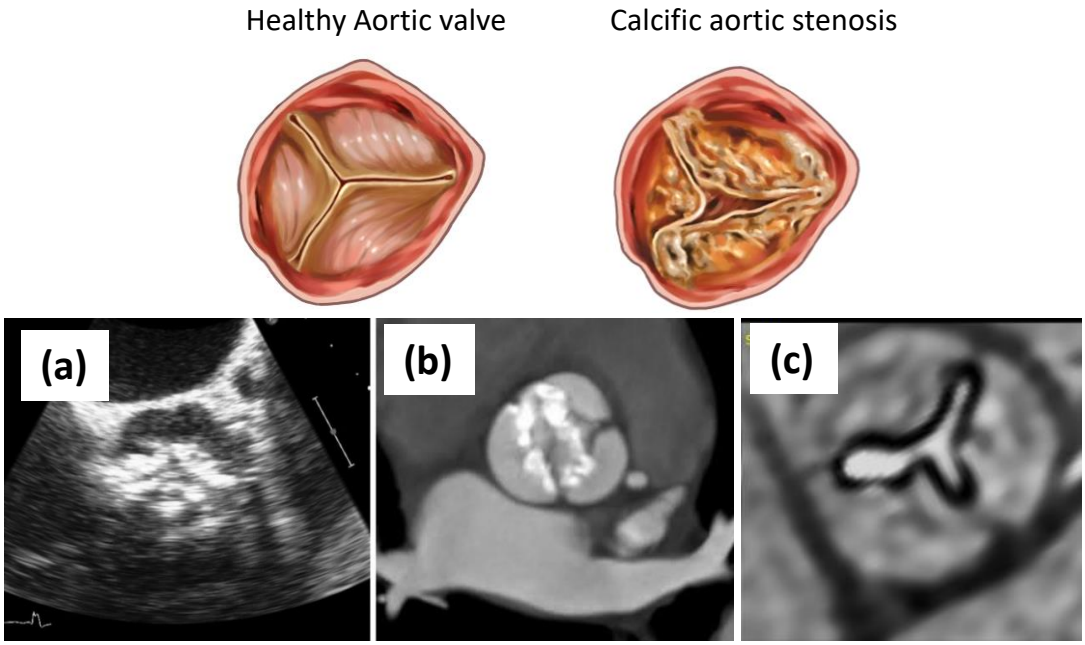

Figure 2.12. Calcific aortic stenosis visualized by (a) echocardiography, (b) CT imaging, (c) MRI. Images were modified from Lindman et al. 2013[2], www.cardiacmri.com, and braile.com.br.

patient. However, it has lower spatial resolution in compare with CT scan which makes it less favorable for quantifying calcification. Additionally, MRI is more expensive than other imaging modalities, which prevents it from being widely used.

2.6.2 Calcific aortic stenosis Treatment

Prevalence of valvular diseases has been led to design and development of artificial heart valves that can replace the native valves. The most common treatment for severe calcific aortic stenosis is the valve replacement. In surgical aortic valve replacement (SAVR), patients undergo an open-heart surgery to replace their aortic valve with a mechanical or a bioprosthetic valve; in this procedure calcified native leaflets are cut and removed. The mechanical or bioprosthetic valve is subsequently sutured to the aortic root. Alternatively, for patients who are at high risk for open

heart surgery, transcatheter aortic valve replacement (TAVR) has become standard of care. TAVR is less invasive and uses a catheter system to deliver and deploy the transcatheter valve to the location of the native aortic valve. The TAV deployment process for two of the most common

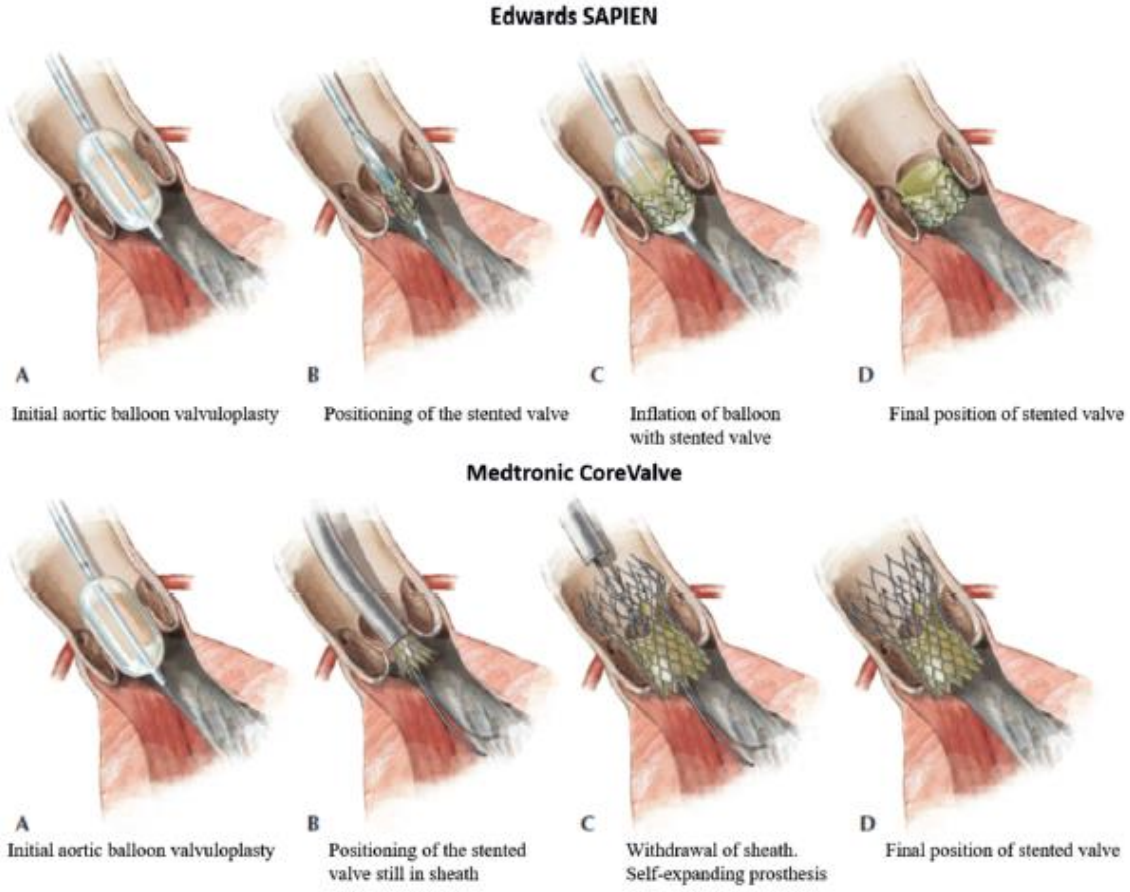

Figure 2.14. Schematic shows the catheter delivery systems for two transcatheter aortic valves: (1st row) an Edwards SAPIEN (Edwards Lifesciences, Irvine, California), (2nd row) a Medtronic CoreValve (Medtronic, Minneapolis, Minnesota). Image is adapted from Bianchi 2019[1]

types of TAV: balloon expandable Edwards SAPIEN valves and self-expandable Medtronic valves is shown in Figure 2.9. Although SAVR and TAVR improve symptoms and survivals, they come with some shortcomings and complications that are discussed in chapter 4.

3. SPECIFIC AIM 1: Right ventricle in Hypoplastic Left Heart Syndrome exhibits altered hemodynamics in the human fetus

3.1 Introduction

Congenital heart disease (CHD) occurs in up to 5% of live births[21]. Structural CHDs can be complex and difficult to treat, such as hypoplastic left heart syndrome (HLHS), which is where the left ventricle is generally underdeveloped, representing ~9% of all CHDs[22]. Under normal conditions, both ventricles contribute to circulation with flow interlinked through the foramen ovale and ductus arteriosus. In HLHS, fetal flow patterns change relative to normal development, with reversal of shunting at the foramen ovale (left atrium to right atrium), and with most flow entering the systemic circulation from the right heart via the ductus arteriosus, resulting in lowered perfusion through the pulmonary arteries[23]. Although stable for fetal circulation, these flow inefficiencies are not sustainable in postnatal circulation. Ultimately there is a chronic volume overload and overstretch in the right ventricle, which can lead to congestive heart failure [24]. Blood circulation in HLHS can be improved after birth through a series of surgeries by completely bypassing the left ventricle, making the right ventricle the only pump for the entire circulatory system[25]. Surgery corrects the volume overload and overstretch. However, the systemic veins become congested and the right ventricle is underloaded due to a low preload caused by a bottleneck at the pulmonary circulation[26], thereby changing the mechanical signals for ventricular remodeling. Hemodynamic analysis of fetal circulation pre-surgery may guide patient selection for the procedure and may provide insight into the volume overloaded state.

The molecular etiology for HLHS has remained poorly defined. However, the structural phenotype is reproduced upon obstruction of the left atrium in otherwise healthy hearts. For

example, ligation of the left atrium leads to an underdeveloped left ventricle in chick embryos [27]. Obstruction in humans can come in the form of an undersized foramen ovale, where 40% of the umbilical venous return passes in healthy hearts[28]. Alternatively, outflow obstruction can also lead to an HLHS phenotype. In the human fetal heart, a severe aortic stenosis can lead to HLHS; yet, alleviating restricted blood flow through valvuloplasty can prevent this progression[29]. Through these findings, researchers postulate that reduced wall shear stress or altered pressure and therefore loading caused by the obstruction could lead to morphological changes characteristic of HLHS. Quantifying detailed flow patterns and energetics in normal and HLHS human hearts may provide more insight into the role of mechanical loading in this disease, especially since size and output from the HLHS right ventricle are known to be larger than normal as the right ventricle compensates for an ill-functioning left ventricle[30].

As experimental approaches are appropriate and accessible to study animal models, noninvasive computational fluid dynamics (CFD) based on medical imaging is of great utility for investigating human fetal heart function. Quantifying blood flow during cardiac development in normal and diseased hearts will help us to identify if specific mechanical environments are correlated with heart malformations. Here, we use a CFD simulation based on patient-specific human fetal ultrasound scans to quantify blood flow patterns in healthy and HLHS hearts. The right ventricle in HLHS is important since its function dominates cardiovascular flow as the left ventricle in HLHS cases is exceedingly small[31]. Therefore, in the current study, intracardiac flow has been simulated in the right ventricle to quantify the demand on the right heart.

3.2 Methods

3.2.1 Data collection

The study protocol complied with the Institutional Review Boards of Children's Hospital Colorado, Colorado State University, and the University of Colorado. Nine fetal hearts (5 HLHS and 4 normal) were scanned using 4D patient-specific spatio-temporal image correlation (STIC) ultrasound with gestational ages listed in Table 3.1. Scans were collected on a GE Voluson E10 system (GE Healthcare, USA) using a RAB6 probe with a frame rate of >70 fps; images were collected at Children's Hospital Colorado during normal patient visits. Doppler velocity waveforms were obtained at the pulmonary and tricuspid valves (Figure 3.1b). Ultrasound scans were taken from normal fetuses (22-35 weeks of gestation) and fetuses diagnosed with HLHS (22-37 weeks of gestation). It was difficult to perfectly match gestational age due to challenges with obtaining patient data.

Table 3.1. List of all the cases and represented numbers

		Case	GA
Normal	Mid-stage	N.1	22
		N.2	26
	Late-stage	N.3	27
		N.4	35
HLHS	Mid-stage	H.1	22
		H.2	25
	Late-stage	H.3	28
		H.4	35
		H.5	37

Abbreviations – GA: gestational age, N: normal, H, HLHS: hypoplastic left heart syndrome

3.2.2 Medical Image Processing

Methods for image processing were performed using prior techniques outlined in Wiputra et al.[32-34]. Briefly, volume ultrasound images were analyzed using 4DView software (GE Healthcare, USA), where images were split into 40-time steps. The right ventricle in 2D ultrasound

images was semi-automatically segmented using a lazy snapping algorithm in a custom-written C++ code and converted into binary images (Figure 3.1a.i). 3D geometries were reconstructed

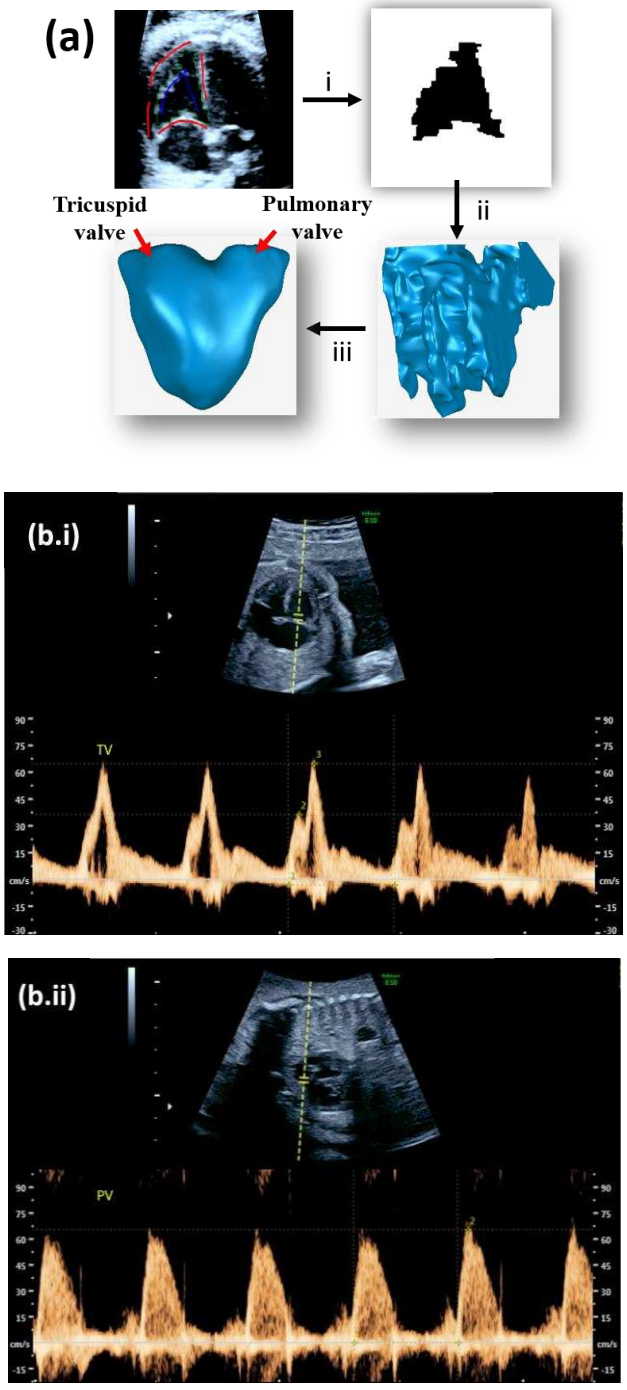

Figure 3.1. (a) Ultrasound images were (i) segmented converted to binary images, (ii) 3D geometry was reconstructed from 2D images, and (iii) surfaces were smoothed. (b) Pulsed Wave Doppler with Doppler measurement locations shown by yellow calipers for the (i) tricuspid and (ii) pulmonary valve.

from these images using VMTK software (www.vmtk.org) (Figure 3.1a.ii) and smoothed using Meshmixer (Autodesk, Inc) and Geomagic software (3D Systems, Morrisville, NC) (Figure 3.1a.iii). We note that internal structure of the ventricle, e.g. trabeculation, papillary muscles, and chordae tendineae, is not modeled due to limited resolution of ultrasound. 3D volumetric data of the fetal heart were extracted at each time point (4D) during the cardiac cycle. Time-dependent 3D volumes were used to model the ventricular wall motion (Figure 3.S1). End diastolic volume (EDV) and stroke volume (SV) were calculated

3.2.3 Ventricular wall motion modeling

To provide a user-defined moving boundary to our CFD simulation, ventricular wall motion was modeled using a Spherical Harmonic Transform algorithm created in MATLAB R2018b (Mathworks Inc., Natick, MA) based on measured volumes from reconstructed 3D geometries. Radial displacement was obtained for a complete cardiac cycle:

$$r_{model}(\theta, \phi, t) = \alpha(\theta, \phi)\Omega(t) + r_0(\theta, \phi), \tag{3.1}$$

where $\Omega(t)$ is the characteristic waveform with respect to time, which was obtained by taking cube root of ventricular volume over time, $\alpha(\theta, \phi)$ is the amplitude of displacement waveform, and $r_0(\theta, \phi)$ is the initial radius. At each time point, the wall motion was modeled as a function of volume and radial displacement, $\alpha(\theta, \phi)$, in θ and ϕ directions, where θ probes from 0 to 180 and ϕ probes from 0 to 360.

3.2.4 Computational fluid dynamics simulation

The modeled wall motion was enforced with a user defined function (UDF), based on Eq. 1. CFD simulations were performed using a dynamic mesh in ANSYS Fluent 17.2 software

(ANSYS Inc., Canonsburg, PA). The pulmonary and tricuspid valve areas were obtained from segmented 3D geometries and by measuring the valve area from 4DView. The valve areas were measured at the end of systole. Area measurements were done manually in 4D view. Simulations were performed using non-Newtonian viscosity with the Carreau-Yasuda model:

$$\eta = \eta_\infty + (\eta_0 - \eta_\infty)[1 + (\lambda\gamma)^2]^{\frac{n-1}{2}}, \tag{3.2}$$

where η_∞ is the viscosity, 0.0035 Pa*s for a Newtonian model, η_0 is the viscosity at zero shear, 0.056 Pa*s, γ is the shear rate, and λ and n are constants; 3.313 and 0.3568 respectively[32]. Four cardiac cycles were simulated to allow flow development (confirmed with a converged time-dependent flow field), after which the results of the last cardiac cycle were analyzed. The simulations were performed with 1-1.5 million mesh cells based on a mesh independence study[35]. Boundary conditions in the simulation were set such that during systole, the tricuspid valve was closed (no-slip wall) and the pulmonary valve (zero pressure outlet) was open, while during diastole, the tricuspid valve was open (zero pressure inlet) and the pulmonary valve was closed (no-slip wall). The boundary conditions were implemented using a script.

3.3 Analysis

Results were analyzed with CFD-post software (ANSYS Inc., Canonsburg, PA). We computed the area-weighted average wall shear stress (WSS) with respect to time since multiple studies have shown that low and oscillatory WSS can alter endothelial cell phenotypes, and has been correlated with diseased conditions in the vasculature[36]. Time-averaged WSS (TAWSS) was calculated using Eq. 3.3 to determine the function of HLHS and normal right ventricles over one cardiac cycle:

$$TAWSS = \frac{1}{T}\int_0^T |\vec{\tau}_w| dt, \tag{3.3}$$

where $\vec{\tau}_w$ is the WSS vector, t is time, and T is the period of one cardiac cycle. Separately, the intraventricular pressure gradient (IVPG) was computed using area-weighted average pressure. Since the inlet and outlet are set a zero pressure boundary condition, the IVPG is equal to the apex pressure for the current study. Kinetic Energy (KE) in the right ventricle and at the inlet and outlet were calculated by Eq. 3.4 and 3.5:

$$KE_{CV} = \int_{CV(t)} \frac{1}{2}\, \rho\, \vec{v}(t)^2\, dV, \tag{3.4}$$

$$KE_{in/out} = \int_0^T \int_{CS(t)} \frac{1}{2}\, \rho\, \vec{v}(t)^2 (\vec{v} \cdot\, \hat{n}\,)\, dA\, dt, \tag{3.5}$$

where ρ is the density of blood, $\vec{v}$ is the velocity of blood flow, V is the volume, CV is control volume that is defined as volume of the entire right ventricle, $\hat{n}$ is a unit normal vector relative to the control surface (CS), and A is the area. KE_{in} is the inflow KE, and KE_{out} is the outflow KE. Work done (Wd) by right ventricle (excluding afterload) was calculated cumulatively for the entire right ventricle during systole through Eq. 3.6:

$$Wd = \int_0^T \int_{CS(t)} P(\vec{v}.\hat{n}\,)\, dA\, dt, \tag{3.6}$$

where P is blood flow pressure with respect to a zero value at the inlet and outlet. Energy loss was calculated by Eq. 3.7, which excludes the afterload:

$$E = Wd - KE_{CV} - KE_{in/out} \tag{3.7}$$

Note that pressure at the valves is set to 0 when they are open. Hemodynamic efficiency is calculated by Eq. 3.8:

$$\eta = \frac{KE_{out}}{Wd} \times 100 \tag{3.8}$$

3.4 Results

3.4.1 Right ventricle function

As gestational age increases, so does the EDV, Figure 3.2a. The relative increase in EDV is greater in HLHS cases, leading to a right ventricle that is 50% larger than a normal right ventricle at 35 weeks gestation. Similar trends are found for the thickness of the right ventricle wall, tricuspid valve and pulmonary valve areas, SV, and CO, Figure 3.2b-f. The CO at mid- and late-stages, in the HLHS right ventricle is respectively 30% and 50% greater than a normal heart, as a single ventricle supplies blood to both systemic and pulmonary circulation. The heart rate remains between 120 and 150 beats per minute for normal and HLHS cases during all gestational ages, Figure 3.2g, while the ejection fraction remains between 40-65%, Figure 3.2h. Overall, the HLHS right ventricle is larger when compared to normal, especially at later gestational ages, with a greater output that correlates with the increasing size.

3.4.2 Hemodynamics

Despite the increasing size and output from the right ventricle in HLHS, many hemodynamic characteristics are similar between normal and HLHS hearts, supplementary videos 1-9 for each heart in Table 3.1. We note that these results exclude the impact of leaflets, which can shift vortex formation further into the ventricle[37,38]. In both heart types, two vortices are generated during diastole, corresponding to the E- and A-waves, respectively resulting from ventricular expansion and atrial contraction. These vortices traverse through the ventricle, creating localized regions of high WSS (Figure 3.3), Figure 3.3 shows the maximum WSS of all cases. Except for

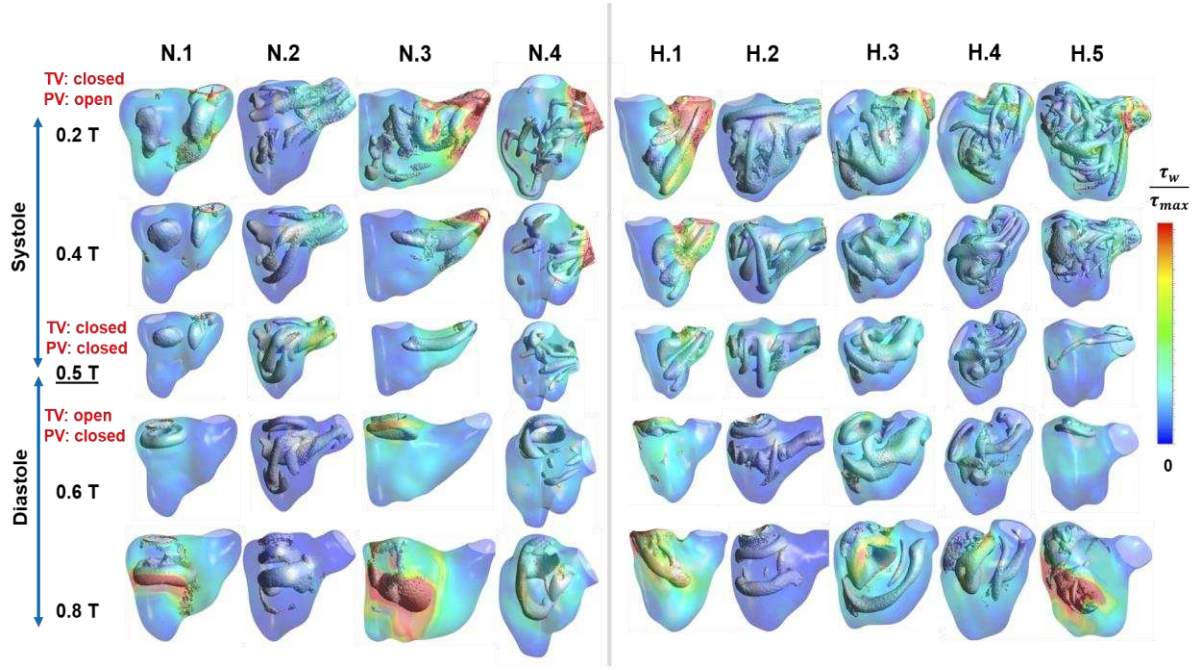

Figure 3.2. Wall shear stress and vortex isosurface at different time points of one cardiac cycle for normal right ventricles at gestation weeks 22 (N.1), 26 (N.2), 27 (N.3), and 35 (N.4), and HLHS right ventricles at gestation weeks 22 (H.1), 25 (H.2), 28 (H.3), 35 (H.4), and 37 (H.5). Vorticity isosurfaces were computed for demonstration of regions with λ2 criterion larger than 0.05. Time-stepped images were extracted from supplementary videos S1-S9.

the H.5 case, the A-wave vortex interacts and combines with E-wave vortex within the ventricle, creating a bigger overall vortex ring close to the apex. For H.5, a single diastolic wave is seen in Doppler measurements, Figure 3.4, which leads to the formation of a single vortex, instead of two. During systole, the vortices change shape and align with the outflow tract prior to dissipating. As the vortex exits the pulmonary valve, it creates a region of localized high WSS that supplements the high shear stress created from the convergence of flow in this region. This leads to the highest TAWSS seen in the right ventricle, Figure 3.5, which increases relative to gestational age for a normal ventricle, but not in HLHS. No discernable TAWSS differences exist between normal and HLHS hearts elsewhere in the ventricle. Overall, despite a larger ventricle and increased CO for HLHS cases, (Figure 3.2a,f), the primary finding is that no observable difference could be seen for TAWSS relative to normal hearts, except at the pulmonary valve during later stages of

development, Figure 3.5. There are no significant differences in WSS during the cardiac cycle other than the WSS at the normal outlet during systole (Figure 3.S2).

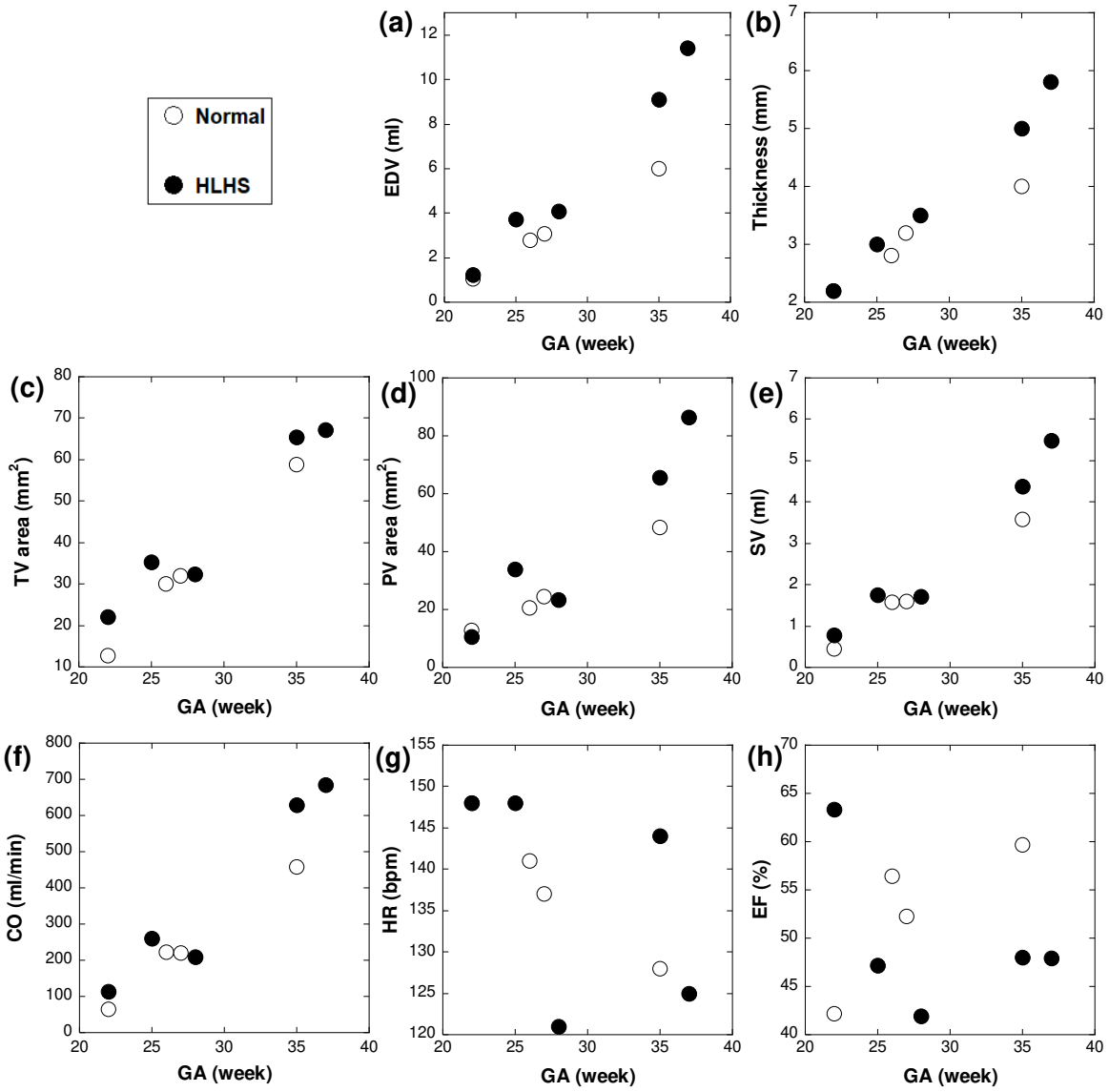

Figure 3.3. Plots show maximum values for (a) end diastolic volume (EDV), (b) ventricular wall thickness, (c) tricuspid valve (TV) area, (d) pulmonary valve (PV) area, (e) stroke volume (SV), (f) cardiac output (CO) (g) heart rate (HR) in beats per minute (bpm), and (h) ejection fraction (EF), with advancement of gestational age for normal and HLHS right ventricles during one cardiac cycle.

3.4.3 Energy and work

Normal and HLHS right ventricles produce a similar amount of work during a cardiac cycle, despite differences in size and SV, Figure 3.6a. In the current context, we note that the calculation excludes work done to overcome the afterload and only pertains the IVPG required to generate fluid inertia, which follows a similar trend, Figure 3.6b. The energy loss, which excludes the effect of afterload in the calculation, is also similar between normal and HLHS right ventricles for all cases, except H.5, Figure 3.6c, while tfficiency is in the range of 70-95% for all cases Note that efficiency would drop when accounting for afterload. For H.5, there is an increase in energy loss relative to other late-stage cases (N.4 and H.4). Note that H.5 also corresponds to the oldest fetus with a large EDV, CO, and the single high-speed diastolic wave, which contributes to a high KE_{in} that increases KE_{CV}, shown in Figure 3.6e, during diastole. Therefore, more energy is lost as a result of the interaction of the high speed single diastolic wave with the ventricular wall when compared to other hearts at a similar gestational age, Figure 3.6c. CO per Wd (Figure 3.6f), and CO per energy loss (Figure 3.6g) are also comparable between normal and HLHS hearts, except N.1 because N1 has a very small Wd. Values would decrease when accounting for afterload. Overall, the difference in work done (excluding work to overcome the afterload) and amount of energy loss is modest, despite notable differences in size and output between HLHS and normal right ventricles.

3.5 Discussion

Our CFD simulations provide detailed insight into the patient-specific hemodynamics of HLHS. Numerous animal studies have shown that prenatal hemodynamic forces sculpt the heart [27,39]. However, the full flow field of many CHDs are undefined in humans, despite the potential

role in remodeling of the fetal heart. We provide a first step toward quantifying these flow fields in HLHS. We found that the right ventricle in HLHS compensates for left ventricle dysfunction through increased size, i.e. EDV. Despite the increased size and output of the right ventricle, there

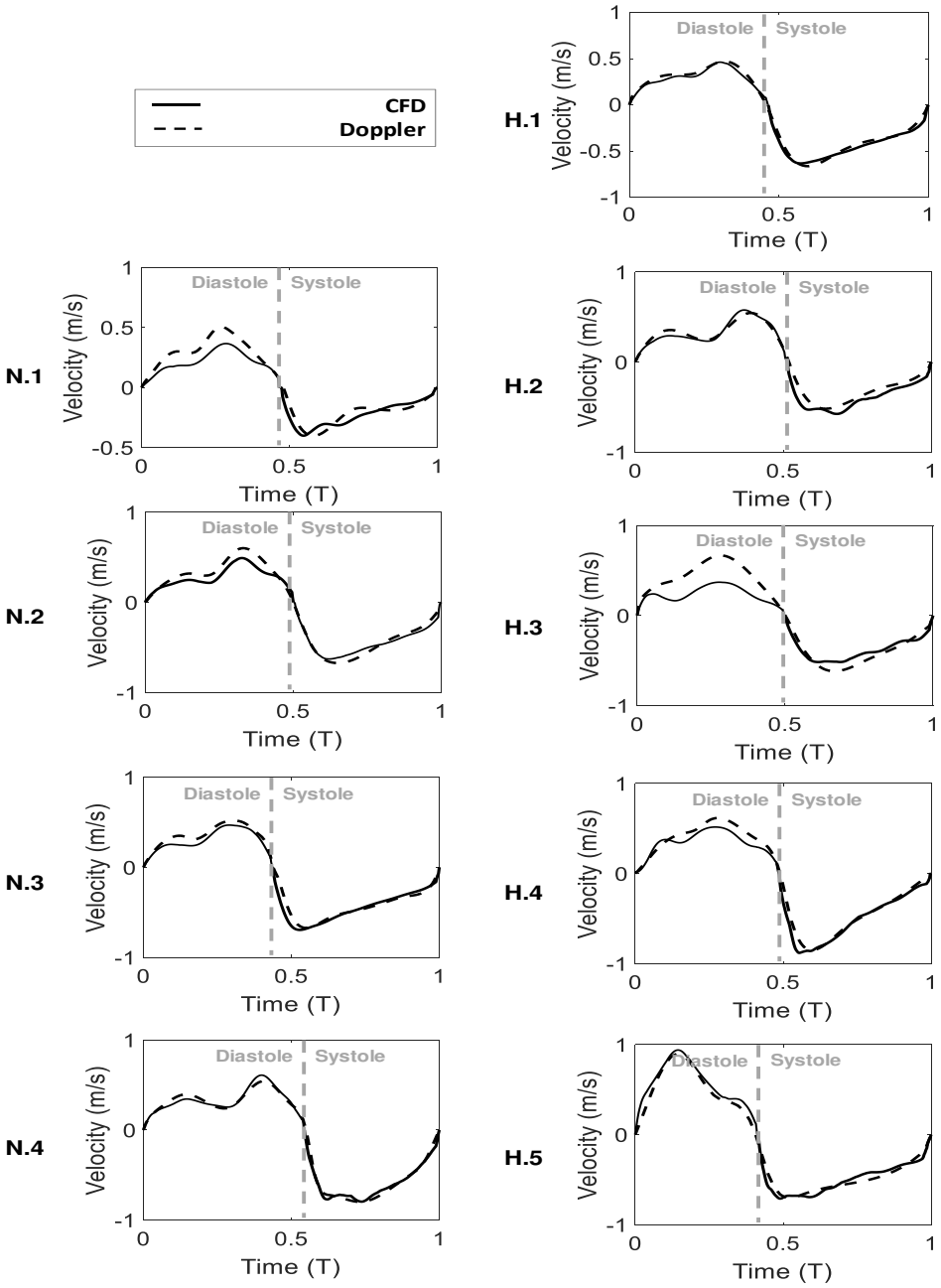

Figure 3.4. CFD-simulated velocity (solid line) compared with Doppler velocity (dashed line) over one cardiac cycle (T) for normal right ventricles at gestation weeks 22 (N.1), 26 (N.2), 27 (N.3), and 35 (N.4), and HLHS right ventricles at gestation weeks 22 (H.1), 25 (H.2), 28 (H.3), 35 (H.4), and 37 (H.5).

was relatively little difference for WSS, Wd, or energy loss between normal and HLHS right ventricles, while noting that Wd and energy loss calculations exclude effects of afterload here.

Functional parameters in the current study are in agreement with the literature, with a general increase in output and size of the right ventricle in HLHS when compared with a normal heart. Note that we measured EDV and SV from the reconstructed geometries, which is different than the clinical approach. EDV, SV, and CO conform to reported values, which are respectively 3.54±1.5 ml, 2.21±0.97 ml, and 321.89 ± 142.02 ml/min for normal hearts at a gestational age of 30.16±3.85 weeks, while for HLHS, these values were 4.18±1.52 ml, 2.30±0.80 ml, and 369.35 ± 118.41 ml/min at 29.12±3.54 weeks. Ejection fractions in that study were also relatively unchanged between right ventricles of normal and HLHS hearts, similar to our results. In addition, reported right ventricle size increases with gestational age, with a mean EDV of 0.8 ml at 20 weeks gestation, increasing to 3.43 ml at 30 weeks gestation in normal right ventricles[40]. Despite the

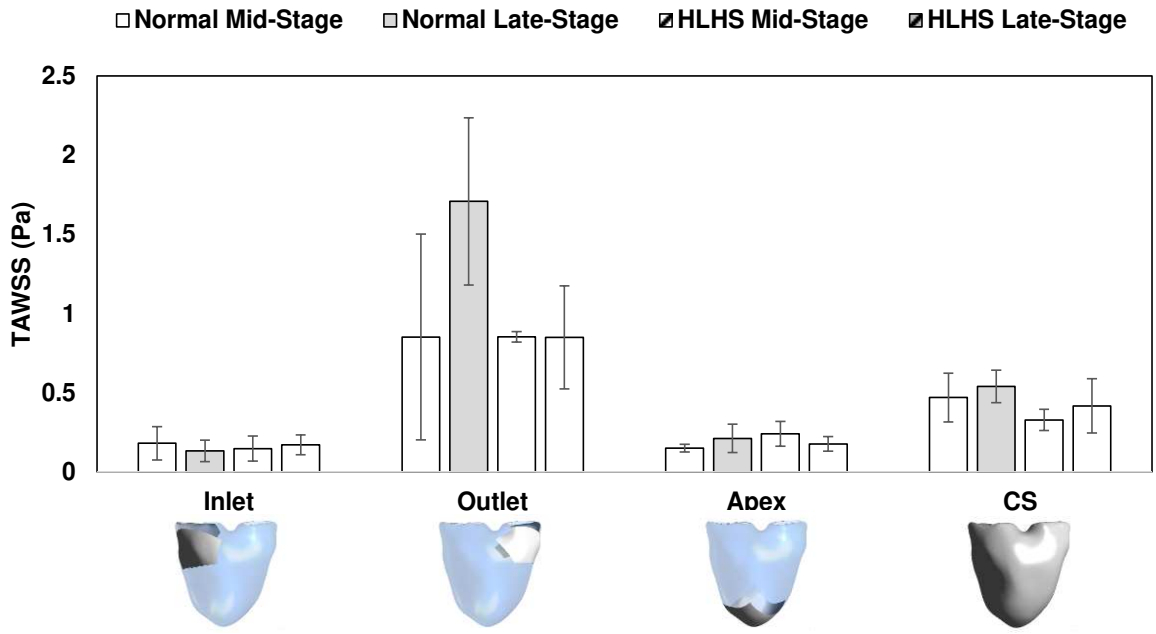

Figure 3.5. Mean time-averaged wall shear stress (TAWSS) with error bars representing standard error of the mean for normal and HLHS for mid- and late-stage at the inlet, outlet, apex, and the entire control surface (CS) of the right ventricle

variability in functional parameters, there is a clear increase in size and output of HLHS relative to normal right ventricles.

TAWSS is relatively conserved across gestational ages for normal and HLHS right ventricles, despite the increased CO, whether as a passive or adaptive response. TAWSS can remain conserved when the heart features, e.g. heart valves, scale with functional output. For example, wall shear stress scales proportionally with flow rate and inversely with radius cubed for laminar flow through a tube. Indeed, CO and SV scale with EDV in Figure 3.2, providing an explanation for conserved TAWSS in Figure 3.5. The PV is an exception in our results. The PV TAWSS changes with age for a normal heart, but not for an HLHS heart. Perhaps, in the overloaded HLHS state, a more drastic increased PV area keeps the TAWSS low, when compared to a normal PV as gestational age increases. Such a situation inconclusively indicates that the valve area is not dictated by an adaptive response, but instead may result from passive scaling. The increases in PV area, Figure 3.2c, d, is in agreement with prior work that reported 0.44±0.11 cm^2 for normal, and 0.55±0.23 cm^2 for HLHS PV areas for 30-32 weeks gestation[41]. TAWSS in normal hearts is also in agreement with previously reported values[33]. Overall, a longitudinal study would improve the ability to dissect out a cause-effect relationship related to conserved TAWSS.

The Wd by the right ventricle and overall energy loss is similar between normal and HLHS hearts (excluding effects from the afterload), while noting that the afterload would lead to Wd that is 10-25x the values required to generate inertia in the current study[42]. When accounting for afterload, the work done would depend on the SV and pulmonary pressure, which is not measured since it requires an invasive procedure. Pulmonary pressure depends on subject-specific left ventricular output and vascular impedance, making it difficult to speculate on trends of total work done. When pulmonary and systemic circulation are connected in series after a Fontan procedure,

the afterload becomes elevated, while the preload and volume overload on the right ventricle decrease, limiting the cardiac output from the ventricle[26,43]. In our work, the calculated Wd (to generate inertia) trends in HLHS right ventricles may be counterintuitive since the size and CO are larger. To gain insight, we studied the biggest contributors to Wd (excluding effects of afterload): SV and IVPG. SV increases with EDV and is larger in HLHS cases relative to normal

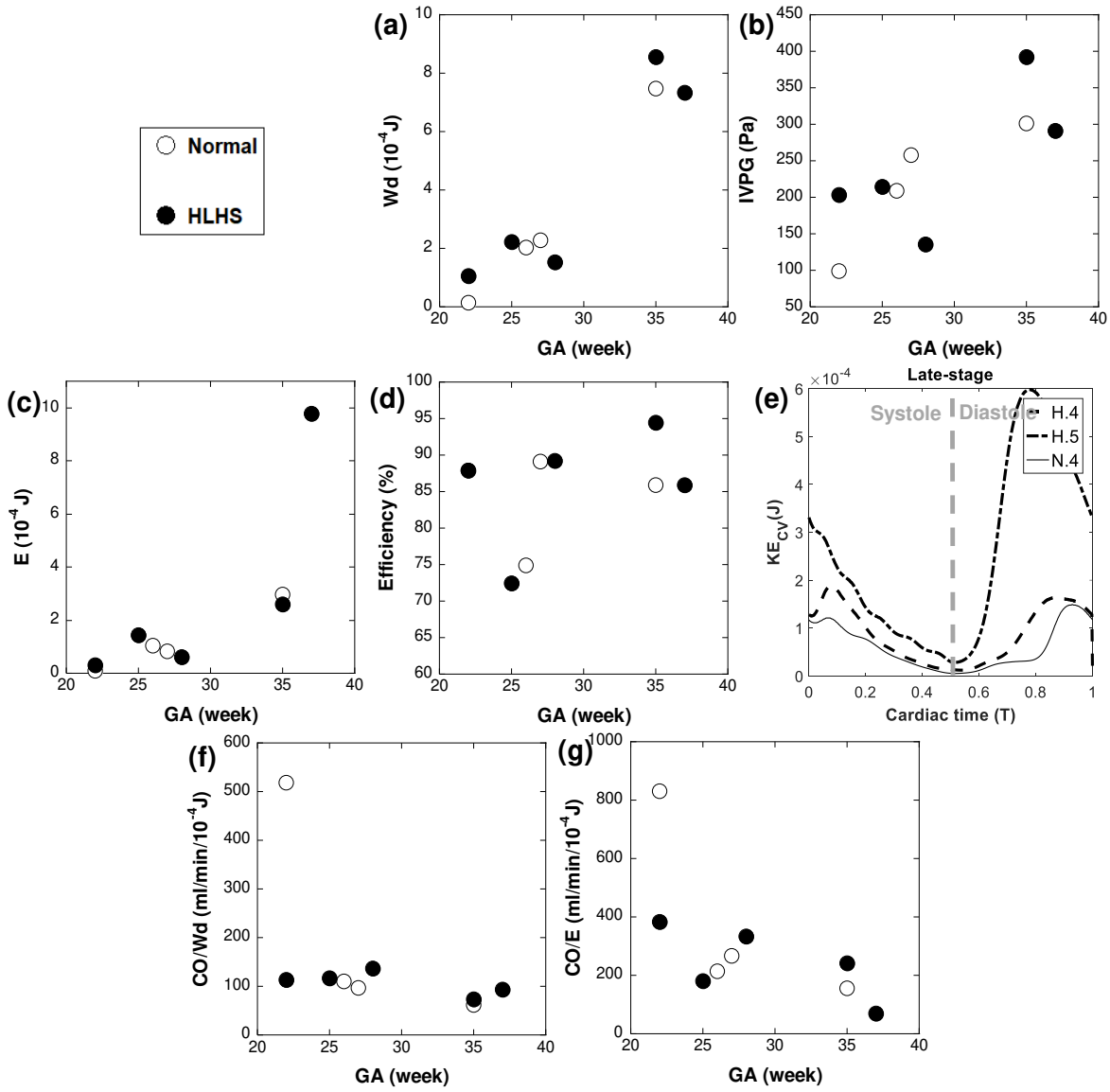

Figure 3.6. Plots show maximum values for (a) work done (Wd), (b) intraventricular pressure gradient (IVPG), (c) energy loss (E), (d) hemodynamic efficiency (η) with advancement of gestational age, (e) kinetic energy in the control volume (KE_CV) at the latest gestational stages studied during one cardiac cycle for normal and HLHS right ventricles, (f) cardiac output per work done (CO/Wd), and (g) cardiac output per energy loss (CO/E).

cases. However, IVPG in HLHS lacked a trend, particularly for H.3 and H.5, where IVPG values were relatively low for a specific fetal age. For H.3, we under-predicted the velocity, Figure 3.4, and therefore the IVPG may be under-predicted. Our under-prediction may be related to our limited ability to segment this case, which exhibited more shadowing than other cases. Case H.5 had flow patterns that differed from all other cases. Energy loss was also similar between HLHS hearts (except H.5) and normal hearts. Without additional HLHS cases to study, we cannot confidently state that Wd to produce inertia is unchanged between normal and HLHS cases, only that our data suggests this could be the case. In our study, the range of the Wd and energy loss when normalized by SV for normal hearts at early- and late-stages are similar to reported values[35]. Overall, results inconclusively indicate that HLHS right ventricles produce similar work with similar energy loss to normal right ventricles when we exclude the effects of afterload.

Various limitations exist in the current study. 4D STIC ultrasound has limited spatial resolution in the small fetal scale, limiting the ability to resolve small ventricular structures. Thus, similar to Uittenbogaard et al.[40], we did not account for the volume of trabeculation, papillary muscles, or chordae tendineae. Due to limited resolution and rapid motion, our technique also restricts us from simulating heart valve leaflet dynamics. Leaflets on the tricuspid valves are expected to shift the diastolic vortex, but otherwise would have little impact on the results, whereas leaflets at the pulmonary valve would have negligible effect on right ventricle flow patterns in the current study. Valves were assumed to be circular-shaped for simplicity of the calculation similar to Rasanen et al. and Allan et al. [41,44]. Valve area in the simulation was designed to match the effective orifice area, which is smaller than a geometric orifice area, with the valve area influencing WSS and energy calculations at the inlet and outlet of the control volume. Additionally, our technique is unable to model isovolumetric contraction and relaxation, and atrial contraction which

may affect flow patterns. We excluded torsional motion of the ventricle since it has been previously found to have minimal impact on fetal cardiac hemodynamics[37]. The calculation for Wd also excludes the effect of afterload, as previously emphasized. Our sample size was small, limiting our ability to apply a statistical analysis, due to the rarity of HLHS and the need for high quality ultrasound images. Overall, due to the challenges of fetal imaging, we had to provide many assumptions, as described previously[33,34].

4. SPECIFIC AIM 2: Calcific Aortic Stenosis – A review on acquired mechanisms of the disease and treatments

4.1 Introduction

Calcific aortic stenosis (AS) is the most common valve disease in developed countries[11,45], in which valves thicken and stiffen, and in some cases nodular deposits form, limiting valve function. This may result in valve regurgitation with concomitant stenosis. Calcific AS is a progressive disease that advances with age[2,46], affecting ~0.2% of people 50-59 years of age and increasing to 9.8% for 80-89 years[47]. As the general population has become older, the prevalence of calcific AS has increased, igniting multiple improvements in its management[11]. In addition to new diagnostic imaging techniques emerging, novel prosthetic valves have been developed as an effective treatment for calcific AS. To date, pharmacotherapy has not been shown to slow down the progression of the disease, or to reverse the calcification process[11]. In this review we highlight engineering perspectives towards recent advancements in the treatment of AS, underlying molecular pathways and mechanisms of the calcification process, clinical characteristics, hemodynamics, complications of calcific AS, diagnoses, and common treatment practices for calcific AS.

4.2 Aortic valve structure and calcification

Aortic valve (AV) leaflets consist of three layers: the ventricularis layer is elastin-rich and located on the ventricular side; the spongiosa is made of proteoglycans that provide lubrication for the other layers; and a fibrosa layer made of a dense collagen network is on the aortic side of the valve[48,49], which provides much of the structural support in response to mechanical forces[50]. These 3 layers are filled with valvular interstitial cells (VICs), and the entire layered structure is covered

by endothelial cells[51] (Figure 4.1). The fibrosa layer is particularly prone to calcification[52], while alterations to the endothelial barrier function could impact propensity for calcification. For years, calcification was thought to be a passive degenerative process in which calcium accumulates on leaflets[46,53], where old age, male gender, diabetes mellitus, coronary artery disease, chronic renal disease, hypertension, hypercholesterolemia, and smoking are known to increase the risk for AV calcification[54]. Now, it is understood that calcification is a complex process involving mechanobiology, molecular signaling, tissue remodeling, and inflammation as the AV opens and closes billions of times during a lifetime.

4.3 Hemodynamics and Endothelial Cell Mechanotransduction

Due to the sensitivity to hemodynamics (blood flow), endothelial cells may contribute to calcification and AS by responding to shear stress experienced on the cells' apical side (Figure 4.1). Indicating a potential link, calcium formation is more common in the non-coronary cusp, where surrounding fluid wall shear stress is lower relative to coronary cusps[45]. Endothelial cells respond to shear stress by changing their morphology, gene regulation, protein expression, transendothelial transport, alignment, and release of molecules and proteins from the surface[12]. These processes can occur as endothelial cells convert mechanical stimuli to biochemical signals to elicit biological responses, known as mechanotransduction, briefly summarized below.

Vascular endothelial cells sense their environment through ion channels (which allows membrane depolarization and cell signaling), integrins, intercellular junction proteins, caveolae, the glycocalyx, G protein-coupled receptors (GPCRs), and tyrosine kinase receptors[55,56], However, only some of these mechanosensors have been observed for valvular endothelial cells (further explained below). Integrins function as signaling receptors and play a crucial role in transmitting physical mechanical forces between the extracellular matrix and the actin cytoskeleton via focal

adhesion complexes. In one example, valvular endothelial cell morphological alignment perpendicular to the direction of flow involves β1 integrin, vinculin and focal adhesion kinase and depends on Rho-kinase and calpain[12]. GPCRs are also highly sensitive to changes in flow and activate downstream signaling by binding to extracellular ligands[57]. The glycocalyx is a mediator for cell-cell adhesion and works as a trap for ions and antibodies that translate to downstream signaling pathways[55]. Using these mechanosensors (and others), mechanical forces are transmitted to the nucleus and can change the nuclear morphology, stiffness, and gene expression[58]. Mechanotransduction in relation to AS calcification continues to be explored and only a brief description of some findings are presented here.

4.4 Inflammation mechanism in aortic valve calcification

Multiple studies indicate a role for an innate and adaptive immune response that leads to calcification. This largely initiates with dysregulated valvular endothelial cells, progresses to excessive remodeling of the leaflet ECM, changes in tissue stiffness, tissue mineralization, osteogenesis (formation of bone), and eventually lead to late-stage calcification[13,59].

The endothelium is most responsive to the magnitude and directionality of fluid shear stress. Physiological unidirectional shear stress is protective by downregulating adhesion proteins, vascular cell adhesion molecule 1 (VCAM-1), platelet endothelial cell adhesion molecule-1 (PECAM-1), and chemokines IL-1β and IL-8. It also leads to expression of nitric oxide (NO), which can help prevent thrombotic responses that could otherwise play a role in calcification[49]. Notch signaling is increased, which helps prevent calcification[60]. There is also increased expression of osteoprotegrin (OPG), which regulates aortic valve calcification by inhibiting receptor activator of the nuclear factor κB ligand (RANKL) signaling[61]. Under oscillatory shear

stress, VCAM-1, intercellular adhesion molecule 1 (ICAM-1), endothelial selectin (E-selectin), VEGF, and TGFβ are upregulated, which leads to increased oxidative stress and inflammatory agents such as bone morphogenic protein (BMP)-4 and cytokines: IL-1β and INFγ. TGFβ and VEGF can induce cell proliferation, fibrosis, and promotes calcification by enhancing irreversible tissue thickening and stiffening[12]. Increased BMP-2 and BMP-4 can upregulate osteogenic pathways involving the Msx2 transcription factor that activates Wnt/LDL receptor-related protein 5 (Lrp5)/β-catenin signaling[62,63], and the Runx2/Cbfa1 transcription factor[63,64] that leads to differentiation of the VICs to an osteoblast-like phenotype. Altogether, low and oscillatory shear

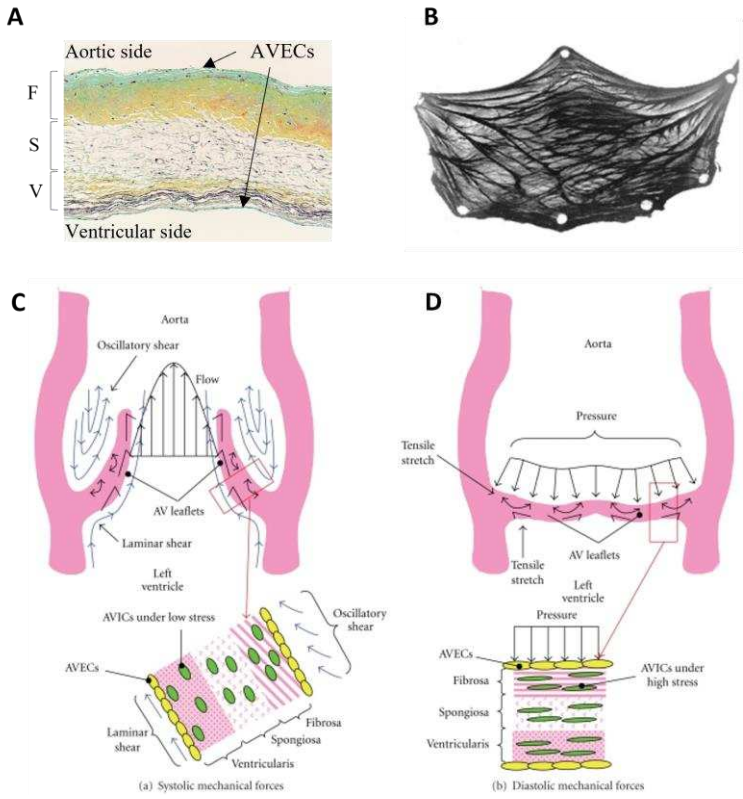

Figure 4.1. Microscopic and macroscopic overview of aortic valve tissue structure: (a) histological section of the aortic valve leaflet showing three layers: fibrosa (F), spongiosa (S), and ventricularis (V) covered by valvular interstitial cells (VICs) and valvular endothelial cells (VlvECs). (b) excised view of the aortic valve leaflet demonstrating fiber structure. Schematic of stress experienced by aortic valve leaflets and valvular cells during (c) systole, and (d) diastole. (a) is from Fishbein et al. (b) is from Driessen et al.; (c) and (d) are from Balachandran et al.

stress found in stagnating regions of aortic valve leaflets are linked to signaling changes in the endothelium that lead to proinflammatory responses that could be linked to calcification.

Endothelial cell responses can also lead to low-density lipoprotein (LDL) deposition in response to altered mechanical forces, which can induce inflammation[13,65]. LDL and lipoprotein (a) derived from cholesterol colocalize in the calcified valve tissue in early calcification[66]. Plasma lipoprotein (a) is an independent risk factor of AS identified through genome-wide association

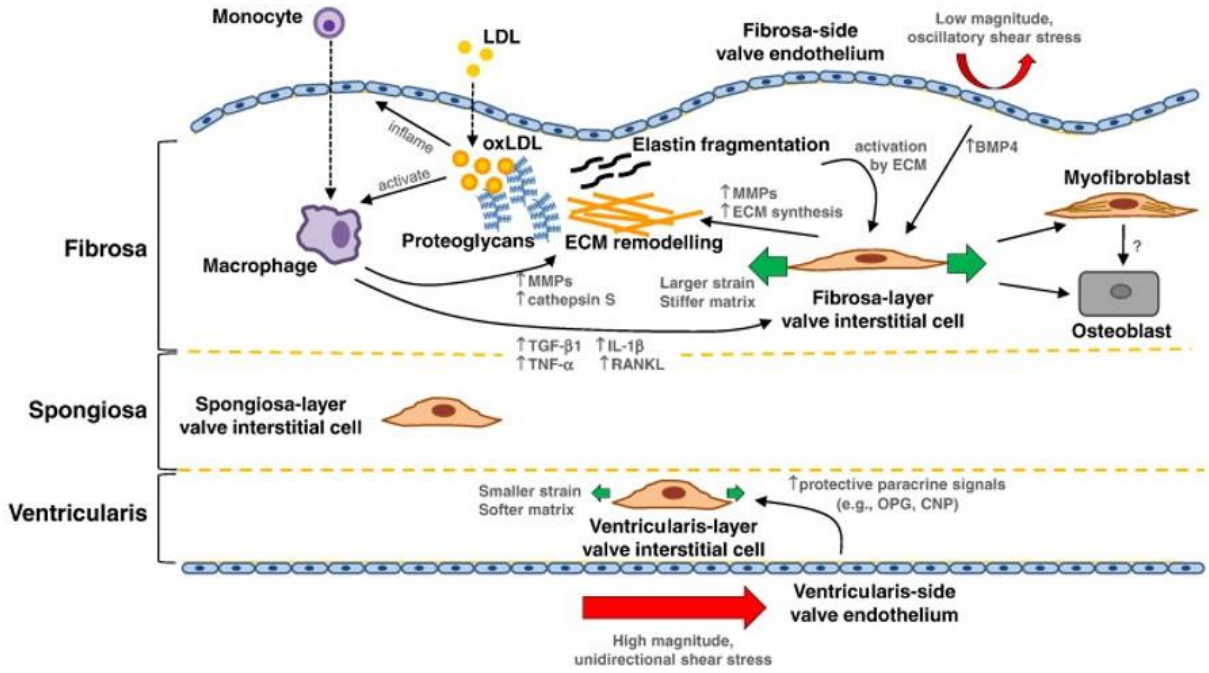

Figure 4.2. Summary of mechanotransduction and pathway of valvular calcification: in the fibrosa layer, the oxidated LDL (oxLDL) can inflame the endothelial cells, bind to monocytes, and activate macrophages. Activated macrophages mediate extracellular matrix (ECM) remodeling and molecular signaling that can potentiate valvular interstitial cell (VIC) pathological differentiation to myofibroblast and osteoblast cells. The ECM further affects VIC activation and differentiation; activated VICs synthesize and remodel the ECM, and produce cytokines, like TGF-β1. Interstitial and endothelial cells on each layer of the tissue exhibit a different phenotype. On the ventricular side, endothelial cells experience high magnitude and unidirectional shear stress, which may inhibit pathological differentiation of the local VICs. Image is from Yip et al.

studies[66-68]. Furthermore, apolipoprotein H (APOH) was identified as a novel locus for lipoprotein (a) levels[68]. Despite the link of LDL with calcification, studies have found that LDL suppression

or lipid-lowering therapy with statins (anti-inflammatory and antioxidant agents) do not slow down the progression of disease even when given at early stages of calcification[69,70].

Macrophages are found in calcified AV leaflets, likely entering through trans-endothelial migration involving ICAM and VCAM[69]. In response to activated endothelial cells, macrophages release pro-osteogenic cytokines like IL-1β, IL-6, tumor necrosis factor-α (TNF-α), and RANKL, all of which could contribute to calcification. Activated macrophages produce enzymes that can cause interstitial cell activation, changes in gene expression, and differentiation to osteoblasts, which then leads to excess synthesis and remodeling of collagen fibers in the fibrosa[52] (Figure 4.2). Cytokines can promote cell proliferation and ECM remodeling. Some fibroblasts can differentiate to activated myofibroblasts[71]. The activation of myofibroblasts further induces inflammation through the expression of BMP, MMP-2 and MMP-9 and releases TNF-α and TGF-β1 and eventually differentiate to osteoblast-like phenotype[72]. TNF-α activates nuclear factor-κB (NF-κB) pathways which leads to expression of proinflammatory genes[73]. Via activation of NF-κB, T cell activation amplifies the inflammatory response by producing cytokine interferon- (IFN-γ) and TNF-α. Macrophages (along with vascular smooth muscle cells) also release calcification-prone extracellular vesicles (EVs)[74]. Excessive production of EVs lead to microcalcification. Overall, macrophages can initiate a number of proinflammatory events that can lead to calcification in response to endothelial signals.

4.5 Pharmacotherapies

Currently there is no approved pharmaceutical treatment for calcific aortic valve stenosis, but literature provides possible future pharmacological approaches in human and animal models. A review by Myasoedova et al. showed that oxidized low density lipoprotein (Ox-LDL),

oxidized phospholipids (Ox-PL), lipoprotein associated phospholipase A2 (Lp-PLA2), Lp(a), proprotein convertase subtilisin/kexin type 9 (PCSK9), high density lipoprotein (HDL), the purinergic receptor 2Y2 (P2Y2R), sodium-dependent phosphate cotransporter (PiT-1), dipeptidyl peptidase-4 (DDP-4) are targetable components for prevention and treatment of calcific AS in human[75]. In efforts to target calcific AS, antisense oligonucleotides (ASOs) 2nd generation (inhibitor of apo(a) mRNA translation) was introduced as a new selective Lp(a) inhibitor[76]. Niacin (nicotinic acid) therapy helps to lower LDL and Lp(a)[77] and increase HDL[78]. Since statins exhibit limited benefit to calcific AS, the lowering of LDL may not provide benefit. Also, a trial study showed that extended-release niacin (ERN) does not reduce the risk of cardiovascular disease despite the favorable effect on lowering Lp(a)[79]. PCSK9 (involve in regulating blood cholesterol) inhibitors can significantly lower LDL and plasma Lp(a)[80] and reduce the risk of cardiovascular disease, but have an unclear impact on calcific AS. Sodium phosphonoformate (PFA) as a PiT-1 inhibitor can inhibit calcification in human VICs[81]. DDP-4 inhibitors inhibit progression of calcific AS by blocking insulin-like growth factors and osteogenic activities in VICs. Additionally, some animal studies suggest that calcification can be reversible. Miller et al. showed that a "genetic switch" in Reversa mice can reduce plasma lipid and oxidative stress and halt the progression of the calcific AS[82]. P2Y2R promotes expression of carbonic anhydrase CAXII, which acidifies the extracellular space and promotes calcification regression by resorbing minerals in mice[83]. There is ongoing effort to develop pharmacotherapies for calcific AS, but due to the complex processes involved, this is a challenging undertaking.

4.6 Clinical and Hemodynamic Characteristics of Aortic Stenosis

Severe AS can result in serious problems. Patients can experience heart murmur, chest pain, shortness of breath, fatigue and syncope. Pressure overload can occur in the left ventricle,

and when left untreated, this can lead to hypertrophy[84]. Presence of long-term pressure overload can even eventually lead to systolic failure and congestive heart failure. AS can also further create bleeding complications described below.

Aortic stenosis severity can be assessed based on valve flow velocity, valve orifice area, and the pressure gradient across the valve[14,85]. The common flow condition for severe stenosis is defined as a peak aortic velocity ≥ 4 (m/s), pressure gradient ≥40 (mmHg), and AV area <1 (cm^2)[86]; however, 5-10% of the patients with severe stenosis have low flow (low cardiac output), low pressure gradient <40 (mmHg) due to reduced left ventricle ejection fraction (LVEF) (<40%)[14], and 10-35% with severe stenosis have paradoxical (Stage 3D Severe AS) low flow and low pressure gradient due to LV hypertrophy (with normal EF). These variations of hemodynamics make the diagnosis and decision making for treatment of AS difficult; therefore other parameters have also been used to make accurate decisions when treating AS; this includes both subjective clinical symptoms and objective data, such as valvulateral impedance, AV resistance, projected AV area at normal flow, and calcium score[14,86]. A review by Saikrishnan et al. provides a comprehensive summary of metrics, units, methods of measurement and the cut-off points for severe AS[14]. In order to score AS, maximum velocity and pressure gradient are measured, and valve effective orifice area (EOA) is calculated.

Blood flow through the valve can be characterized using techniques and imaging modalities described below. Blood flowing from left ventricle outflow tract (LVOT), passing through a stiff narrow valve opening, creates a jet with maximum velocity at vena contracta (VC). VC is a location where fluid pathlines converge, and the velocity is the highest. The area of the VC is known as the EOA. Using Doppler echocardiography, pressure drop is approximated using a simplified Bernoulli equation, assuming that proximal velocity is negligible, $\Delta P = 4v^2$, where

ΔP is the transaortic valve pressure gradient (between VC and LVOT), and v is maximum velocity of blood[15] (Figure 4.3). EOA is calculated using the continuity equation; the volume flow rate passing through LVOT equals to the flow rate passing through VC, i.e. $EOA \cdot VTI_{VC} = CSA_{LVoT} \cdot VTI_{LVoT}$, where VTI_{VC} and VTI_{LVoT} are the velocity time integrals measured from the parasternal long-axis view at the location of LVOT and VC, and EOA and CSA_{LVoT} are cross sectional areas

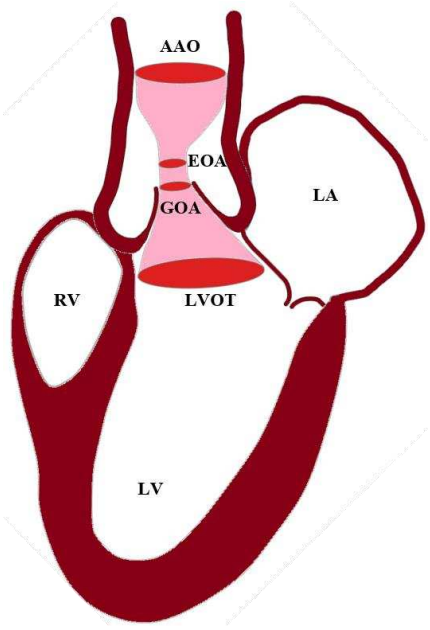

Figure 4.3. Schematic of blood passing through a stenosed aortic valve. Using continuity equation, the effective orifice area (EOA) can be calculated based on velocity time integral (VTI) at vena contracta (VC), cross-sectional area (CSA) of left ventricle outflow tract (LVOT), and VTI at LVOT. AAO- ascending aorta, LA- left atrium, LV- left ventricle, RV- right ventricle, GOA- geometric orifice area.

of VC and LVOT[14,15,87]. In rare cases when there are discrepancies in Doppler echocardiography measurements, cardiac catheterization is used to obtain a more accurate measurement of pressure directly from the blood vessel. Using the Gorlin equation, the geometric orifice area (GOA) is calculated from the flow rate and the pressure drop between the LVOT and VC, which is related to the EOA through the contraction coefficient. The GOA the area formed by free edges of the leaflets when valves are fully opened. Thus, catheterization measurements are performed at peak systole. A review by Saikrishnan et al. provides a detailed description of diagnostic modalities and

formulations[14]. Calcific AS can be additionally assessed by computed tomography (CT) which provides high-resolution assessment of calcification, and enables accurate measurement of leaflet anatomy and annulus geometry. Calcific deposits have higher density compared with surrounding soft tissues. CT imaging uses attenuation coefficients expressed by Hounsfield unit (HU). High density calcific deposits have a high attenuation value (>130 HU) which makes the calcific area appear bright in the image. A calcium score is quantified by multiplying calcified area by Hounsfield unit, and is known as Agatston score[19]. Different Agatston scores are used for men and women to diagnose severe stenosis[20]. Recent studies highlighted that calcification deposits are more prevalent in men, while fibrosis may be more significantly involved in valvular dysfunction in women[88,89]; presence of estrogen in women inhibits aortic valve calcification via suppression of RANKL signaling[90] and suppression of TGFβ-dependent ECM production[91]. Animal studies showed that sex-related differences in calcific aortic valve disease are due to different pathogenetic and signaling pathways in male and female[89].

In addition to impacting energy loss and hemodynamics, an aortic stenosis has a significant impact on the hemostatic capacity of blood. It can lead to gastrointestinal, skin, and mucosal bleeding, which may, in-part, be attributed to acquired von Willebrand syndrome (AVWS) also known as Heydes Syndrome[92,93]. It appears as though the AVWS stems from turbulence that can occur in an aortic stenosis, whereas it is often alleviated once a diseased valve is replaced, eliminating pathological flow[93,94,95].

4.7 Calcific Aortic Valve Stenosis Treatment

At late stages of calcific AS, no therapies can manage the progression of calcification and the only effective treatment is valve repair or replacement[85].

Valve Repair – Valve repair surgery can be used and is one of the oldest cardiovascular surgical interventions dating back to the early 1920s[96]. Native aortic valve (root and leaflets) repair comes with low mortality risk and is free of most valve-related complications, yet durability of treatments remained limited and reoperation is often required in the short term[97]. This has largely fallen out of favor in modern practice and is not utilized often, except in some centers.

Valvuloplasty – Balloon aortic valvuloplasty (BAV) is a catheter-based technique that dilates native valve's narrowed opening by delivering and inflating a balloon at the site of stenosed valve through femoral artery[98]. BAV increases leaflet mobility by creating a fracture in calcified lesions, expanding the aortic annulus and separating calcified commissures[99]. It has become a tool that can even be used in fetal aortic stenosis, to avoid progression into a more complex congenital heart malformation[100]. Use of an oversized balloon can cause infractions in the valve ring, separation between leaflets and the root, and leaflet tearing[99]. Additionally, balloon inflation may cause complications like coronary ostia occlusion that could lead to myocardial ischemia and dysfunction of left ventricle. BAV procedures do not provide long term improvements in adults, as the dilated valve can become restenosed; therefore, BAV is a temporary improvement option and a bridge to SAVR or TAVR for patients who are at high risk and need an urgent intervention[101]. Utilization of BAV is also practiced as a palliative treatment option in terminal patients with less than one-year life expectancy to improve quality of life in the short term, often seen in the hospice population.

Valve Replacement – Surgical aortic valve replacement (SAVR) has become the most common treatment for severe calcific aortic stenosis in which patients undergo an open-heart surgery to replace their aortic valve with a mechanical or a bioprosthetic valve; in this procedure calcified native leaflets are cut and removed. The mechanical or bioprosthetic valve is subsequently sutured

to the aortic root. SAVR improves symptoms and survival, but it comes with risks of thrombosis in mechanical valves that can cause stroke or heart attack, or in the case of bioprosthetic valves, durability is an issue with these valves often calcifying over time[102]. Initially, in older patients who are inoperable or are at high risk for surgery, transcatheter aortic valve replacement (TAVR) was an alternative option. However, this option is now common practice for lower risk patients, as the devices and procedures have advanced with equal to improved outcomes compared to SAVR[103]. The first in-human TAVR was performed in 2002[104]; since then, more than 50,000 TAVR interventions have been done worldwide[105]. TAVR is a less invasive technology in which a stented valve is delivered to the location of native valve through a catheter and is expanded to replace the calcified native aortic valve and leaflets.

Current guidelines set by the American College of Cardiology (ACC) and American Heart Association (AHA) advocate for Aortic Valve Replacement in the setting of symptomatic severe aortic stenosis. Timing of intervention depends on the development of clinical symptoms once the valve is classified as severe. The main reason is due to durability of bioprosthetic valves. Due to the relative development of TAVR being in its infancy within the last decade, long term durability has not been well established, although expert consensus agree 10 years is a reasonable time frame before expected degeneration and failure of the bioprosthesis. However, investigators are currently attempting to determine the benefit of treatment of severe aortic stenosis before the development of symptoms and potentially remodeling and other stressful changes to the heart. An ongoing study titled Evaluation of Transcatheter Aortic Valve Replacement Compared to Surveillance for Patients With Asymptomatic Severe Aortic Stenosis (EARLY TAVR) trial is ongoing to address the timing of intervention in severe aortic stenosis[106]. Furthermore, there is another school of thought that goes beyond waiting for symptoms with severe AS, but in fact challenges the

traditional belief to only treat severe AS. A clinical trial is being developed, called PROGRESS: Management of Moderate Aortic Stenosis by Clinical Surveillance or TAVR. As such, investigators are now looking to examine the benefit of treating moderate AS with TAVR intervention, although facing the same challenges regarding the issue of durability

SAVR and TAVR have various advantages. A study of 699 high-risk patients with severe aortic stenosis who were randomly treated with SAVR and TAVR in PARTNER 1 trial showed that one-year mortality rates were similar between the transcatheter and surgically treated groups (24.2% TAVR vs. 26.8% SAVR), but hemodynamics and post-operative outcomes were significantly different. The transcatheter group had a shorter hospitalization with a slightly better mean AV pressure gradient and mean AV area at one-year. However, vascular complications were significantly higher in the transcatheter group at one-month (11% TAVR vs 3.2% SAVR). The rate of major strokes at one-year were more than twice as high in the transcatheter group (5.1% TAVR vs 2.4% SAVR). Moderate and severe paravalvular regurgitation was more frequent in the transcatheter group than in the surgical group at one-year (6.8% TAVR vs 1.9% SAVR). Meanwhile, major bleeding was more frequent in the surgical group (19.5% SAVR vs 9.3% TAVR)[107]. Other follow-up studies have confirmed similar mortality rates and post-procedural outcomes; at 5 years, Gleason et al. reported mortality rates of 55.3% and 55.4% for TAVR and SAVR, respectively[108], and Mack et al. reported that risk of death at 5 years increases to 67.8% in TAVR and 62.4% in SAVR[109].

In low-risk patients, with severe aortic stenosis that were randomly treated with SAVR and TAVR in PARTNER 3 trial, TAVR was associated with significantly lower risk of mortality at one year (2.1% TAVR vs 3.5% SAVR) and life threatening bleeding (3.9% TAVR vs.11.2% SAVR); no significant differences in stroke (3.0% TAVR vs 4.2% SAVR), major vascular

complications (3.6% TAVR vs 2.4% SAVR), and myocardial infarction (1.7% TAVR vs 2.1% SAVR); and significantly higher moderate to severe paravalvular leak (PVL) (3.6% TAVR vs 1.7% SAVR)[110]. With 3 trials (PARTNER 1, 2, and 3), TAVR vs. SAVR have been studied in high-, intermediate-, and low-risk patients.

The TAVR utilization among underserved and underrepresented populations are lower. This was initially thought to be related to lower incident of AS among Black and Hispanic populations[111], but further studies suggested that this might be due to limited access to care, low socioeconomic status, and treatment biases in the non-White population[111,112]. This calls the need for advance clinical care accessible to all patients regardless of their race and ethnicity.

4.7.1 Mechanical Heart valves

Currently implanted mechanical heart valves (MHVs) typically have a bileaflet structure in shape of two discs made of pyrolytic carbon that can open pivotally. MHVs are highly durable when compared with other artificial heart valves; they can last up to 25 years in patients without major complications, but they have high risk of thrombosis[102]. High durability makes these valves more suitable for patients younger than age 50, as MHVs have a lower risk of reoperation[113].

Fluid high shear stress in the hinge region of these valves can initiate thrombotic events[114]. Patients treated with mechanical valves need a lifelong anticoagulant drug therapy to prevent thrombosis and thromboembolism[115]; however these drugs increase the risk of bleeding, stroke, systemic embolism, cardiac tamponade and death[116]. Therefore, multiple groups are attempting to improve the blood-material interactions through surface treatments[117]. However, the hemodynamic impact on blood from the hinge remains a concern, even with these treatments.

4.7.2 Bioprosthetic Heart valves

Bioprosthetic heart valves (BHV) are made of porcine or bovine pericardium. They have the advantage of being less thrombotic, requiring only short-term anticoagulation after surgery. The main disadvantage of BHVs is that they often require reoperation due to structural valve deterioration and calcification, making the average BHV lifetime only ~15 years. In recent years, BHVs durability has been improved by anti-calcification and anti-mineralization treatments. Therefore, nowadays BHVs are more commonly recommended for implantation, even in younger patients, due to their improved durability and lower risk of structural deterioration[118]. Otherwise, pediatric patients previously exhibited severe complications with calcification of BHVs.

4.7.3 Transcatheter Heart valves

Transcatheter heart valves (THVs) are gaining traction due to novel designs and delivery systems to replace the calcified aortic valve. In TAVR procedures, TAVs are deployed to the location of a calcified aortic valve with stent expansion through one of two main mechanisms: balloon expansion or self-expansion through shape memory alloys. The stent permanently opens the native valve by pushing against calcified leaflets. Some of the most frequent complications occurring with TAVR procedures are TAV malpositioning, coronary obstruction, paravalvular leak, crimped-induced leaflet damage, thrombosis, conduction abnormalities, and prosthetic-patient mismatch[119]. There are also less common, but potentially fatal complications including valve embolization and annular rupture. TAV crimping causes significant structural changes and damages in leaflet tissue that affects the durability of the tissue, and can lead to early thrombosis, early calcification and endocarditis in tissue[120]. Prosthetic-patient mismatch is a condition in which

EOA of the TAV is too small relative to patient's body size[121] causing elevated flow resistance at the valve which should be overcome by increased pressure in the heart[119].

Valve positioning has an important role in TAV hemodynamics; it has been suggested that TAV be positioned about 5 mm below the annulus of the valve for the best outcome[122]; however, the deployment site is dependent on the type of the TAV and in recent years, many attempts have been made to customize TAV deployment according to the patient-specific aortic root anatomy. If the implant is too-high or a too-low, it can result in moderate to severe paravalvular aortic regurgitation (AR) or PVL[122]. The malpositioned TAV can be manually repositioned; if ineffective, an alternative solution is to deploy a second TAV inside the first TAV, this is known as valve-in-valve (ViV) procedure[122]. Using new generation of TAVR devices, ViV has shown to be very effective in reducing post-procedural AR; a study of 63 patient who had ViV procedure using Edwards SAPIEN transcatheter valve showed that only 7.9% of the patient still had significant AR after procedure, however, ViV is associated with higher prevalence of cardiac conduction abnormalities which requires permanent pacemaker implantation in patients[123].

Additionally, undersizing a TAV can lead to malpositioning, valve dislodgement, and embolization[124]. It has been recommended that slightly oversizing the TAV can minimize PVL without causing injury and rupture in aortic root and annulus[124,125]. Another cause of PVL after TAVR procedure for calcified AS is the gap between the TAV and soft tissue resulting from stiffened calcified native leaflets and a calcified annulus[126]. The new generation of TAVR devices are designed to reduce some of these complications. Edwards SAPIEN family of valves are balloon expandable TAVs comprised of a cobalt-chromium frame; an inner and an outer sealing skirt made from polyethylene terephthalate (PET) fabric to reduce PVL; and bovine pericardial leaflet tissue treated with anticalcification treatment, ThermaFix, to reduce mineralization. In contrast, the

Medtronic CoreValve family are self-expandable, owing to nitinol stent material, and are comprised of porcine pericardial leaflet tissue with an antimineralization treatment. Numerous studies have investigated performance of Medtronic CoreValve and Edwards SAPIEN valves with respect to postprocedural PVL. Some reported that moderate to severe post-procedural PVL is more common with Medtronic CoreValve[127]. However, a recent longitudinal study showed that the severity and frequency of PVL at pre-discharge was significantly higher in Medtronic CoreValve (56.7% Medtronic CoreValve vs 43.2% Edwrads SAPIEN, p=0.06), but after one year, there was no major differences in frequency and severity of PVL between the two groups, possibly due to coaptation of self-expandable nitinol stent with aortic annulus[128].

Conduction abnormalities can be caused by tissue damage during valve deployment. In general, balloon-expandable valves have lower rates of pacemaker requirements compared to self-expandable TAVs. Studies show that the risk of conduction abnormalities and the need for permanent pacemaker implantation is higher after Medtronic CoreValve implantation compared to Edwards SAPIEN[129,130], possibly due to the valve design and its self-expansion mechanism; Medtronic CoreValves have a higher height and are implanted deeper into the LVOT. The self-expandable nitinol stent may apply pressure on and below the annulus that could result in atrioventricular node and left bundle branches damage[130,131].

4.8 Coronary Obstruction

Surgical bioprosthetic valves are likely to degenerate within 10-20 years[132]. Since reoperation is a high-risk procedure for elderly patients and increases their mortality risk, in recent years, non-invasive implantation of a TAV inside the degenerative bioprosthetic valve has become an alternative intervention for these patients[132-134]. However, it may come with the risk of coronary obstruction. Coronary obstruction is a rare consequence of TAVR that occurs during the procedure

in <1% of patients, but it is life-threatening[122,135,136] as it restricts blood flow circulation in coronary arteries. Coronary obstruction can occur following a TAV implantation in native aortic valve or following a ViV procedure which includes TAV implantation inside another TAV or TAV implantation inside a surgical bioprosthetic valve. Coronary obstruction is more common during ViV procedure (about four times greater) than during TAVR in a native aortic valve[132,133,136], and more frequently occurs with use of balloon expandable valves (0.81% balloon expandable vs. 0.34% self-expandable)[136]. This is possibly due to the differences in design and deployment mechanism of the transcatheter valves[135,136]. Coronary obstruction following a surgical bioprosthetic ViV procedure occurs more frequently in patients who had stentless or stented valves with bioprosthetic leaflets mounted externally[133]. Additionally, it is proposed that coronary obstruction in surgical bioprosthetic ViV procedures is more related to the model and positioning of the surgical bioprosthetic valve, and is independent of the type of TAV, particularly if a surgical valve is implanted in a non-coaxial tilted position, decreasing the distance between leaflets and coronary ostia[135]. Other surgical bioprosthetic valve risk factors were supra-annular implantation, high leaflet profile, valve design, stentless valves, or bulky bioprosthetic leaflets[135].

Clinical studies showed that anatomical factors such as low-laying coronary ostium and narrow sinus of Valsava (SOV), narrow sinotubular junction, and low sinus height are associated with coronary occlusion[135,136], while the left coronary artery (LCA) more commonly becomes obstructed (88.6%)[136]. In this study, the average height of LCA ostia in patients with coronary obstruction was 11 mm in men, and 10 mm in women. Most patients with SOV <30 mm and LCA ostium height <12 mm had coronary obstruction [133]. Initially, female sex was identified as a risk factor for coronary obstruction[135,136], but when aortic root dimensions were adjusted to body surface area, female anatomy was no longer an independent factor for coronary obstruction[135,137].

Coronary obstruction can be caused by calcium deposits, a native leaflet blocking the coronary ostia, a TAV that is positioned too high within the annulus, or through thrombosis [122]. In native TAVR procedures, coronary obstruction was linked to presence of bulky calcified lesions on the aortic leaflet blocking the coronary ostium (97.7%); however, the degree of calcification was not a predictor of coronary obstruction[136]. Even though the location of the calcification is an important factor in coronary obstruction[135], to-date no study has been done to evaluate coronary obstruction with respect to anatomical features of coronary ostium and the location of the calcium nodules.

Coronary obstruction might be prevented by a novel intervention technique called bioprosthetic or native aortic scallop intentional laceration (BASILICA)[138].

4.9 Bioprosthetic or Native Aortic Scallop Intentional Laceration of Coronary Artery (BASILICA)

The first BASILICA human procedure was performed in 2011 during a surgical bioprosthetic ViV procedure in two patients using Edwards SAPIEN and Medtronic CoreValve to prevent coronary obstruction[134]. This technique has been originated from the LAMPOON (Intentional Laceration of the Anterior Mitral leaflet to Prevent left ventricular Outflow Obstruction during transcatheter mitral valve implantation) technique[138]. In this procedure, a guiding catheter carrying an electrified wire is directed toward aortic valve through the femoral artery and is positioned at the base of the leaflet; the electrified wire lacerates the leaflet from base to its free edge[139] and creates a split leaflet that would allow blood flow through the coronary arteries. Since the first BASILICA procedure in 2011, some clinical and computational studies have been performed to show the feasibility of BASILICA procedure and to evaluate its overall

outcomes and outcomes relative to thrombosis and post-operation coronary obstruction[138-140,141-143]; however implications of this procedure on outcomes remain unclear (Figure 4.4).

Leaflet thrombosis remains a concern for TAVR after the BASILICA procedure, despite theoretically creating more washout in the target aortic sinus and neosinus. A recent experimental

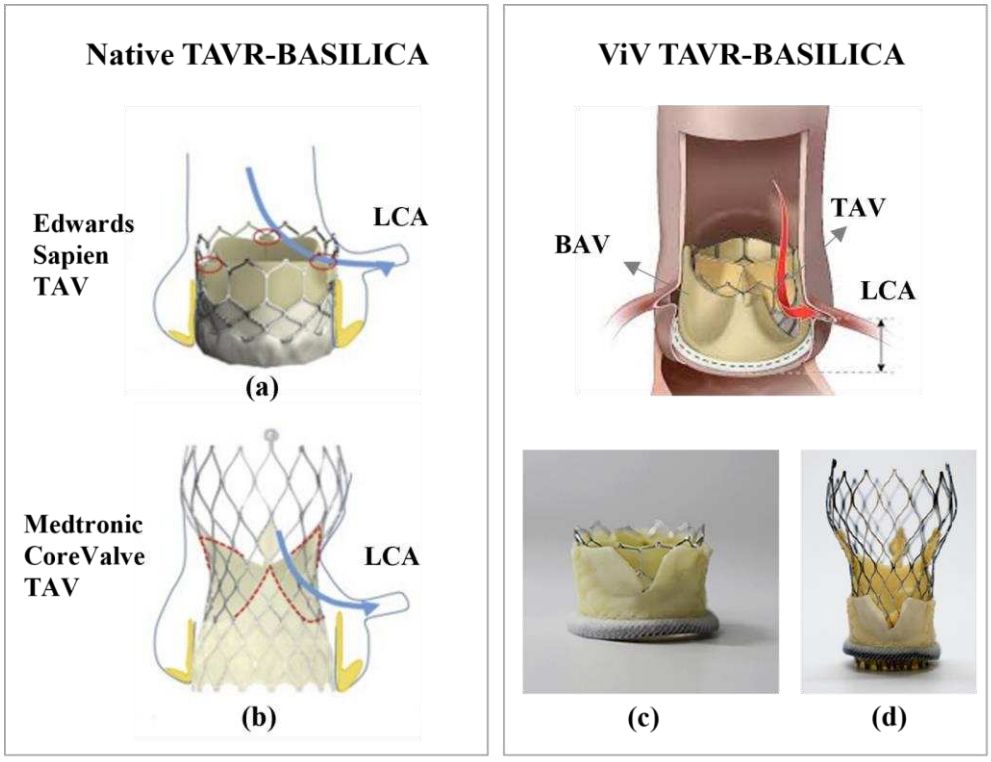

Figure 4.4. Schematic of a native TAVR-BASILICA and a valve-in-valve TAVR-BASILICA: (a) a Edwards Sapien 3 transcatheter aortic valve (TAV) and (b) a Medtronic CoreValve Evolut R TAV replaced in a native aortic valve. (c) A Edwards Sapien 3 TAV and (d) a Medtronic CoreValve Evolut R TAV replaced in a bioprosthetic aortic valve (BAV). Red and blue arrows show the location of the lacerated leaflet (native or bioprosthetic) relative to the left coronary artery (LCA). (a) and (b) are from Krishnaswamy et al., (c) and (d) are from Khodaee et al.

study showed that leaflet laceration can mitigate the risk of thrombosis, while improving washout, with increases in velocity in the sinus and the neosinus by 50% for a Medtronic Evolve ViV, and more than 60% in Edwards SAPIEN 3 ViV[143]. Similarly, a computational study showed that the average blood residence time (BRT) on the leaflets of BASILICA computational model was about 10% less than that in the ViV computational model without leaflet laceration. It has been

hypothesized that thrombus is more likely to form in regions with low flow, which can better support fibrin formation due to low advective transport (or increased BRT)[142,144,145]. Therefore, the BASILICA procedure appears to reduce the risk of leaflet thrombosis in the lacerated leaflets [142]. Additionally, a computational study showed that the hemodynamic outcome of a two-leaflet-lacerated BASILICA model is improved when compared with a one-lacerated BASILICA model and the model without laceration, but no significant difference was observed for additional leaflet laceration (three-leaflet-lacerated model)[141]. Overall, the BASILICA technique is still relatively new and require additional studies to better understand the benefits and when the procedure may be most effective.

4.10 Discussion

As the general population has become older, the prevalence of calcific AS has increased in the recent decades; this has led to extensive research to reveal the complex underlying mechanisms of the valvular calcification, which involves mechanobiology, molecular signals, tissue remodeling, and inflammation, and yet our understanding of this complex process is limited.

Since pharmacotherapy has been ineffective in preventing progression of the calcification, treatment of calcific AS has become narrowed down to surgical and minimally-invasive interventions to repair or replace the native valve; this has led to design and development of artificial valves such as MHVs, BHVs, and TAVs that can mimic the function of the native valve. An immense amount of research has been performed to evaluate the performance of these artificial valves, and to develop better designs that can improve their flaws. Yet, there are undesirable post-interventional outcomes that are related to shortcomings of each valve design.

TAVR has gained favor as procedures and designs have undergone many improvements in recent decades. Despite this, there are still unresolved complications. New procedures aimed at overcoming challenges, like the BASILICA procedure continue to be investigated. Despite precise measurements on a patient's aortic valve anatomy and calcification, calcified lesions continue to complicate TAVR. Other tools like computational modeling have helped surgeons with pre-procedural planning, and with understanding the underlying biomechanics of post-procedural complications. However, these many of these tools continue to be validated. Overall, more studies are required to evaluate the relationships between new procedures and valves with hemodynamics, patient-specific anatomical characteristics, and deployment. This would help surgeons to select patients with suitable characteristics for specific procedures or valves that could improve outcomes.

5. SPECIFIC AIM 3: Predictive factors and clinical outcomes following a native aortic scallop intentional laceration intervention – a case study

5.1 Introduction

More than 400,000 people with aortic valve stenosis had transcatheter aortic valve replacement (TAVR) in the last decade[146]. In TAVR, expansion of a transcatheter aortic valve (TAV) forces calcified native aortic leaflets to permanently open, and in rare cases, this can obstruct the coronary artery. Coronary obstruction during TAVR is a rare and potentially fatal complication that occurs in <1% of the population[122,136]. In efforts to prevent coronary obstruction, the bioprosthetic or native aortic scallop intentional laceration (BASILICA) technique has been developed, in which the leaflet facing a coronary artery is typically lacerated from its base to its outer edge using a catheter and an electrified guidewire [138,139,147,148]. Some computational studies have shown that leaflet laceration is effective in improving the hemodynamics by increasing washout, thereby mitigating some of the risk of thrombosis within the target sinus and neo-sinus [142,143]. Ideally, the BASILICA procedure is expected to free coronary arteries from obstruction by allowing blood to flow through the lacerated leaflet. However, the lacerated leaflet may not always open properly in front of the ostia to allow coronary perfusion. Leaflet material or calcium deposits may displace toward coronary ostia or TAV-related thrombosis may develop and embolize in the coronary arteries, leaving patients with post-procedural complications, despite successful laceration of the leaflets.

The efficacy of the BASILICA procedure remains unclear, in part since this technique is highly specialized and is not a standard of practice at most TAVR sites. High success rates have been reported for post-BASILICA outcomes[95,139], but this is possibly due to the exclusion of high-risk patients for coronary obstruction from the study, as post-BASILICA outcomes are highly

dependent on the patient selection[147]. There are many risks for the procedure including increased risk of hemodynamically unstable severe aortic regurgitation, laceration of the aortic annulus that can lead to annular rupture upon TAVR implant, ventricular perforation that can lead to cardiac tamponade, or laceration of the papillary muscle leading to hemodynamically unstable severe mitral regurgitation (MR). Coronary obstruction also remains a concern even with this procedure. Outcomes may depend on patient-specific anatomy relative to implant placement. During the procedure, calcific leaflets can enter into the coronary ostium, blocking flow. Multicenter data has shown that post-TAVR coronary obstruction (without BASILICA) is associated with anatomical dimensions such as narrow sinus of valsava (SOV), low coronary ostium height, narrow sinotubular junction (STJ) and low sinus height[136]. Overall, more studies are needed to identify which patients may best benefit from the BASILICA procedure.

No study to our knowledge has been performed to identify the role of patient-specific characteristics in post-BASILICA coronary obstruction. Yet, identifying these characteristics, hemodynamics, and anatomical features in relation to post-BASILICA outcomes can provide guidance when picking patients. This is the goal of the current work, which may provide more insight into the BASILICA procedure and may help with procedural planning.

5.2 Methods

5.2.1 Data Collection – The study was approved by Institutional Review Board of the Medical Center of the Rockies, Colorado State University, and Washington University in St. Louis. A total of 12 patients underwent a native TAVR-BASILICA procedure (with exception of one having a TAVR-BASILICA procedure in homograft aortic valve and root). The clinical screening includes (1) computed tomography (CT) examination prior to the procedure to evaluate patients' valve calcification severity and anatomy; (2) echocardiography (ECG) to examine patients' valve

function including left ventricle end-systolic volume (ESV), end-diastolic volume (EDV), stroke volume (SV), ejection fraction (EF), aortic jet velocity and pressure gradients across the aortic valve (AV); and (3) intra-procedural transesophageal echocardiography (TEE) to evaluate post-procedural paravalvular leak (PVL) and coronary obstruction through leaflet material/calcification or thrombosis. Through angiography, calcium is seen as a bright lesion and thrombus is identified with a radio-opaque lesion with multiple layers of irregularities as contrast coats the outside of the thrombus when passing through the vessel.

5.2.2 Assessment of aortic valve morphology and valve selection – All patients in this study had medium sized native valves (18.5-26.6 mm) and were treated with Edwards SAPIEN valves sized either at 23- or 26-mm. ECG-gated CT was used in the peri-interventional evaluation, allowing for objective three-dimensional assessment of anatomical features to assist with device selection. The aortic annulus was assessed in its true plane immediately below the hinge point of the aortic valve cusps. The long and short axis were measured, allowing for the calculation of a mean diameter. Derived mean diameter was used to calculate the annulus area on the basis of the formula for the area of a circle. This is a given limitation as we know true aortic anatomy is not purely circular, therefore accurate sizing and even overexpansion of a TAV in some cases can help mitigate the risk of PVL. Dimensions such as SOV, STJ and annulus diameter were measured in short and long axis views, and the average values were calculated and used in comparisons. The location of anatomical measurements is summarized in Figure 5.1.

Calcium on aortic valve leaflets and on the aortic annulus was scored to obtain information about anatomic details related to PVL predisposition, as severe calcification may impair complete apposition of the sealing skirt on the valve to the native commissures. Additionally, the shape and the location of the calcification were assessed in the left ventricle outflow tract (LVOT) and on the STJ to provide further information for perioperative evaluation that can lead to differences in valve selection, implant height or even prohibition of TAVR procedure entirely. 3D-TEE, using Philips Epic, was utilized intra-procedurally to assist with positioning of guide-catheter placement prior to laceration during the BASILICA procedure. This modality has the added benefit in assessing for real time outcomes or complications including pericardial effusion, valve function, PVL and valvular gradients.

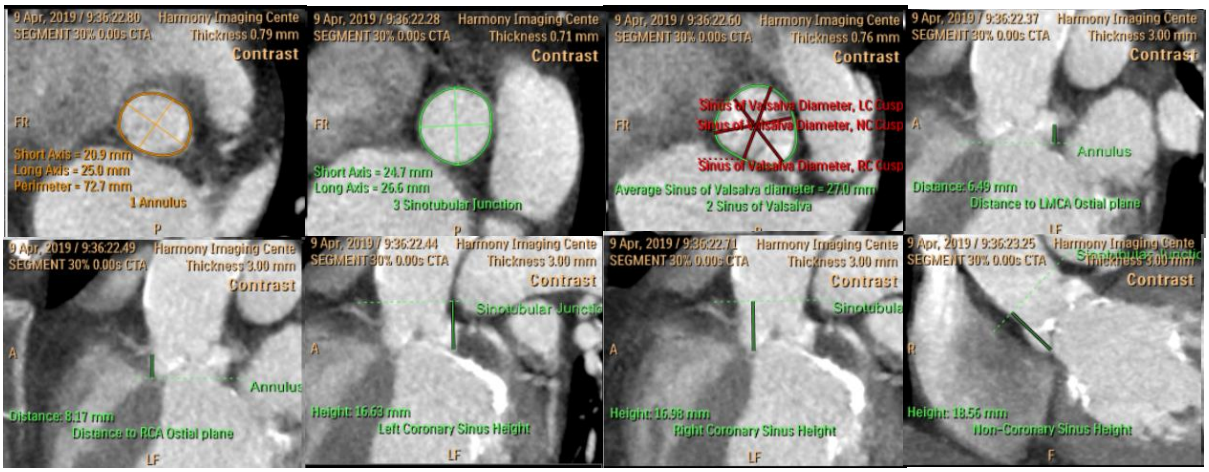

Figure 5.1. The annulus and STJ diameters were measured from long and short axis views. The SOV diameter was measured for each left, right and non-coronary sinus. The coronary height was measured from the annulus plane to the lower level of the left and right coronary ostia opening. The sinus heights were measured from the base of the cusp/leaflet on the annulus plane to the STJ plane.

5.2.3 Implantation technique – Patient selection is primarily based on those patients who have a high risk of coronary artery obstruction from the TAVR implant based on anatomical features. BASILICA is considered in patients where the bottom of the coronary ostium is <10 mm from the annular plane. It is also considered, in cases of "stove-pipe" root features or those that have small

sinuses where the leaflet can reach or cover a significant portion of the coronary ostium. Lastly, long leaflets that could reach the STJ are considered for a BASILICA procedure.

BASILICA procedures are planned in conjunction with a standard TAVR protocol with a few extra steps to lacerate the aortic valve leaflet of interest prior to the TAV implant. It is important to consider the geometrical relationships between the aortic cusp anatomy and the catheters used to engage the critical hinge points in which laceration is to be performed. After careful selection of equipment, attempts are made to engage the base of the aortic cusp utilizing 3D TEE and fluoroscopy. Although catheter selection and technique differ among various centers (ie, guide-in-guide approach), ultimately a catheter is selected that has the best chance of success to engage the targeted aortic leaflet scallop to direct a guidewire across it. This is aimed at a snare that is on the opposite side of the leaflet, which is positioned by crossing the aortic valve with a separate retrograde catheter. Once in position, a 0.014-inch guidewire is traversed through the leaflet scallop while electrically advanced. The tip of this long wire is then snared and externalized from the body, creating a loop from two different entry points into the body. The wire still straddles the punctured leaflet and therefore the scallop is lacerated by pulling both ends of the free wire while simultaneously delivering electricity with short burst of radiofrequency energy. After the equipment is removed, TAVR is performed immediately, especially due to heightened risk of severe aortic regurgitation (AR), which can lead to hemodynamic instability. Typically, position is already gained into the left ventricle for quick access and rapid deployment of the TAV.

Analysis - The average values for patients' general parameters, hemodynamic measures, anatomical features, and calcium scores are compared for groups with and without coronary obstruction. Similar to anatomical features, anatomical aspect ratios can vary in patients; therefore, ratios including sinus width to sinus height, sinus width to annulus width, annulus width to STJ

width, leaflet length to sinus and ostia heights, TAV height to sinus height, and TAV width to annulus width are quantified because differences in anatomy can results in variations in hemodynamics and valve dynamics. Numerical variables are reported as mean ± standard deviation.

5.3 Results

Of 12 patients between age 63 and 89 who underwent the BASILICA procedure for native aortic valve stenosis, 2 female patients had left main coronary obstruction, one possibly due to leaflet material and one possibly due to thrombosis. Summary characteristics of patients with post-BASILICA complications are shown in Table 5.1.

5.3.1 Coronary obstruction – Post-BASILICA coronary obstruction was associated with low post-procedural EDV, ESV, and LVOT stroke volume (SV) (Figure 5.2). Anatomical dimensions including small STJ, low sinus height, low ostia height, small SOV were seen for post-BASILICA coronary obstruction incidence (Figure 5.3). Anatomical ratios including large TAV height to sinus and ostia height ($\frac{H_{TAV}}{H_{Sinus}}, \frac{H_{TAV}}{H_{Ostia}}$), small TAV to annulus diameter ($\frac{D_{TAV}}{D_{Ann}}$), large annulus to STJ diameter ($\frac{D_{Ann}}{D_{STJ}}$), large left leaflet length to left ostia and sinus height ($\frac{L_{L\,leaflet}}{H_{L\,ostia}}, \frac{L_{L\,leaflet}}{H_{sinus}}$) were associated with post-BASILICA coronary obstruction (Figure 5.4). Post-BASILICA coronary obstruction was not linked to more calcification; patients in the coronary obstruction group had mild and moderate leaflet calcification with none to mild annular calcification. Comparisons of the clinical characteristics of patients with and without coronary obstruction are shown in Table 5.2.

5.4 Discussion

Through this work, we found that low-laying coronary ostium, narrow SOV, narrow STJ, and low sinus height are associated with post-BASILICA coronary obstruction. These findings are similar to the Ribeiro et al. study that reports a link between patients' anatomical root dimension and the post-TAVR coronary obstruction[136]. Additionally, through this study, some aortic dimension aspect ratios were found to be associated with post-BASILICA coronary obstruction that are further discussed below.

5.4.1 Effect of patient-specific aortic sinus and ostia anatomy, and TAV height on post-BASILICA coronary obstruction – The anatomy of a patient can affect hemodynamics and sinus washout. If blood stasis occurs, this can lead to the accumulation of coagulation factors, which can lead to thrombosis and coronary obstruction [142,144,149,150]. One feature that can assist washout is the formation of vortices in the aortic sinus during systole. In a narrow sinus, the vortex and the shear layers are not fully formed and dissipate by late systole[151]; this underdeveloped vortex in the narrow sinus causes flow stagnation within the sinus. Our results show a trend toward a narrow sinus in coronary obstruction cases, as demonstrated by SOV parameter. This could be related to the increased risk for thrombosis with a narrow sinus, as reported by Moore. Additionally, low EDV, ESV and LVOT SV (with an average HR of 70 and 75 bpm) can lead to reduced sinus washout and are associated with post-BASILICA coronary obstruction in the current study. Supporting this idea, the in-vitro flow model of Midha et al. shows that low cardiac output

increases the size of stagnation regions in the neo-sinus by more than 4 times without a BASILICA procedure [152].

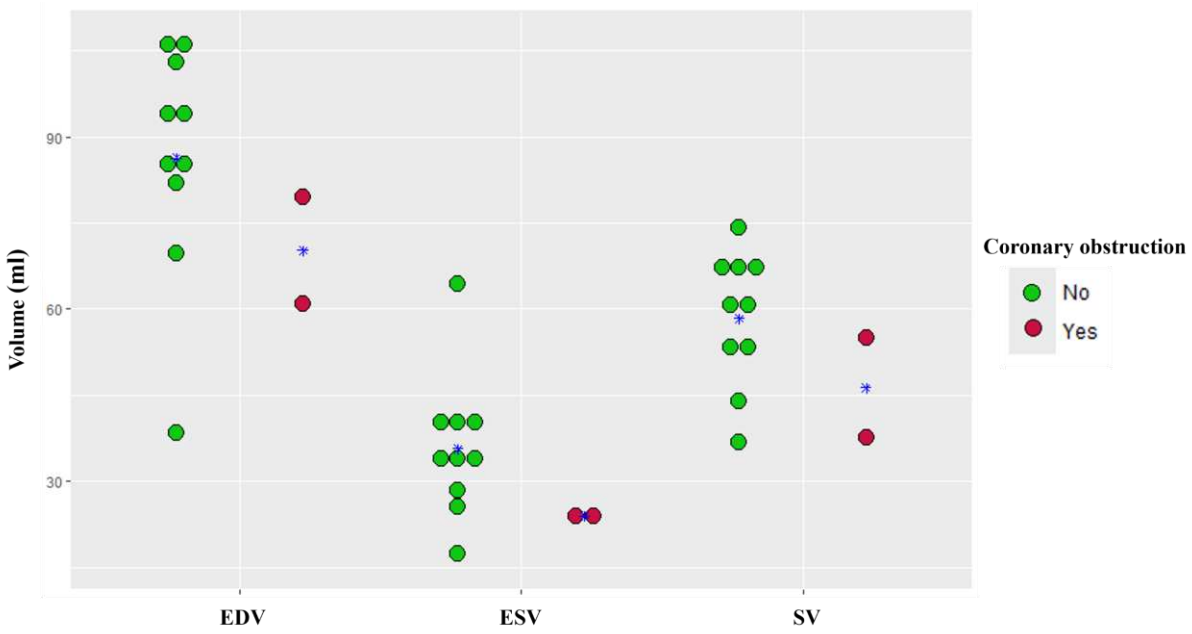

Figure 5.2. Dot plots of end diastolic volume (EDV), end systolic volume (ESV), stroke volume (SV) for the groups with and without coronary obstruction. The blue marker shows the mean in each group.

Short sinus height (<18) and/or low ostia (<10 mm), seen with coronary obstruction in the current study leaves less space for the flow to circulate within the sinus and coronary arteries. Moreover, the large ratio of TAV height to sinus height and ostia height ($\frac{H_{TAV}}{H_{Sinus}}, \frac{H_{TAV}}{H_{Ostia}}$) associated with post-BASILICA coronary obstruction (through thromboembolism/thrombosis) might lead to flow stagnation within the sinus and neo-sinus, since a tall TAV relative to sinus height (considering that the sinus width and STJ in the coronary obstruction group are also narrowed) can prevent a sinus vortex from fully forming and can limit washout[153]. High implantations, i.e. >6 mm, have been shown to increase thrombosis risk through heightened flow stagnation and reduced washout[154]. In a low implantation, neo-sinus thrombus severity increases due to limited flow circulation in this region because a great portion of the TAV leaflet is restricted by the native leaflet[152,155].

On this subject, computational studies have shown that leaflet laceration can mitigate the risk of thrombosis and improve hemodynamics within the target sinus and neo-sinus by allowing more washout and by reducing the blood residence time (BRT) as more blood flows through the coronary arteries[142,143]. However, leaflet laceration success depends on patient-specific aortic root and TAV characteristics, which has not been well-studied yet. In the current study, a patient aortic root-TAV interaction parameter as described by $\frac{H_{TAV}}{H_{Ostia}}$ ratio appears to be a substantial factor in determining the success of the BASILICA procedure. In this regard, Moore et al. showed that the presence of coronary flow can pull the sinus vortex deeper into the sinus[156]. However, we postulate that a low ostium relative to TAV height can lose its interaction with the vortex, considering that

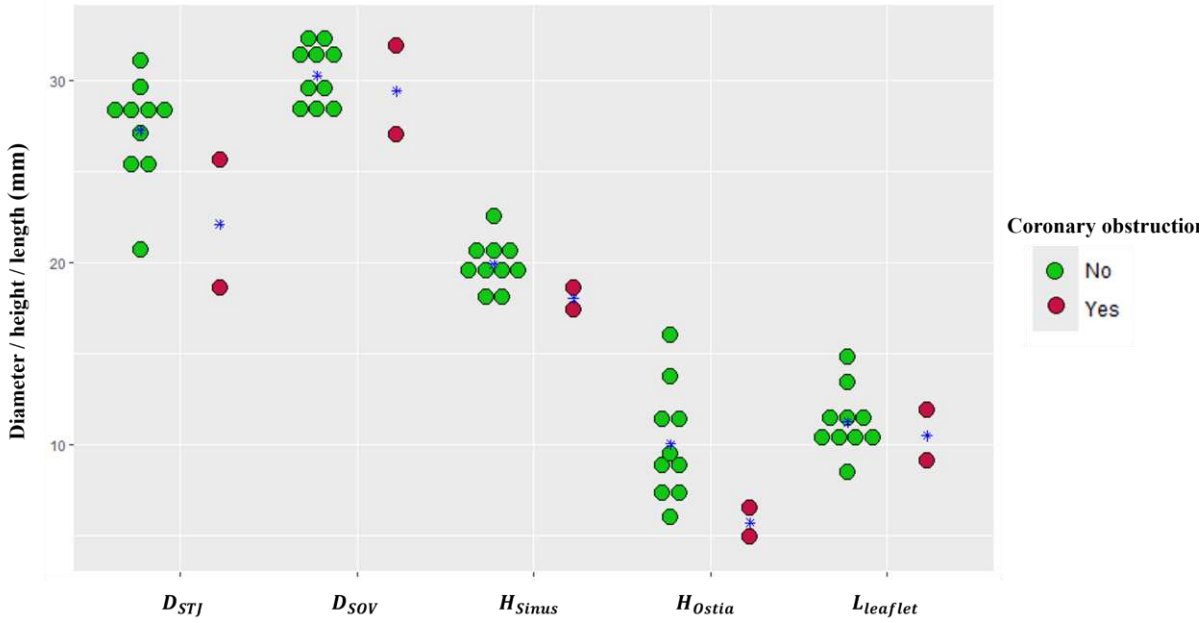

Figure 5.3. Dot plots of sinotubular junction (STJ) diameter, sinus of valsava (SOV) diameter, sinus height, left coronary ostia height, left leaflet length for the groups with and without coronary obstruction. The blue marker shows the mean in each group.

the flow circulation through the sinus might be reduced due to other factors associated with coronary obstruction such as low flow, and narrow sinus and STJ. Therefore, with a high $\frac{H_{TAV}}{H_{Ostia}}$ ratio (a TAV height more than 3 times longer than the ostia height), the native leaflet laceration

may not be as effective in improving flow circulation in the sinus. This state is seen in one patient of the study with post-BASILICA coronary obstruction due to thrombosis.

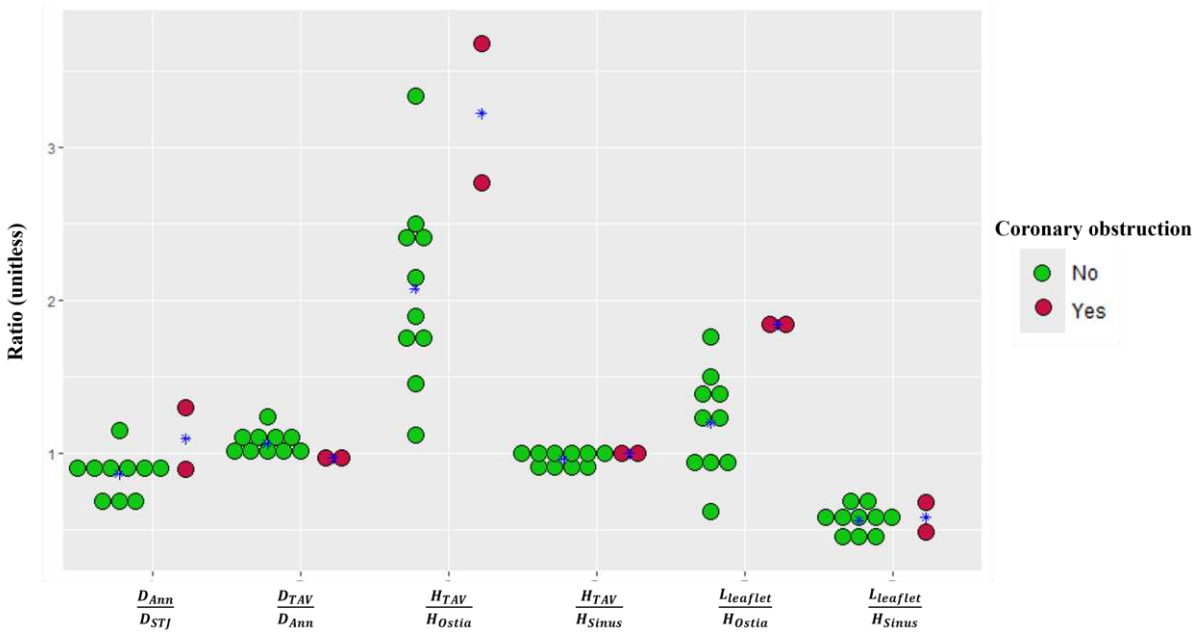

Figure 5.4. Dot plots of anatomical ratios including annulus diameter to sinotubular junction diameter, transcatheter aortic valve diameter to annulus diameter, transcatheter aortic valve height to sinus and ostia height, left leaflet length to left ostia and sinus height for the groups with and without coronary obstruction. The blue marker shows the mean in each group. D- diameter, H- heigh, L- length, Ann- annulus, STJ-sinotubular junction, TAV-transcatheter aortic valve.

A computational study showed that the sinus hemodynamics (washout) of a two-leaflet-lacerated BASILICA model is improved when compared with a one-lacerated BASILICA model and the model without laceration, but no significant difference was observed for additional laceration[141]. Although these studies show improved sinus washout, it is unknown how leaflet laceration relative to patient aortic root-TAV interaction affects the left coronary obstruction.

5.4.2 Effect of patient-specific aortic leaflet anatomy on post-BASILICA coronary obstruction – Despite the smaller average left native leaflet length in the coronary obstruction group, the ratios of left leaflet length to left ostia height and sinus height ($\frac{L_{L\ leaflet}}{H_{L\ ostia}}$, $\frac{L_{L\ leaflet}}{H_{sinus}}$) were larger in the patient with coronary obstruction due to thrombosis when compared to the control

group; this may support post-BASILICA coronary obstruction, because the closer the leaflet tip is to the STJ than the annulus, the less blood can circulate through the sinus and coronary arteries. Furthermore, the lacerated native leaflet may become extended and occupy more space in the narrow sinus of the coronary obstruction group. This adversely affects the vortex formation in the sinus, which may lead to a rise in the BRT and thrombus formation within the sinus region[149]. Additionally, in an extended lacerated native leaflet, leaflet material and/or calcium deposits may unfavorably displace and obstruct the coronary artery. Our proposed parameters are supported by a similar study that introduced the ratio of leaflet length to curved coronary sinus height (L/C >1) as a novel predictor of post-TAVR coronary obstruction[157]. However, in the current study, the curved coronary sinus height measurement was not available; therefore, we used sinus and ostia heights for comparisons.

5.4.3 Effect of patient-specific aortic annulus, sinotubular junction anatomy and TAV size on post-BASILICA coronary obstruction – In this study, the TAV was slightly undersized and possibly overexpanded in the coronary obstruction group, while for most patients in the control group oversized TAVs were selected (Table 5.3). The ratio of TAV to annulus diameter ($\frac{D_{TAV}}{D_{Ann}}$) <1 linked to post-BASILICA coronary obstruction could be explained with overexpansion of the TAV increasing the risk of flow stagnation in the neo-sinus due to reduced leaflet motion in the neo-

sinus [152,155]. In contrast, a slight (10%) underexpansion (oversizing) of the TAV reduces the tension

Table 5.1. Summary characteristics of all patients in the BASILICA procedure.

Clinical	
Age (years)	78 (63-89)
Male	4
Female	8
Weight (kg)	77.8 (45.3-116.6)
Height (m)	1.6 (1.4-1.7)
HR	76 (56-96)
BSA (m2)	1.8 (1.3-2.1)
Hemodynamics	
EDV (ml)	83 (38-106)
ESV (ml)	33 (17-64)
LVOT SV (ml)	56 (36-74)
EF (%)	60 (36-70)
Max AV velocity (m/s)	2.24 (1.69-2.65)
Mean AV velocity (m/s)	1.58 (1.31-1.95)
AV VTI (cm)	47 (29-68)
Peak AV pressure gradient (mmHg)	20 (11-28)
Mean AV pressure gradient (mmHg)	11 (3 -17)
Anatomy	
Annulus Area (cm2)	4.3 (3.4-5.4)
LVOT Area (cm2)	4.3 (3.6-5.5)
Annulus Diameter (mm)	23.4 (18.5-26.8)
Average SOV diameter (mm)	30.1 (27-32.4)
Right SOV	29.8 (25.8-33)
Left SOV	30.7 (27.3-34.2)
Non SOV	29.8 (26.8-32.9)
STJ Diameter (mm)	26 (18.6-31.1)
Sinus height (mm)	19.7 (17.4-22.5)
LM height (mm)	9.3 (4.9-14.8)
RCA height (mm)	13 (8.2-16.3)
Right leaflet length (mm)	11.3 (9-13.4)
Left leaflet length (mm)	11.2 (9.1-13.4)
Calcification	
Leaflet Calcification Score (Agatston score)	1908 (0*-5671)
Leaflet Calcification	None: 1 Mild: 4 Moderate: 4 Severe: 3

Annular Calcification		*None: 4* *Mild: 6* *Moderate: 2*
LCA calcification		7
RCA calcification		3
Edwards SAPIEN 3 valve size (mm)		
	23 mm	6
	26 mm	6
Outcomes		
LM coronary obstruction		2
PVL		8

Abbreviations: HR- heart rate, BSA- body surface area, EDV- end diastolic volume, ESV- end systolic volume, SV- stroke volume, LVOT- left ventricle outflow tract, EF- ejection fraction, AV- aortic valve, VTI-velocity time integral, SOV- sinus of valsava, STJ- sinotubular junction, LM- left main, LCA- left coronary artery, RCA- right coronary artery, PVL-paravalvular leak

* One patient had a TAV in Homograft operation, therefore there was no calcium lesions on the aortic root and leaflets

in the TAV leaflets, therefore systolic opening motion of the leaflets can push more flow out of the neo-sinus and improve flow dynamics in this region. Drastic underexpansion (25%) yields a higher pressure gradient and narrower effective orifice area (higher velocity), resulting in a jet of blood that raises concerns as this hemodynamic condition can adversely affect blood[158]; and TAV leaflets can fold during the opening creating large regions with stagnant flow that support thrombosis. Therefore, a slight (10%) valve underdeployment has been recommended, as it can improve neo-sinus washout with minimal increase in pressure gradients and velocity[155].

In the coronary obstruction group, the average STJ diameter was narrower, but the annulus to STJ diameter ratio ($\frac{D_{Ann}}{D_{STJ}} > 1$) was larger indicating that flow coming through the relatively large annulus is obstructed by a small STJ; this may further facilitate flow stagnation within the sinuses that laceration may not be able to mitigate; the flow trapped within the aortic sinuses may

also push the native leaflet toward coronary artery and physically obstruct it. Whereas $\frac{D_{Ann}}{D_{STJ}} < 1$ in the control group suggests a more balanced flow circulation in and out of the aortic root and

Table 5.2. Comparison of the clinical characteristics of patients with and without coronary obstruction

General	***No Coronary obstruction (10)***	***Coronary obstruction (2)***
Age (years)	79 ± 6	73 ± 14
Male	4	0
Female	6	2
Weight (kg)	72.3 ± 19	105.4 ± 15.7
Height (m)	1.6 ± 0.08	1.5 ± 0.05
BSA (m2)	1.7 ± 0.28	2.03 ± 0.16
Hemodynamic		
EDV (ml)	86.4 ± 20	70.2 ± 13
ESV (ml)	35.7 ± 12	23.95 ± 0.9
LVOT SV (ml)	76.7 ± 20	62.5 ± 9.1
EF (%)	59 ± 9.3	65 ± 5.1
Peak AV velocity (m/s)	2.22 ± 0.29	2.38 ± 0.37
Mean AV velocity (m/s)	1.58 ± 0.22	1.61 ± 0.06
AV VTI (cm)	47.3 ± 11	50.3 ± 20
Peak AV pressure gradient (mmHg)	20.1 ± 5.3	23 ± 7
Mean AV pressure gradient (mmHg)	10.6 ± 4.1	12 ± 1.4
Anatomy		
Annulus Area (cm2)	4.27 ± 0.63	4.43 ± 0.2
LVOT Area (cm2)	4.39 ± 0.7	4.27 ± 0.02
Annulus Diameter (mm)	23.4 ± 2.4	23.6 ± 0.8
Average SOV diameter (mm)	30.3 ± 1.6	29.4 ± 3.4
Right SOV	29.8 ± 1.8	29.4 ± 4.2
Left SOV	30.9 ± 1.7	29.5 ± 3.1
Non SOV	29.9 ± 2.4	29.4 ± 2.8
STJ Diameter (mm)	27.2 ± 2.8	22.1 ± 4.9
Sinus height (mm)	20 ± 1.31	18 ± 0.84
LM height (mm)	10.3 ± 3.1	5.7 ± 1.1
RCA height (mm)	13.7 ± 2.06	9.15 ± 1.34
Right leaflet length (mm)	11.04 ± 1.79	10.5 ± 0.56
Left leaflet length (mm)	11.03 ± 1.42	10.5 ± 1.97

Ratio factors		
$\frac{D_{Ann}}{D_{STJ}}$	0.86 ± 0.13	1.1 ± 0.27
$\frac{L_{leaflet}}{H_{Sinus}}$	0.56 ± 0.08	0.58 ± 0.13
$\frac{L_{leaflet}}{H_{Ostia}}$	1.2 ± 0.33	1.84 ± 0.01
$\frac{H_{TAV}}{H_{Sinus}}$	0.96 ± 0.05	1.0 ± 0.04
$\frac{H_{TAV}}{H_{Ostia}}$	2.07 ± 0.62	3.22 ± 0.63
$\frac{D_{TAV}}{D_{Ann}}$	1.06 ± 0.08	0.97 ± 0.02
$\frac{D_{TAV}}{D_{STJ}}$	0.91 ± 0.09	1.06 ± 0.23
Calcification		
Leaflet Calcification Score (Agatston score)	2056 ± 1673	1165 ± 54
Leaflet Calcification		
None	1	0
Mild	3	1
Moderate	3	1
Severe	3	0
Annular Calcification		
None	3	1
Mild	5	1
Moderate	2	0

Abbreviations: HR- heart rate, BSA- body surface area, EDV- end diastolic volume, ESV- end systolic volume, SV- stroke volume, LVOT- left ventricle outflow tract, EF- ejection fraction, AV- aortic valve, VTI-velocity time integral, SOV- sinus of valsava, STJ- sinotubular junction, LM- left main, RCA- right coronary artery, TAV- transcatheter aortic valve, Ann- annulus, D- diameter, H- height, L- length

sinuses. Although the data reported in Ribeiro et al. confirms this finding, the importance, and the effect of small STJ on sinus hemodynamics has not been thoroughly studied in the literature.

5.4.4 Aortic valve calcification and post-BASILICA coronary obstruction – Similar to the Ribeiro et al. study the degree of valve calcification was not a predictor of post-BASILICA

coronary obstruction incidence suggesting that hemodynamic and anatomical factors play a more significant role in post-BASILICA coronary obstruction than calcification.

5.5 Limitation

The available data for this study was limited because BASILICA intervention is a relatively new technique. Still, TAVR without a BASILICA procedure is the standard practice for treatment of aortic stenosis in many medical centers and hospitals. Further post-BASILICA coronary obstruction is very rare Due to these complications, the collected patient data was relatively small with only 2 cases in the coronary obstruction group, which limited our ability in applying a reasonable statistical analysis. Because previous studies stated that female anatomy is not an independent predictor of coronary obstruction[135,137], and we have a small and uneven number of observation for male and female patients, the sex-rated differences were not investigated.

The current work does not account for patient-specific blood, which can impact the risk for coronary obstruction through thrombosis. The data on TAV implantation depth and its angle relative to the aortic annulus was unavailable, limiting our ability to evaluate outcomes relative to these parameters. The usual limitations on imaging with CT scans include scan quality and resolution depending on the specific slice depth of the CT scanner, motion artifact, and arrhythmias. Limitations with 3D-TEE imaging include visualization of the valve and shadowing artifacts with severe calcification, which may limit a surgeon's ability to assess a patient's condition. Limitations specific to the procedure include patient selection bias, as these patients are all high-risk for coronary obstruction even without BASILICA. Also, the aortic root anatomy can limit favorable angulation of the guide catheter to slice at the desired location in the deep base of the scallop. There is very limited literature available on post-BASILICA outcomes. To draw conclusions about the underlying mechanisms of post-BASILICA coronary obstruction in relation

to predictors, we had to investigate the TAVR-related causes and consequences that may not accurately represent the BASILICA outcome because BASILICA changes the hemodynamics considerably.

Table 5.3. Edwards SAPIEN 3 transcatheter aortic valve diameter compared with aortic valve diameter for groups with and without coronary obstruction

	TAV Diameter (mm)	***Annulus Diameter (mm)***
with coronary obstruction	23	23.2
	23	24.2
without coronary obstruction	26	23
	26	22.8
	23	22.7
	26	26.6
	26	24.4
	26	24.2
	23	18.5
	23	23.8
	26	26.8
	23	20.8

Abbreviations: TAV- transcatheter aortic valve

5.6 Conclusion

The present study is the first to provide an understating of the link between patient-specific characteristics and the post-BASILICA coronary obstruction. The outcomes of our study were evaluated relative to the left main coronary artery and left main obstruction, as only the left leaflet was lacerated. Coronary obstruction is a multivariate process involving patient-specific aortic valve anatomy, blood, aortic valve function, TAV-aortic root interaction, complex flow patterns and blood-flow interactions. The coronary obstruction following a BASILICA procedure was

associated with low left ventricle EDV, low ESV, low LVOT SV, narrow STJ, low sinus height, low ostia height, large $\frac{H_{TAV}}{H_{Sinus}}$, $\frac{H_{TAV}}{H_{Ostia}}$, small $\frac{D_{TAV}}{D_{Ann}}$, large $\frac{D_{Ann}}{D_{STJ}}$, and large $\frac{L_{L\,leaflet}}{H_{L\,ostia}}$, $\frac{L_{L\,leaflet}}{H_{sinus}}$.

Since BASILICA is an extension of the TAVR procedure, some TAVR-related causes and consequences leading to coronary obstruction may also be relevant to BASILICA results. Some studies have shown that specific-patient characteristics can be used as predictors for coronary obstruction following a TAVR, but it was not clear whether these characteristics are linked to coronary obstruction following a BASILICA procedure. Very limited studies have been performed on the mechanisms of this new technique so far and still we do not have much clarity on how patient-specific characteristics can impact the BASILICA outcomes.

The importance and effect of anatomical aspect ratios on sinus hemodynamics have not been well-researched. We characterized anatomical aspect ratios in addition to direct anatomical dimensions of the patient's aortic root because aspect ratios can provide more details about patient's aortic root environment and eliminate the size dependency of the dimensions that appears in the data due to gender and age variations. In addition, the effect of leaflet laceration relative to patient-specific anatomy and TAV-aortic root interactions is a new topic and so many aspects of it are unknown that require more investigation. Larger multi-center patient populations, experimental and computational studies are needed to confirm the results of this study and to define cut off values that can be used for patient selection and procedural planning.

6. CONCLUSION

Aim 1 – Despite limited spatial resolution in the ultrasound images of small fetal hearts, we were able to accurately process images and obtain geometric boundaries. Our CFD simulations provided detailed insight into the patient-specific hemodynamics of HLHS. Numerous animal studies have shown that prenatal hemodynamic forces play an important role in development of the cardiovascular structures. However, the full flow field of many CHDs were undefined in humans, despite the potential role in remodeling of the fetal heart. We provided detailed quantitative flow patterns for HLHS, which has the potential to guide future prevention and therapeutic interventions, while more immediately providing additional functional detail to cardiologists to aid in decision making.

Aim 2 – Calcific aortic stenosis is a progressive disease that has become more prevalent in recent decades. Despite advances in pharmacotherapies, and research to uncover underlying biomechanisms, and development of new generations of prosthetic valves and replacement techniques, management of calcific aortic stenosis still comes with unresolved complications. We highlighted underlying molecular mechanisms of acquired aortic stenosis calcification in relation to hemodynamics, complications related to the disease, diagnostic methods, and evolving treatment practices for calcific aortic stenosis. TAVR has become the standard of care due to its favorable clinical outcomes, however it still comes with some complications, e.g. coronary obstruction is a rare fatal complication that occurs following a TAVR procedure, which may be eliminated using BASILICA procedure.

Aim 3 – Despite precise measurements on a patient's aortic valve anatomy and calcification, calcified lesions and native leaflet material continue to complicate TAVR-BASILICA. We provided predictive factors based on anatomical measurements and ratios of patient's aortic root

and valve, that are associated with post-BASILICA coronary obstruction. Although BASILICA procedure is reported to be effective in preventing coronary obstruction, the presence of multiple predictors in a patient might be too unfavorable that would make the laceration of the leaflet ineffective. The proposed predictors can further be used to create a non-dimensional parameter for surgeons to be able to predict the coronary obstruction during procedural planning. This would provide insight into the patient-specific outcome, which may help surgeons to select patients with suitable characteristics for specific procedures or valves that could improve the outcomes. The anatomical rations $\frac{H_{TAV}}{H_{Ostia}}$ and $\frac{L_{leaflet}}{H_{Ostia}}$ are considerably different between the groups and their increasing value is associated with the coronary obstruction group, similarly a large $\frac{D_{Ann}}{D_{STJ}}$ ratio and

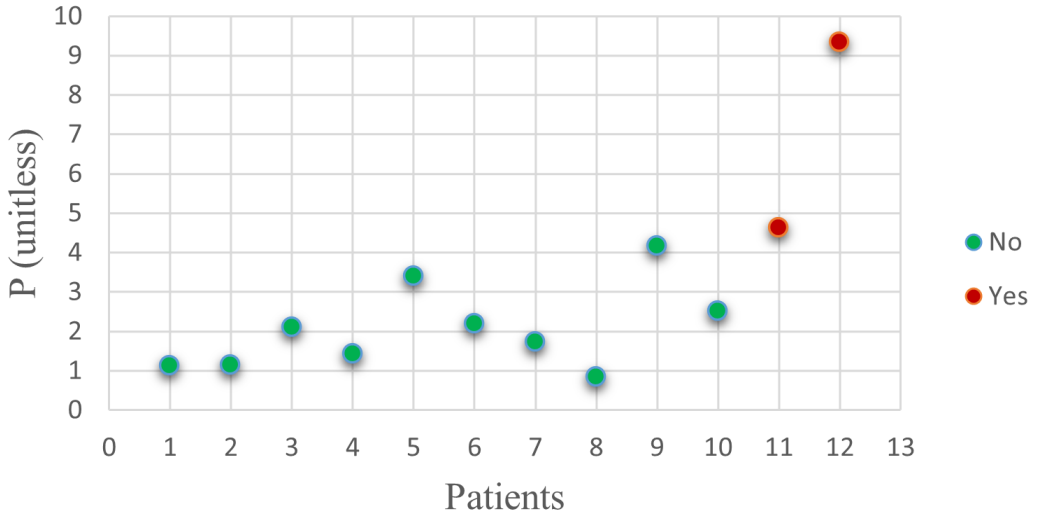

Figure 6.1. Non-dimensional parameter P can be used as a single predictor to distinguish which patients are likely to have post-BASILICA coronary obstruction. The red circle shows the patients with post-BASILICA coronary obstruction.

a small $\frac{D_{TAV}}{D_{Ann}}$ ratio were shown to be contributors to the coronary obstruction following a BASILICA procedure (as seen in Figure 5.4). Therefore a non-dimensional parameter as described by $P = \frac{\frac{D_{Ann}}{D_{STJ}} \times \frac{H_{TAV}}{H_{Ostia}} \times \frac{L_{leaflet}}{H_{Ostia}}}{\frac{D_{TAV}}{D_{Ann}}}$ can successfully distinguish which patients are likely to have coronary

obstruction following a BASILICA procedure based on their anatomical features. The non-dimensional parameter P > 4.5 is seen for the patients with coronary obstruction in this study. The non-dimensional parameter P is plotted for all patients; the red data points show the patients who had post-BASILICA coronary obstruction (Figure 6.1.)

Additionally, using Buckingham Pi theorem approach, we normalized the anatomical ratios by the annulus diameter and plotted the normalized features relative to the Reynolds number (Figure 6.2). Reynold number is a non-dimensional parameter with a wide range of applications, and it can predict flow patterns and behavior. The Reynolds number is defined as $Re = \frac{4\rho CO}{\pi D_{Ann}\mu}$, where ρ is the density of the fluid, CO is the cardiac output, D_{Ann} is the annulus diameter as a characteristic dimension, and μ is the dynamic viscosity of the fluid. Reynolds number can quantify the flow behavior relative to inertial and viscous forces. A low Reynolds number in addition to patient's unfavorable anatomical features may further contribute to coronary obstruction.

In this study pre-intervention velocity and cardiac output were not available for all cases, therefore Reynolds numbers were calculated based on the post-intervention data. Due to this limitation, this comparison may not be helpful in predicting post-BASILICA outcome. Further studies with a complete patient dataset before intervention are needed to investigate and propose a predictive parameter relative to Reynold number and anatomical features that can be used by surgeons to identify the outcome of the intervention for each patient.

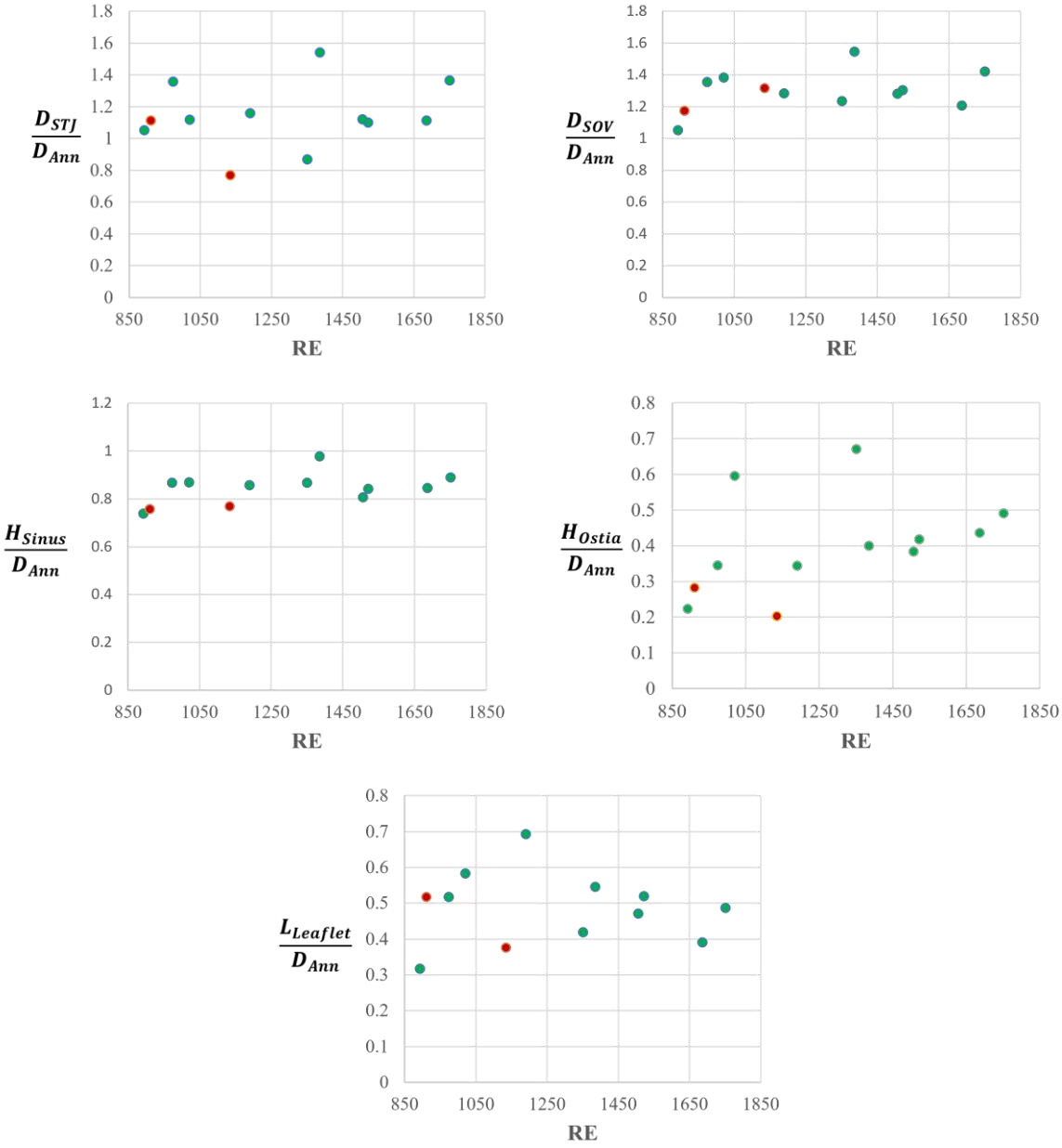

Figure 6.2. Plots of normalized anatomical dimensions relative to Reynolds numbers for all patients. The green and red data points correspond to normal cases and patients with post-BASILICA coronary obstruction, respectively. D- diameter, H- heigh, L- length, Ann- annulus, STJ-sinotubular junction, ostia- left coronary ostia, leaflet- left leaflet.

7. FUTURE WORK

7.1 Hypoplastic left heart syndrome (HLHS)

Accurate assessment of cardiac function requires novel tools and techniques to eliminate the errors in measurements and modeling. The future direction for this research is to eliminate some of the limitations of the current study by applying a robust technique that uses a pairwise image registration approach to provide a more accurate spatio-temporal model for myocardial motion from the ultrasound image[4] (Figure 7.1). This technique can reduce motion estimation error caused by noise that appears in the ultrasound data due to movement of the fetus or shadowing

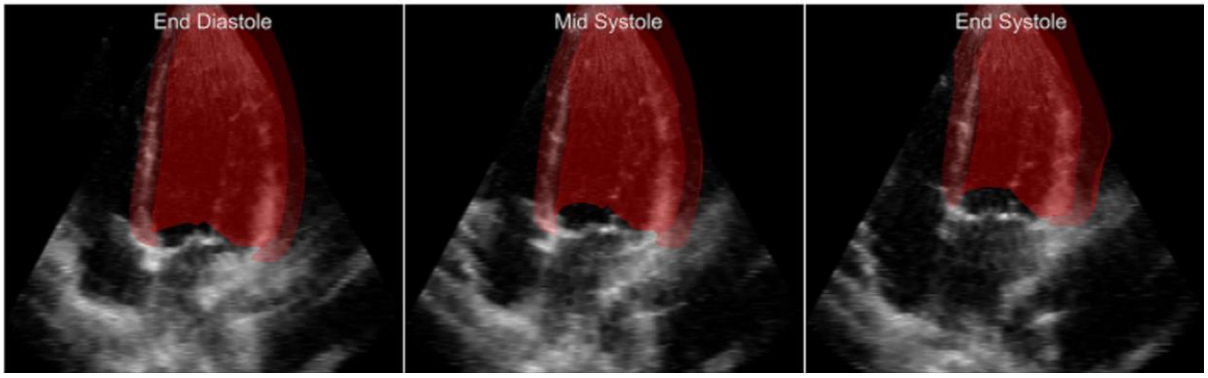

Figure 7.1. Example of a spatio-temporal model for myocardial motion from the ultrasound image[4] during systole and diastole.

from fetal bones. Additionally, applying a lumped parameter model is crucial to realistically model the afterload and the diseased condition in the fetal heart that would provide deeper insight into the disease. Since HLHS is a very rare disease, the data that can be collected from one medical center is limited. A multicenter study can be helpful in collecting a large sample size that would qualify for an accurate statistical analysis, that would provide more information about the trends and patterns in the HLHS disease.

7.2 Computational modeling of BASILICA

A few computational studies have shown that BASILICA intervention can improve hemodynamics within the sinus and neo-sinus. These studies have used an ideal aortic valve geometry; thus, the effect of patient-specific aortic valve geometry on the success of this novel interventional technique has not been well researched. In this dissertation, a computational model was partially developed to investigate the outcome of the BASILICA procedure relative to the patient-specific aortic root geometry and TAV-aortic root interaction.

7.2.1 TAV Modeling

A 26 mm Edwards SAPIEN 3 model was designed in SolidWorks 2020 to mimic the TAVs that were implanted in our clinical cases. An Edwards SAPIEN valve has 4 main components: stent, inner skirt, outer skirt, and leaflets. Since the exact dimensions were unknown, the sketch

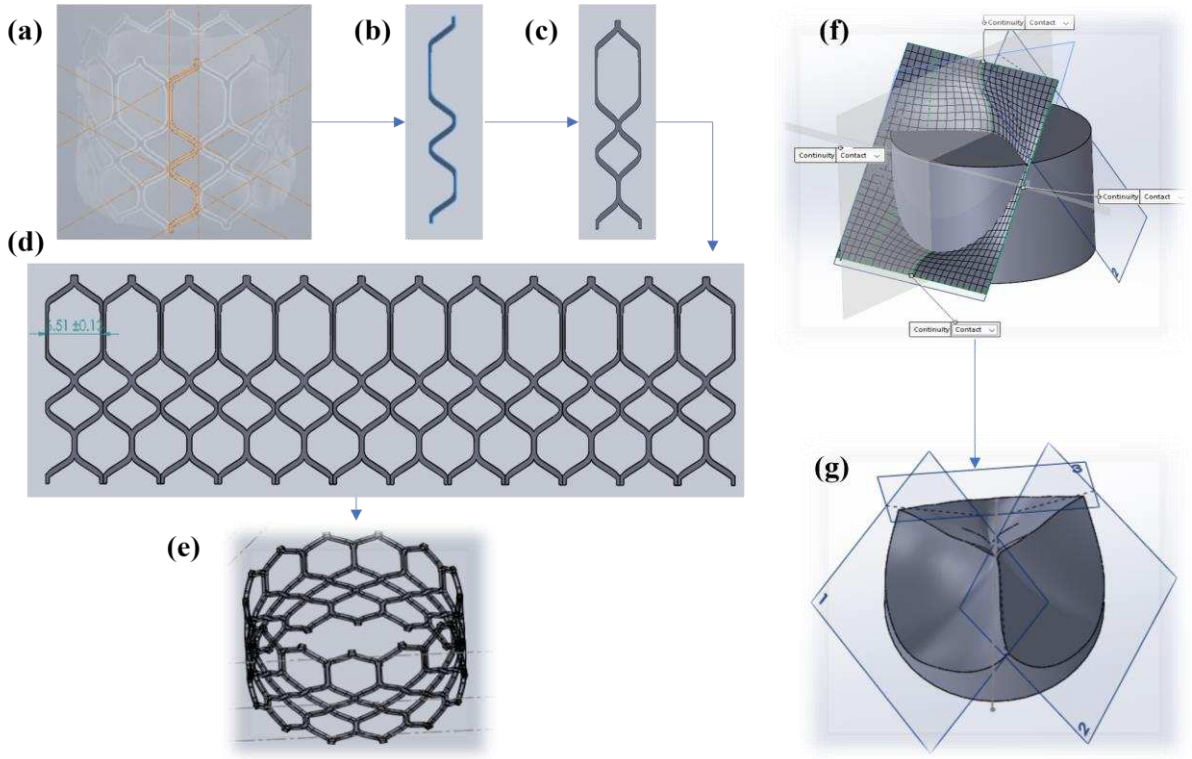

Figure 7.2. Steps for designing a TAV in SolidWorks: (a) create a sketch from picture, (b) extrude the sketch, (c) mirror the extruded structure to create one stent unit, (d) copy the unit 12 times to create a flat stent, (e) bend the flat model 360-degrees to create the final model of the stent. (f) create a curved surface to cut the cylinder with, (g) rotate the surface 120-degree from the previous surface to create all three leaflets.

for the stent, inner and outer skirts were created from the picture of the TAV that was taken from the manufacturing website. The leaflet's profile was created by slicing a 20-mm-long-cylinder using a curved surface that was positioned in 120-degree angle from the previous surface to create all three leaflets. The reconstructed steps for the stent and the leaflets are shown in Figure 7.2.

7.2.2 TAV Assembly

As seen in Figure 7.2, the final geometry does not include the bridge where skirts and leaflets are being sutured to the stent. For simplicity of the modeling, the stent was modeled as a one-piece structure. All components were being assembled in SolidWorks Assembly to create the final geometry of the Edwards SAPIEN 3 (Figure 7.3).

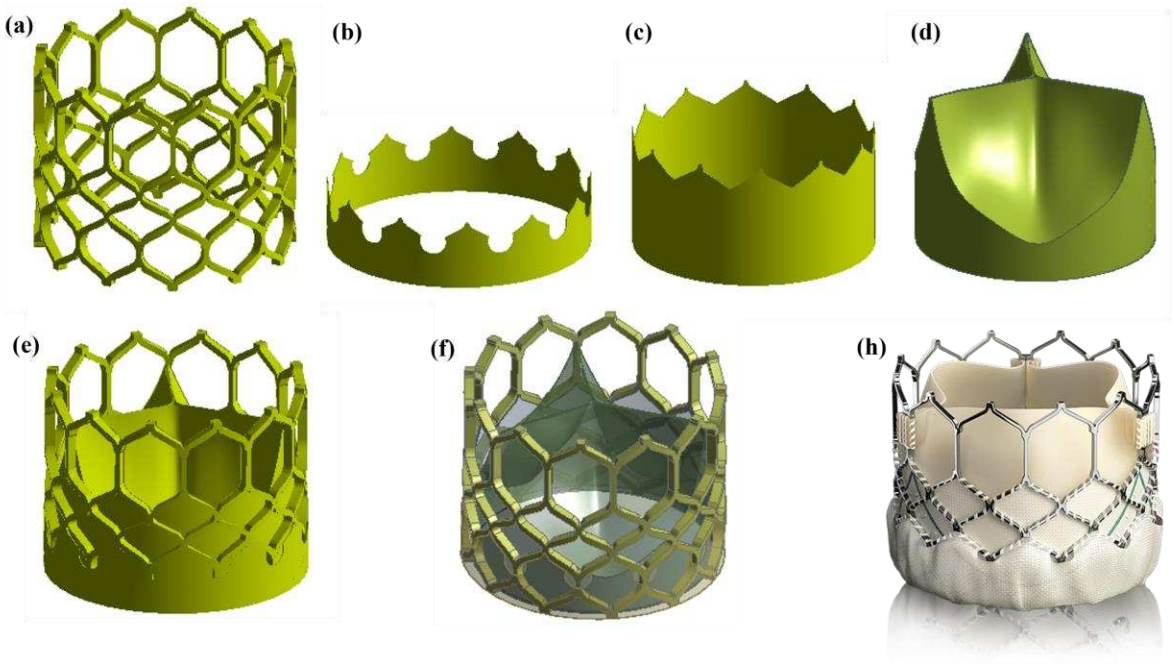

Figure 7.3. All the TAV components modeled and assembled in SolidWorks: (a) stent, (b,c) inner and outer skirts, (d) leaflets in the closed position. (e) a complete TAV assembly and (f) a transparent TAV modeled from (h) the Edwards SAPIEN 3 valve (in open position).

7.2.3 TAV Crimping

To deploy a TAV inside the patient-specific aortic root, the TAV must be crimped. The assembled geometry was then imported in ANSYS to be prepared for crimping. All components in the modeled TAV were discretized using a hexahedron and a tetrahedron methods. The target mesh element size for the stent, inner and outer skirts was 0.5 mm, and for leaflets was 0.2 mm, to capture the complex folding motion of the leaflets during crimping (Figure 7.4 a).

An Edwards SAPIEN 3 valve is made of a stainless-steel stent, polyethylene terephthalate (PET) skirts, and bovine pericardium leaflets. The stainless steel stent was modeled with ρ= 7760 kg/m^3, E= 193 GPa, σy = 340 MPa, σ_U = 670 MPa, υ=0.29[1]. The bioprosthetic leaflets were modeled using a hyperplastic material model (Ogden, 3rd degree)[1]. The skirts were modeled using the default polyethylene material setup in ANSYS Static Structural. All components have bonded

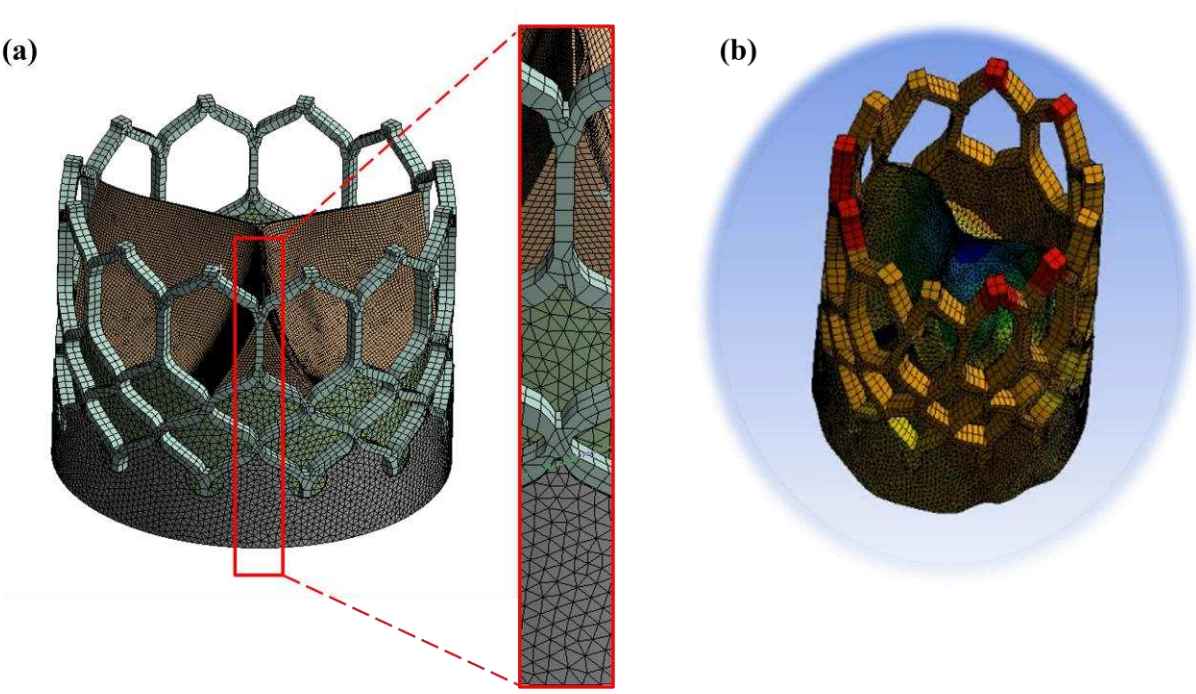

Figure 7.4. (a) Meshed model of the TAV with a detailed view at the location shared between the two stent units, (b) crimped model of the TAV.

contacts. A displacement boundary condition is assigned to circular surface of each component to model the crimped valve (Figure 7.4 b).

7.2.4 Patient Aortic Root and Native Leaflet Modeling

Patient's aortic root anatomy was automatically segmented from the CT scans using a threshold technique and a snake algorithm in ITK-SNAP 3.8. The threshold technique uses Hounsfield unit filtration to highlight the borders of the aortic root in the region of interest. The snake algorithm segments the borders using parameters that control propagation and curvature forces. Aortic valve leaflets in the CT scans have clear boundaries (Figure 7.5 a) but due to limitation of the technique, leaflets cannot be properly segmented using the same automated technique. Therefore, to obtain an accurate model, aortic leaflets were manually segmented. Reconstructed geometries were then processed in Geomagic software to get a smooth surface and clear boundaries for the ANSYS simulation. Aortic root and leaflet models were then assembled in SolidWorks to create the final patient-specific model (Figure 7.5 b)

7.2.5 TAV Deployment

Future work for this study includes a TAV deployment inside a patient-specific aortic root geometry and modeling BASILICA procedure which is relatively a complex computational simulation that requires a fluid-structure interaction (FSI) setup. The initial step of the deployment was performed by taking the crimped TAV model inside the root and between the leaflets (Figure 7.5 c. To expand the crimped TAV, proper material, contacts and boundary conditions need to be defined for all components in the TAV and native leaflets.

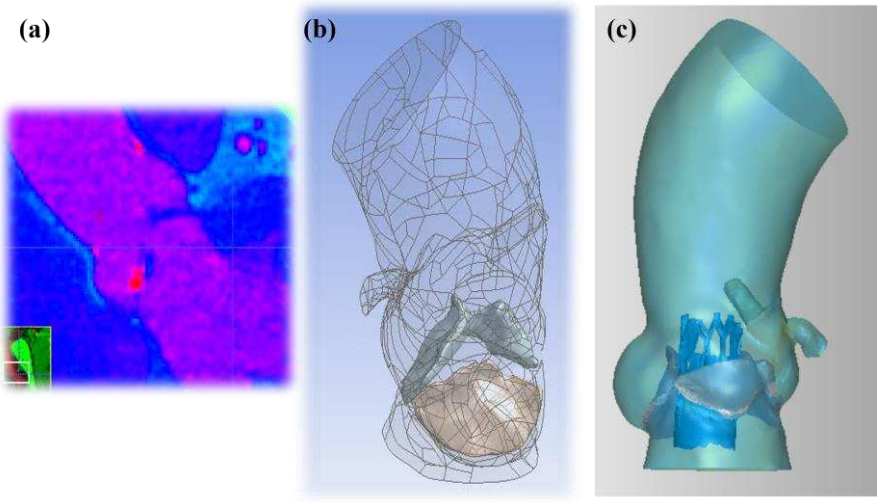

Figure 7.5. (a) Raw CT image in DICOM format showing a clear contrast that separates the aortic root and the leaflets from the unwanted area, (b) 3D reconstructed model of the aortic root and the leaflets, (c) TAV placement inside the aortic root for deployment.

Coronary obstruction following a BASILICA procedure is a multi-factorial process. A FSI simulation is crucial for realistic modeling of blood flow in the aortic root of the patients who have BASILICA procedure. Flow stagnation is an important factor in this simulation, which can be quantified by a parameter known as blood/particle residence time measured using a Lagrangian particle tracking method. In this approach, the spatial position of the particles that are released in the flow are traced to identify how long each particle stays in the domain[159]. Long particle residence time in the sinus domain is reported to be linked to higher risk of thrombus formation within the sinus. Flow stagnation should further be quantified in patients with normal aortic root characteristics and patients whom aortic root is more susceptible to cause post-interventional coronary obstruction (based on parameters reported in the chapter 5). This would help us understand the effect of leaflet laceration relative to sinus hemodynamics, patient-specific aortic environment, and TAV-aortic root interaction.

REFERENCES

1 Matteo Bianchi, State University of New York at Stony Brook, 2019.

2 Brian R Lindman, Robert O Bonow, and Catherine M Otto, "Current management of calcific aortic stenosis," Circulation research **113** (2), 223-237 (2013).

3 Efstratios I Charitos and Hans-Hinrich Sievers, "Anatomy of the aortic root: implications for valve-sparing surgery," Annals of cardiothoracic surgery **2** (1), 53 (2013).

4 Hadi Wiputra, Wei Xuan Chan, Yoke Yin Foo, Sheldon Ho, and Choon Hwai Yap, "Cardiac motion estimation from medical images: a regularisation framework applied on pairwise image registration displacement fields," Scientific reports **10** (1), 1-14 (2020).

5 S Yagel, SM Cohen, I Shapiro, and DV Valsky, "3D and 4D ultrasound in fetal cardiac scanning: a new look at the fetal heart," Ultrasound in Obstetrics and Gynecology: The Official Journal of the International Society of Ultrasound in Obstetrics and Gynecology **29** (1), 81-95 (2007).

6 Abraham M Rudolph, "Fetal and neonatal pulmonary circulation," Annual Review of Physiology **41** (1), 383-395 (1979).

7 Claudia Schmidtke, Hans-Hinrich Sievers, Alex Frydrychowicz, Michael Petersen, Michael Scharfschwerdt, Antje Karluss, Ulrich Stierle, and Doreen Richardt, "First clinical results with the new sinus prosthesis used for valve-sparing aortic root replacement," European Journal of Cardio-Thoracic Surgery **43** (3), 585-590 (2013); BJ Bellhouse and FH Bellhouse, "Mechanism of closure of the aortic valve," Nature **217** (5123), 86-87 (1968); Mano Thubrikar, *The aortic valve*. (Routledge, 2018).

8 Ala Alwan, *Global status report on noncommunicable diseases 2010*. (World Health Organization, 2011).

9 Roberts Gobergs, Elza Salputra, and Ingūna Lubaua, "Hypoplastic left heart syndrome: a review," Acta medica Lituanica **23** (2), 86 (2016).

10 Orlando Petrucci, Philip R Khoury, Peter B Manning, and Pirooz Eghtesady, "Outcomes of the bidirectional Glenn procedure in patients less than 3 months of age," The journal of thoracic and cardiovascular surgery **139** (3), 562-568 (2010).

11 Brian R Lindman, Marie-Annick Clavel, Patrick Mathieu, Bernard Iung, Patrizio Lancellotti, Catherine M Otto, and Philippe Pibarot, "Calcific aortic stenosis," Nature reviews Disease primers **2** (1), 1-28 (2016).

12 Jonathan T Butcher and Robert M Nerem, "Valvular endothelial cells and the mechanoregulation of valvular pathology," Philosophical Transactions of the Royal Society B: Biological Sciences **362** (1484), 1445-1457 (2007).

13 Jesper Hjortnaes, Sophie EP New, and Elena Aikawa, "Visualizing novel concepts of cardiovascular calcification," Trends in cardiovascular medicine **23** (3), 71-79 (2013).

14 Neelakantan Saikrishnan, Gautam Kumar, Fadi J Sawaya, Stamatios Lerakis, and Ajit P Yoganathan, "Accurate assessment of aortic stenosis: a review of diagnostic modalities and hemodynamics," Circulation **129** (2), 244-253 (2014).

15 Helmut Baumgartner, Judy Hung, Javier Bermejo, John B Chambers, Arturo Evangelista, Brian P Griffin, Bernard Iung, Catherine M Otto, Patricia A Pellikka, and Miguel Quiñones, "Echocardiographic assessment of valve stenosis: EAE/ASE recommendations for clinical practice," Journal of the American Society of Echocardiography **22** (1), 1-23 (2009).

16 SR Cannon, KL Richards, and MICHAEL Crawford, "Hydraulic estimation of stenotic orifice area: a correction of the Gorlin formula," Circulation **71** (6), 1170-1178 (1985).

17 Jerome Segal, Daniel J Lerner, D Craig Miller, R Scott Mitchell, Edwin A Alderman, and Richard L Popp, "When should Doppler-determined valve area be better than the Gorlin formula?: variation in hydraulic constants in low flow states," Journal of the American College of Cardiology **9** (6), 1294-1305 (1987).

18 Helmut Baumgartner, Steven Khan, Michele DeRobertis, Lawrence Czer, and Gerald Maurer, "Effect of prosthetic aortic valve design on the Doppler-catheter gradient correlation: an in vitro study of normal St. Jude, Medtronic-Hall, Starr-Edwards and Hancock valves", (Elsevier, 1992).

19 Arthur S Agatston, Warren R Janowitz, Frank J Hildner, Noel R Zusmer, Manuel Viamonte, and Robert Detrano, "Quantification of coronary artery calcium using ultrafast computed tomography," Journal of the American College of Cardiology **15** (4), 827-832 (1990); Ralf Koos, Andreas Horst Mahnken, Anil Martin Sinha, Joachim Ernst Wildberger, Rainer Hoffmann, and Harald Peter Kühl, "Aortic valve calcification as a marker for aortic stenosis severity: assessment on 16-MDCT," American Journal of Roentgenology **183** (6), 1813-1818 (2004).

20 Tania Pawade, Marie-Annick Clavel, Christophe Tribouilloy, Julien Dreyfus, Tiffany Mathieu, Lionel Tastet, Cedric Renard, Mesut Gun, William Steven Arthur Jenkins, and Laurent Macron, "Computed tomography aortic valve calcium scoring in patients with aortic stenosis," Circulation: Cardiovascular Imaging **11** (3), e007146 (2018); Marie-Annick Clavel, David Messika-Zeitoun, Philippe Pibarot, Shivani R Aggarwal, Joseph Malouf, Phillip A Araoz, Hector I Michelena, Caroline Cueff, Eric Larose, and Romain

Capoulade, "The complex nature of discordant severe calcified aortic valve disease grading: new insights from combined Doppler echocardiographic and computed tomographic study," Journal of the American College of Cardiology **62** (24), 2329-2338 (2013); Marie-Annick Clavel, Philippe Pibarot, David Messika-Zeitoun, Romain Capoulade, Joseph Malouf, Shivani R Aggarwal, Phillip A Araoz, Hector I Michelena, Caroline Cueff, and Eric Larose, "Impact of aortic valve calcification, as measured by MDCT, on survival in patients with aortic stenosis: results of an international registry study," Journal of the American College of Cardiology **64** (12), 1202-1213 (2014).

21 Julien IE Hoffman and Samuel Kaplan, "The incidence of congenital heart disease," Journal of the American College of Cardiology **39** (12), 1890-1900 (2002).

22 David J Barron, Mark D Kilby, Ben Davies, John GC Wright, Timothy J Jones, and William J Brawn, "Hypoplastic left heart syndrome," The Lancet **374** (9689), 551-564 (2009); William I Norwood, "Hypoplastic left heart syndrome," The Annals of thoracic surgery **52** (3), 688-695 (1991).

23 Jeffrey A Feinstein, D Woodrow Benson, Anne M Dubin, Meryl S Cohen, Dawn M Maxey, William T Mahle, Elfriede Pahl, Juan Villafañe, Ami B Bhatt, and Lynn F Peng, "Hypoplastic left heart syndrome: current considerations and expectations," Journal of the American college of cardiology **59** (1 Supplement), S1-S42 (2012).

24 HM Gardiner, "Response of the fetal heart to changes in load: from hyperplasia to heart failure," Heart **91** (7), 871-873 (2005).

25 William I Norwood Jr, Marshall L Jacobs, and John D Murphy, "Fontan procedure for hypoplastic left heart syndrome," The Annals of thoracic surgery **54** (6), 1025-1030 (1992); Shunji Sano, Kozo Ishino, Masaaki Kawada, Sadahiko Arai, Shingo Kasahara,

Tomohiro Asai, Zen-ichi Masuda, Mamoru Takeuchi, and Shin-ichi Ohtsuki, "Right ventricle–pulmonary artery shunt in first-stage palliation of hypoplastic left heart syndrome," The journal of thoracic and cardiovascular surgery **126** (2), 504-509 (2003).

26 Marc Gewillig, "The fontan circulation," Heart **91** (6), 839-846 (2005).

27 Kimimasa Tobita and Bradley B Keller, "Right and left ventricular wall deformation patterns in normal and left heart hypoplasia chick embryos," American Journal of Physiology-Heart and Circulatory Physiology **279** (3), H959-H969 (2000).

28 LR Feit, JA Copel, and CS Kleinman, "Foramen ovale size in the normal and abnormal human fetal heart: an indicator of transatrial flow physiology," Ultrasound in Obstetrics and Gynecology: The Official Journal of the International Society of Ultrasound in Obstetrics and Gynecology **1** (5), 313-319 (1991).

29 W Tworetzky, L Wilkins-Haug, and RW Jennings, "Balloon dilation of severe aortic stenosis in the fetus; potential for prevention of hypoplastic left heart syndrome; candidate selection, technique, and results of successful intervention," ACC Current Journal Review **2** (14), 93 (2005); LE Wilkins-Haug, CB Benson, W Tworetzky, AC Marshall, RW Jennings, and JE Lock, "In-utero intervention for hypoplastic left heart syndrome—a perinatologist's perspective," Ultrasound in Obstetrics and Gynecology: The Official Journal of the International Society of Ultrasound in Obstetrics and Gynecology **26** (5), 481-486 (2005).

30 Meryl S Cohen, Nicholas Dagincourt, Victor Zak, Jeanne Marie Baffa, Peter Bartz, Andreea Dragulescu, Gul Dudlani, Heather Henderson, Catherine D Krawczeski, and Wyman W Lai, "The Impact of the Left Ventricle on Right Ventricular Function and

Clinical Outcomes in Infants with Single–Right Ventricle Anomalies up to 14 Months of Age," Journal of the American Society of Echocardiography **31** (10), 1151-1157 (2018).

31 Jing Zhang, Qichang Zhou, Yili Zhao, Qinghai Peng, Zheli Gong, and Xiangdang Long, "Evaluation of right ventricular function in fetal hypoplastic left heart syndrome using spatio-temporal image correlation (STIC)," Cardiovascular ultrasound **14** (1), 12 (2015).

32 Chang Quan Lai, Guat Ling Lim, Muhammad Jamil, Citra Nurfarah Zaini Mattar, Arijit Biswas, and Choon Hwai Yap, "Fluid mechanics of blood flow in human fetal left ventricles based on patient-specific 4D ultrasound scans," Biomechanics and modeling in mechanobiology **15** (5), 1159-1172 (2016).

33 Hadi Wiputra, Chang Quan Lai, Guat Ling Lim, Joel Jia Wei Heng, Lan Guo, Sanah Merchant Soomar, Hwa Liang Leo, Arijit Biwas, Citra Nurfarah Zaini Mattar, and Choon Hwai Yap, "Fluid mechanics of human fetal right ventricles from image-based computational fluid dynamics using 4D clinical ultrasound scans," American Journal of Physiology-Heart and Circulatory Physiology **311** (6), H1498-H1508 (2016).

34 Hadi Wiputra, Guat Ling Lim, Dawn Ah Kiow Chia, Citra Nurfarah Zaini Mattar, Arijit Biswas, and Choon Hwai Yap, "Methods for fluid dynamics simulations of human fetal cardiac chambers based on patient-specific 4D ultrasound scans," Journal of Biomechanical Science and Engineering **11** (2), 15-00608-00615-00608 (2016).

35 Hadi Wiputra, Ching Kit Chen, Elias Talbi, Guat Ling Lim, Sanah Merchant Soomar, Arijit Biswas, Citra Nurfarah Zaini Mattar, David Bark, Hwa Liang Leo, and Choon Hwai Yap, "Human Fetal Hearts with Tetralogy of Fallot have Altered Fluid Dynamics and Forces," American Journal of Physiology-Heart and Circulatory Physiology (2018).

36 Alex Frydrychowicz, Aurélien F Stalder, Maximilian F Russe, Jelena Bock, Simon Bauer, Andreas Harloff, Alexander Berger, Mathias Langer, Jürgen Hennig, and Michael Markl, "Three-dimensional analysis of segmental wall shear stress in the aorta by flow-sensitive four-dimensional-MRI," Journal of Magnetic Resonance Imaging: An Official Journal of the International Society for Magnetic Resonance in Medicine **30** (1), 77-84 (2009); Johannes V Soulis, Olga P Lampri, Dimitrios K Fytanidis, and George D Giannoglou, presented at the Biomedical Engineering, 2011 10th International Workshop on, 2011 (unpublished).

37 Vivek Vasudevan, Hadi Wiputra, and Choon Hwai Yap, "Torsional motion of the left ventricle does not affect ventricular fluid dynamics of both foetal and adult hearts," Journal of biomechanics **96**, 109357 (2019).

38 Vivek Vasudevan, Adriel Jia Jun Low, Sarayu Parimal Annamalai, Smita Sampath, Chih-Liang Chin, Asad Abu Bakar Ali, and Choon Hwai Yap, "Role of diastolic vortices in flow and energy dynamics during systolic ejection," Journal of biomechanics **90**, 50-57 (2019).

39 Jay R Hove, Reinhard W Köster, Arian S Forouhar, Gabriel Acevedo-Bolton, Scott E Fraser, and Morteza Gharib, "Intracardiac fluid forces are an essential epigenetic factor for embryonic cardiogenesis," Nature **421** (6919), 172 (2003); Brennan Johnson, David Bark, Ilse Van Herck, Deborah Garrity, and Lakshmi Prasad Dasi, "Altered mechanical state in the embryonic heart results in time-dependent decreases in cardiac function," Biomechanics and modeling in mechanobiology **14** (6), 1379-1389 (2015); A Wayne Orr, Brian P Helmke, Brett R Blackman, and Martin A Schwartz, "Mechanisms of mechanotransduction," Developmental cell **10** (1), 11-20 (2006).

40 Lukas B Uittenbogaard, Monique C Haak, Marieke D Spreeuwenberg, and John MG van Vugt, "Fetal cardiac function assessed with four-dimensional ultrasound imaging using spatiotemporal image correlation," Ultrasound in Obstetrics and Gynecology **33** (3), 272-281 (2009).

41 Juha Rasanen, RH Debbs, DC Wood, S Weiner, SR Weil, and JC Huhta, "Human fetal right ventricular ejection force under abnormal loading conditions during the second half of pregnancy," Ultrasound in Obstetrics and Gynecology: The Official Journal of the International Society of Ultrasound in Obstetrics and Gynecology **10** (5), 325-332 (1997).

42 P Johnson, DJ Maxwell, MJ Tynan, and LD Allan, "Intracardiac pressures in the human fetus," Heart **84** (1), 59-63 (2000).

43 Hideaki Senzaki, Satoshi Masutani, Jun Kobayashi, Toshiki Kobayashi, Nozomu Sasaki, Haruhiko Asano, Shunei Kyo, Yuji Yokote, and Akira Ishizawa, "Ventricular afterload and ventricular work in Fontan circulation: comparison with normal two-ventricle circulation and single-ventricle circulation with Blalock-Taussig shunts," Circulation **105** (24), 2885-2892 (2002).

44 LD Allan, SUNDER K Chita, WIDAD Al-Ghazali, DC Crawford, and M Tynan, "Doppler echocardiographic evaluation of the normal human fetal heart," Heart **57** (6), 528-533 (1987).

45 Marc R Dweck, Nicholas A Boon, and David E Newby, "Calcific aortic stenosis: a disease of the valve and the myocardium," Journal of the American College of Cardiology **60** (19), 1854-1863 (2012).

46 Catherine M Otto, "Calcific aortic stenosis—time to look more closely at the valve", (Mass Medical Soc, 2008).

47 Jessica Joseph, Syed Yaseen Naqvi, Jay Giri, and Sheldon Goldberg, "Aortic stenosis: pathophysiology, diagnosis, and therapy," The American journal of medicine **130** (3), 253-263 (2017); Gry Wisthus Eveborn, Henrik Schirmer, Geir Heggelund, Per Lunde, and Knut Rasmussen, "The evolving epidemiology of valvular aortic stenosis. the Tromsø study," Heart **99** (6), 396-400 (2013).

48 Michael S Sacks, David B Smith, and Erik D Hiester, "The aortic valve microstructure: effects of transvalvular pressure," Journal of Biomedical Materials Research: An Official Journal of The Society for Biomaterials, The Japanese Society for Biomaterials, and the Australian Society for Biomaterials **41** (1), 131-141 (1998).

49 Sarah T Gould, Suthan Srigunapalan, Craig A Simmons, and Kristi S Anseth, "Hemodynamic and cellular response feedback in calcific aortic valve disease," Circulation research **113** (2), 186-197 (2013).

50 John A Stella and Michael S Sacks, "On the biaxial mechanical properties of the layers of the aortic valve leaflet," (2007).

51 Arkady Rutkovskiy, Anna Malashicheva, Gareth Sullivan, Maria Bogdanova, Anna Kostareva, Kåre-Olav Stensløkken, Arnt Fiane, and Jarle Vaage, "Valve interstitial cells: the key to understanding the pathophysiology of heart valve calcification," Journal of the American Heart Association **6** (9), e006339 (2017).

52 Cindy Ying Yin Yip and Craig A Simmons, "The aortic valve microenvironment and its role in calcific aortic valve disease," Cardiovascular Pathology **20** (3), 177-182 (2011).

53 Nalini M Rajamannan, Robert O Bonow, and Shahbudin H Rahimtoola, "Calcific aortic stenosis: an update," Nature clinical practice Cardiovascular medicine **4** (5), 254-262 (2007); Nalini M Rajamannan, "Calcific aortic stenosis: lessons learned from

experimental and clinical studies," Arteriosclerosis, thrombosis, and vascular biology **29** (2), 162-168 (2009); Nalini M Rajamannan, Frank J Evans, Elena Aikawa, K Jane Grande-Allen, Linda L Demer, Donald D Heistad, Craig A Simmons, Kristyn S Masters, Patrick Mathieu, and Kevin D O'Brien, "Calcific aortic valve disease: Not simply a degenerative process a review and agenda for research from the National Heart and Lung and Blood Institute Aortic Stenosis Working Group," Circulation **124** (16), 1783 (2011);

Nalini M Rajamannan and Catherine M Otto, "Targeted therapy to prevent progression of calcific aortic stenosis", (Am Heart Assoc, 2004); Daniel Alejandro Lerman, Sai Prasad, and Nasri Alotti, "Calcific aortic valve disease: molecular mechanisms and therapeutic approaches," European Cardiology Review **10** (2), 108 (2015); Linda L Demer and Yin Tintut, "Vascular calcification: pathobiology of a multifaceted disease," Circulation **117** (22), 2938-2948 (2008).

54 Emile R Mohler, R Nichols, WP Harvey, MJ Sheridan, BF Waller, and Bruce F Waller, "Development and progression of aortic valve stenosis: atherosclerosis risk factors—a causal relationship? A clinical morphologic study," Clinical cardiology **14** (12), 995-999 (1991).

55 Joan Fernández Esmerats, Jack Heath, and Hanjoong Jo, "Shear-sensitive genes in aortic valve endothelium," Antioxidants & redox signaling **25** (7), 401-414 (2016).

56 John M Tarbell, Zhong-Dong Shi, Jessilyn Dunn, and Hanjoong Jo, "Fluid mechanics, arterial disease, and gene expression," Annual review of fluid mechanics **46**, 591-614 (2014).

57 Vsevolod Katritch, Vadim Cherezov, and Raymond C Stevens, "Structure-function of the G protein–coupled receptor superfamily," Annual review of pharmacology and toxicology **53**, 531-556 (2013).

58 Maria L Lombardi, Diana E Jaalouk, Catherine M Shanahan, Brian Burke, Kyle J Roux, and Jan Lammerding, "The interaction between nesprins and sun proteins at the nuclear envelope is critical for force transmission between the nucleus and cytoskeleton," Journal of Biological Chemistry **286** (30), 26743-26753 (2011).

59 Elena Aikawa, Matthias Nahrendorf, Jose-Luiz Figueiredo, Filip K Swirski, Timur Shtatland, Rainer H Kohler, Farouc A Jaffer, Masanori Aikawa, and Ralph Weissleder, "CLINICAL PERSPECTIVE," Circulation **116** (24), 2841-2850 (2007).

60 Vishal Nigam and Deepak Srivastava, "Notch1 represses osteogenic pathways in aortic valve cells," Journal of molecular and cellular cardiology **47** (6), 828-834 (2009); Katherine E Yutzey, Linda L Demer, Simon C Body, Gordon S Huggins, Dwight A Towler, Cecilia M Giachelli, Marion A Hofmann-Bowman, Douglas P Mortlock, Melissa B Rogers, and Mehran M Sadeghi, "Calcific aortic valve disease: a consensus summary from the Alliance of Investigators on Calcific Aortic Valve Disease," Arteriosclerosis, thrombosis, and vascular biology **34** (11), 2387-2393 (2014).

61 Ryo Kawakami, Hironori Nakagami, Takahisa Noma, Koji Ohmori, Masakazu Kohno, and Ryuichi Morishita, "RANKL system in vascular and valve calcification with aging," Inflammation and regeneration **36** (1), 1-6 (2016); Jens J Kaden, Svetlana Bickelhaupt, Rainer Grobholz, Karl K Haase, Aslıhan Sarıkoç, Martina Brueckmann, Siegfried Lang, Ingrid Zahn, Christian Vahl, and Siegfried Hagl, "Receptor activator of nuclear factor κB

ligand and osteoprotegerin regulate aortic valve calcification," Journal of molecular and cellular cardiology **36** (1), 57-66 (2004).

62 Nalini M Rajamannan, Malayannan Subramaniam, Frank Caira, Stuart R Stock, and Thomas C Spelsberg, "Atorvastatin inhibits hypercholesterolemia-induced calcification in the aortic valves via the Lrp5 receptor pathway," Circulation **112** (9_supplement), I-229-I-234 (2005).

63 Kevin D O'Brien, "Pathogenesis of calcific aortic valve disease: a disease process comes of age (and a good deal more)," Arteriosclerosis, thrombosis, and vascular biology **26** (8), 1721-1728 (2006).

64 Mattabhorn Phimphilai, Zhouran Zhao, Heidi Boules, Hernan Roca, and Renny T Franceschi, "BMP signaling is required for RUNX2-dependent induction of the osteoblast phenotype," Journal of Bone and Mineral Research **21** (4), 637-646 (2006).

65 Gaia Favero, Corrado Paganelli, Barbara Buffoli, Luigi Fabrizio Rodella, and Rita Rezzani, "Endothelium and its alterations in cardiovascular diseases: life style intervention," BioMed research international **2014** (2014).

66 George Thanassoulis, "Lipoprotein (a) in calcific aortic valve disease: from genomics to novel drug target for aortic stenosis," Journal of lipid research **57** (6), 917-924 (2016).

67 Benjamin J Cairns, Sean Coffey, Ruth C Travis, Bernard Prendergast, Jane Green, James C Engert, Mark Lathrop, George Thanassoulis, and Robert Clarke, "A Replicated, Genome-Wide Significant Association of Aortic Stenosis With a Genetic Variant for Lipoprotein (a) Meta-Analysis of Published and Novel Data," Circulation **135** (12), 1181-1183 (2017).

68 Mary Hoekstra, Hao Yu Chen, Jian Rong, Line Dufresne, Jie Yao, Xiuqing Guo, Michael Y Tsai, Sotirios Tsimikas, Wendy S Post, and Ramachandran S Vasan, "Genome-wide association study highlights APOH as a novel locus for lipoprotein (a) levels—brief report," Arteriosclerosis, thrombosis, and vascular biology **41** (1), 458-464 (2021).

69 Livia SA Passos, Adrien Lupieri, Dakota Becker-Greene, and Elena Aikawa, "Innate and adaptive immunity in cardiovascular calcification," Atherosclerosis (2020).

70 Ibrahim Akin and Christoph A Nienaber, "Is there evidence for statins in the treatment of aortic valve stenosis?," World journal of cardiology **9** (8), 667 (2017); S Joanna Cowell, David E Newby, Robin J Prescott, Peter Bloomfield, John Reid, David B Northridge, and Nicholas A Boon, "A randomized trial of intensive lipid-lowering therapy in calcific aortic stenosis," New England Journal of Medicine **352** (23), 2389-2397 (2005); Kwan Leung Chan, Koon Teo, Jean G Dumesnil, Andy Ni, and James Tam, "Effect of Lipid lowering with rosuvastatin on progression of aortic stenosis: results of the aortic stenosis progression observation: measuring effects of rosuvastatin (ASTRONOMER) trial," Circulation **121** (2), 306-314 (2010); Anne B Rossebø, Terje R Pedersen, Kurt Boman, Philippe Brudi, John B Chambers, Kenneth Egstrup, Eva Gerdts, Christa Gohlke-Bärwolf, Ingar Holme, and Y Antero Kesäniemi, "Intensive lipid lowering with simvastatin and ezetimibe in aortic stenosis," New England Journal of Medicine **359** (13), 1343-1356 (2008).

71 Rosario V Freeman and Catherine M Otto, "Spectrum of calcific aortic valve disease: pathogenesis, disease progression, and treatment strategies," Circulation **111** (24), 3316-3326 (2005).

72 Juan Francisco Santibáñez, Javier Guerrero, Miguel Quintanilla, Angels Fabra, and Jorge Martínez, "Transforming growth factor-β1 modulates matrix metalloproteinase-9 production through the Ras/MAPK signaling pathway in transformed keratinocytes," Biochemical and biophysical research communications **296** (2), 267-273 (2002).

73 Frank Helderman, Dolf Segers, Rini de Crom, Berend P Hierck, Rob E Poelmann, Paul C Evans, and Rob Krams, "Effect of shear stress on vascular inflammation and plaque development," Current opinion in lipidology **18** (5), 527-533 (2007); Jens J Kaden, Carl-Erik Dempfle, Rainer Grobholz, Carolin S Fischer, Daniela C Vocke, Refika Kılıç, Aslıhan Sarıkoç, Rafael Piñol, Siegfried Hagl, and Siegfried Lang, "Inflammatory regulation of extracellular matrix remodeling in calcific aortic valve stenosis," Cardiovascular Pathology **14** (2), 80-87 (2005); Patrick Mathieu, Rihab Bouchareb, and Marie-Chloé Boulanger, "Innate and adaptive immunity in calcific aortic valve disease," Journal of immunology research **2015** (2015).

74 Sophie EP New, Claudia Goettsch, Masanori Aikawa, Julio F Marchini, Manabu Shibasaki, Katsumi Yabusaki, Peter Libby, Catherine M Shanahan, Kevin Croce, and Elena Aikawa, "Macrophage-derived matrix vesicles: an alternative novel mechanism for microcalcification in atherosclerotic plaques," Circulation research **113** (1), 72-77 (2013); Alexander N Kapustin, Martijn LL Chatrou, Ignat Drozdov, Ying Zheng, Sean M Davidson, Daniel Soong, Malgorzata Furmanik, Pilar Sanchis, Rafael Torres Martin De Rosales, and Daniel Alvarez-Hernandez, "Vascular smooth muscle cell calcification is mediated by regulated exosome secretion," Circulation research **116** (8), 1312-1323 (2015).

75 Veronika A Myasoedova, Alessio L Ravani, Beatrice Frigerio, Vincenza Valerio, Donato Moschetta, Paola Songia, and Paolo Poggio, "Novel pharmacological targets for calcific aortic valve disease: Prevention and treatments," Pharmacological research **136**, 74-82 (2018).

76 Mark J Graham, Nick Viney, Rosanne M Crooke, and Sotirios Tsimikas, "Antisense inhibition of apolipoprotein (a) to lower plasma lipoprotein (a) levels in humans," Journal of lipid research **57** (3), 340-351 (2016); Sotirios Tsimikas, Nicholas J Viney, Steven G Hughes, Walter Singleton, Mark J Graham, Brenda F Baker, Jennifer L Burkey, Qingqing Yang, Santica M Marcovina, and Richard S Geary, "Antisense therapy targeting apolipoprotein (a): a randomised, double-blind, placebo-controlled phase 1 study," The Lancet **386** (10002), 1472-1483 (2015).

77 Evan A Stein and Frederick Raal, "Future directions to establish lipoprotein (a) as a treatment for atherosclerotic cardiovascular disease," Cardiovascular drugs and therapy **30** (1), 101-108 (2016).

78 Aakash Garg, Abhishek Sharma, Parasuram Krishnamoorthy, Jalaj Garg, Deepti Virmani, Toishi Sharma, Giulio Stefanini, John B Kostis, Debabrata Mukherjee, and Ekaterina Sikorskaya, "Role of niacin in current clinical practice: a systematic review," The American journal of medicine **130** (2), 173-187 (2017).

79 John J Albers, April Slee, Kevin D O'Brien, Jennifer G Robinson, Moti L Kashyap, Peter O Kwiterovich, Ping Xu, and Santica M Marcovina, "Relationship of apolipoproteins A-1 and B, and lipoprotein (a) to cardiovascular outcomes: the AIM-HIGH trial (Atherothrombosis Intervention in Metabolic Syndrome with Low HDL/High Triglyceride

and Impact on Global Health Outcomes)," Journal of the American College of Cardiology **62** (17), 1575-1579 (2013).

80 Frederick J Raal, Robert P Giugliano, Marc S Sabatine, Michael J Koren, Dirk Blom, Nabil G Seidah, Narimon Honarpour, Armando Lira, Allen Xue, and Padmaja Chiruvolu, "PCSK9 inhibition-mediated reduction in Lp (a) with evolocumab: an analysis of 10 clinical trials and the LDL receptor's role [S]," Journal of lipid research **57** (6), 1086-1096 (2016); Marc S Sabatine, Robert P Giugliano, Anthony C Keech, Narimon Honarpour, Stephen D Wiviott, Sabina A Murphy, Julia F Kuder, Huei Wang, Thomas Liu, and Scott M Wasserman, "Evolocumab and clinical outcomes in patients with cardiovascular disease," New England Journal of Medicine **376** (18), 1713-1722 (2017).

81 Kazuhiko Seya, Ken-Ichi Furukawa, Mari Chiyoya, Zaiqiang Yu, Haruhisa Kikuchi, Kazuyuki Daitoku, Shigeru Motomura, Manabu Murakami, Yoshiteru Oshima, and Ikuo Fukuda, "1-Methyl-2-undecyl-4 (1H)-quinolone, a derivative of quinolone alkaloid evocarpine, attenuates high phosphate-induced calcification of human aortic valve interstitial cells by inhibiting phosphate cotransporter PiT-1," Journal of pharmacological sciences **131** (1), 51-57 (2016).

82 Jordan D Miller, Robert M Weiss, Kristine M Serrano, Robert M Brooks, Christopher J Berry, Kathy Zimmerman, Stephen G Young, and Donald D Heistad, "Lowering plasma cholesterol levels halts progression of aortic valve disease in mice," Circulation **119** (20), 2693-2701 (2009).

83 Rihab Bouchareb, Nancy Côté, Khai Le Quang, Diala El Husseini, Jérémie Asselin, Fayez Hadji, Dominic Lachance, Elnur Elyar Shayhidin, Ablajan Mahmut, and Philippe Pibarot,

"Carbonic anhydrase XII in valve interstitial cells promotes the regression of calcific aortic valve stenosis," Journal of molecular and cellular cardiology **82**, 104-115 (2015).

84 Blase A Carabello, "How does the heart respond to aortic stenosis: let me count the ways", (Am Heart Assoc, 2013).

85 S Joanna Cowell, David E Newby, Nicholas A Boon, and Andrew T Elder, "Calcific aortic stenosis: same old story?," Age and ageing **33** (6), 538-544 (2004).

86 Susan Kwon and Aasha Gopal, "Hemodynamic Classifications of Aortic Stenosis and Relevance to Prognosis," Aortic Stenosis-Current Perspectives (2019).

87 Julio Garcia, Lyes Kadem, Eric Larose, Marie-Annick Clavel, and Philippe Pibarot, "Comparison between cardiovascular magnetic resonance and transthoracic Doppler echocardiography for the estimation of effective orifice area in aortic stenosis," Journal of Cardiovascular Magnetic Resonance **13** (1), 1-9 (2011).

88 Martine Voisine, Maxime Hervault, Mylène Shen, Anne-Julie Boilard, Benoît Filion, Mickael Rosa, Yohan Bossé, Patrick Mathieu, Nancy Côté, and Marie-Annick Clavel, "Age, Sex, and Valve Phenotype Differences in Fibro-Calcific Remodeling of Calcified Aortic Valve," Journal of the American Heart Association **9** (10), e015610 (2020);

Marie-Ange Fleury and Marie-Annick Clavel, "Sex and race differences in the pathophysiology, diagnosis, treatment, and outcomes of valvular heart diseases," Canadian Journal of Cardiology (2021).

89 Volha I Summerhill, Donato Moschetta, Alexander N Orekhov, Paolo Poggio, and Veronika A Myasoedova, "Sex-specific features of calcific aortic valve disease," International Journal of Molecular Sciences **21** (16), 5620 (2020).

90 Mariana Kiomy Osako, Hironori Nakagami, Nobutaka Koibuchi, Hideo Shimizu, Futoshi Nakagami, Hiroshi Koriyama, Munehisa Shimamura, Takashi Miyake, Hiromi Rakugi, and Ryuichi Morishita, "Estrogen inhibits vascular calcification via vascular RANKL system: common mechanism of osteoporosis and vascular calcification," Circulation research **107** (4), 466-475 (2010); Emma Harper, Hannah Forde, Colin Davenport, Keith D Rochfort, Diarmuid Smith, and Philip M Cummins, "Vascular calcification in type-2 diabetes and cardiovascular disease: Integrative roles for OPG, RANKL and TRAIL," Vascular pharmacology **82**, 30-40 (2016).

91 Bin Zhang, Virginia M Miller, and Jordan D Miller, "Influences of sex and estrogen in arterial and valvular calcification," Frontiers in endocrinology **10**, 622 (2019).

92 Maxwell L Gelfand, Theodore Cohen, John J Ackert, Marjorie Ambos, and Manuel Mayadag, "Gastrointestinal bleeding in aortic stenosis," American Journal of Gastroenterology (Springer Nature) **71** (1) (1979); André Vincentelli, Sophie Susen, Thierry Le Tourneau, Isabelle Six, Olivier Fabre, Francis Juthier, Anne Bauters, Christophe Decoene, Jenny Goudemand, and Alain Prat, "Acquired von Willebrand syndrome in aortic stenosis," New England Journal of Medicine **349** (4), 343-349 (2003); Vuyisile T Nkomo, Julius M Gardin, Thomas N Skelton, John S Gottdiener, Christopher G Scott, and Maurice Enriquez-Sarano, "Burden of valvular heart diseases: a population-based study," The Lancet **368** (9540), 1005-1011 (2006); Senan J Yasar, Obai Abdullah, William Fay, and Sudarshan Balla, "Von Willebrand factor revisited," Journal of interventional cardiology **31** (3), 360-367 (2018).

93 Theodore E Warkentin, Jane C Moore, and David G Morgan, "Gastrointestinal angiodysplasia and aortic stenosis," N. Engl. J. Med. **347** (11), 858-859 (2002).

94 Sophie Susen, Andre Vincentelli, Thierry Le Tourneau, Claudine Caron, Christophe Zawadzki, Alain Prat, Jenny Goudemand, and Brigitte Jude, "Severe Aortic and Mitral Valve Regurgitation Are Associated with von Willebrand Factor Defect", (American Society of Hematology, 2005); JL Blackshear, EM Wysokinska, RE Safford, CS Thomas, BP Shapiro, S Ung, ME Stark, P Parikh, GS Johns, and D Chen, "Shear stress-associated acquired von Willebrand syndrome in patients with mitral regurgitation," Journal of Thrombosis and Haemostasis **12** (12), 1966-1974 (2014); Eric Van Belle, Antoine Rauch, Flavien Vincent, Emmanuel Robin, Marion Kibler, Julien Labreuche, Emmanuelle Jeanpierre, Marie Levade, Christopher Hurt, and Natacha Rousse, "Von Willebrand factor multimers during transcatheter aortic-valve replacement," New England Journal of Medicine **375** (4), 335-344 (2016); Maria Bortot, Katrina Bark, Keith Neeves, Nathan Clendenen, David J Bark, and Jorge DiPaola, "Impaired Primary Hemostasis in Patients on Cardiopulmonary Bypass," Arteriosclerosis, thrombosis, and vascular biology **39** (Suppl_1), A130-A130 (2019).

95 Eric Van Belle, Flavien Vincent, Antoine Rauch, Caterina Casari, Emmanuelle Jeanpierre, Valentin Loobuyck, Mickael Rosa, Cedric Delhaye, Hughes Spillemaeker, and Camille Paris, "von Willebrand factor and management of heart valve disease: JACC review topic of the week," Journal of the American College of Cardiology **73** (9), 1078-1088 (2019).

96 Lawrence H Cohn, Vakhtang Tchantchaleishvili, and Taufiek K Rajab, "Evolution of the concept and practice of mitral valve repair," Annals of cardiothoracic surgery **4** (4), 315 (2015).

97 Diana Aicher, Roland Fries, Svetlana Rodionycheva, Kathrin Schmidt, Frank Langer, and Hans-Joachim Schäfers, "Aortic valve repair leads to a low incidence of valve-related complications," European Journal of Cardio-Thoracic Surgery **37** (1), 127-132 (2010).

98 Alain Cribier, Nadir Saoudi, Jacques Berland, Thierry Savin, Paulo Rocha, and Brice Letac, "Percutaneous transluminal valvuloplasty of acquired aortic stenosis in elderly patients: an alternative to valve replacement?," The Lancet **327** (8472), 63-67 (1986).

99 Robert D Safian, Valerie S Mandell, Robert E Thurer, Grover M Hutchins, Stuart J Schnitt, William Grossman, and Raymond G McKay, "Postmortem and intraoperative balloon valvuloplasty of calcific aortic stenosis in elderly patients: mechanisms of successful dilation," Journal of the American College of Cardiology **9** (3), 655-660 (1987).

100 W Arzt, D Wertaschnigg, I Veit, F Klement, R Gitter, and G Tulzer, "Intrauterine aortic valvuloplasty in fetuses with critical aortic stenosis: experience and results of 24 procedures," Ultrasound in obstetrics & gynecology **37** (6), 689-695 (2011); Audrey C Marshall, Wayne Tworetzky, Lisa Bergersen, Doff B McElhinney, Carol B Benson, Russell W Jennings, Louise E Wilkins-Haug, Gerald R Marx, and James E Lock, "Aortic valvuloplasty in the fetus: technical characteristics of successful balloon dilation," The Journal of pediatrics **147** (4), 535-539 (2005); Wayne Tworetzky, Louise Wilkins-Haug, Russell W Jennings, Mary E van der Velde, Audrey C Marshall, Gerald R Marx, Steven D Colan, Carol B Benson, James E Lock, and Stanton B Perry, "Balloon dilation of severe aortic stenosis in the fetus: potential for prevention of hypoplastic left heart syndrome: candidate selection, technique, and results of successful intervention," Circulation **110** (15), 2125-2131 (2004); Kevin G Friedman, Renee Margossian, Dionne A Graham, David M Harrild, Sitaram M Emani, Louise E Wilkins-Haug, Doff B

McElhinney, and Wayne Tworetzky, "Postnatal left ventricular diastolic function after fetal aortic valvuloplasty," The American journal of cardiology **108** (4), 556-560 (2011).

101 Polonca Kogoj, Rok Devjak, and Matjaz Bunc, "Balloon aortic valvuloplasty (BAV) as a bridge to aortic valve replacement in cancer patients who require urgent non-cardiac surgery," Radiology and oncology **48** (1), 62 (2014).

102 Stuart J Head, Mevlüt Çelik, and A Pieter Kappetein, "Mechanical versus bioprosthetic aortic valve replacement," European heart journal **38** (28), 2183-2191 (2017).

103 Philippe Pibarot, Erwan Salaun, Abdellaziz Dahou, Eleonora Avenatti, Ezequiel Guzzetti, Mohamed-Salah Annabi, Oumhani Toubal, Mathieu Bernier, Jonathan Beaudoin, and Géraldine Ong, "Echocardiographic results of transcatheter versus surgical aortic valve replacement in low-risk patients: the PARTNER 3 trial," Circulation **141** (19), 1527-1537 (2020); Joao Braghiroli, Kunal Kapoor, Torin P Thielhelm, Tanira Ferreira, and Mauricio G Cohen, "Transcatheter aortic valve replacement in low risk patients: a review of PARTNER 3 and Evolut low risk trials," Cardiovascular diagnosis and therapy **10** (1), 59 (2020).

104 Alain Cribier, Helene Eltchaninoff, Assaf Bash, Nicolas Borenstein, Christophe Tron, Fabrice Bauer, Genevieve Derumeaux, Frederic Anselme, François Laborde, and Martin B Leon, "Percutaneous transcatheter implantation of an aortic valve prosthesis for calcific aortic stenosis: first human case description," Circulation **106** (24), 3006-3008 (2002).

105 Arash Kheradvar, Elliott M Groves, Craig J Goergen, S Hamed Alavi, Robert Tranquillo, Craig A Simmons, Lakshmi P Dasi, K Jane Grande-Allen, Mohammad RK Mofrad, and Ahmad Falahatpisheh, "Emerging trends in heart valve engineering: Part II. Novel and

standard technologies for aortic valve replacement," Annals of biomedical engineering **43** (4), 844-857 (2015).

106 Patrizio Lancellotti and Mani A Vannan, "Timing of intervention in aortic stenosis," The New England journal of medicine **382** (2) (2020); Marko Banovic, Bernard Iung, Svetozar Putnik, Serge Nikolic, Martin Penicka, Marek Deja, and Jozef Bartunek, "Addressing the Treatment Dilemma in Asymptomatic Aortic Stenosis: The AVATAR Trial," JACC: Cardiovascular Imaging **12** (9), 1896-1897 (2019); Russell James Everett, Marie-Annick Clavel, Philippe Pibarot, and Marc Richard Dweck, "Timing of intervention in aortic stenosis a review of current and future strategies," (2018); Brian R Lindman, Marc R Dweck, Patrizio Lancellotti, Philippe Généreux, Luc A Piérard, Patrick T O'Gara, and Robert O Bonow, "Management of asymptomatic severe aortic stenosis: evolving concepts in timing of valve replacement," Cardiovascular Imaging **13** (2_Part_1), 481-493 (2020).

107 Craig R Smith, Martin B Leon, Michael J Mack, D Craig Miller, Jeffrey W Moses, Lars G Svensson, E Murat Tuzcu, John G Webb, Gregory P Fontana, and Raj R Makkar, "Transcatheter versus surgical aortic-valve replacement in high-risk patients," New England Journal of Medicine **364** (23), 2187-2198 (2011).

108 Thomas G Gleason, Michael J Reardon, Jeffrey J Popma, G Michael Deeb, Steven J Yakubov, Joon S Lee, Neal S Kleiman, Stan Chetcuti, James B Hermiller, and John Heiser, "5-Year outcomes of self-expanding transcatheter versus surgical aortic valve replacement in high-risk patients," Journal of the American College of Cardiology **72** (22), 2687-2696 (2018).

109 Michael J Mack, Martin B Leon, Craig R Smith, D Craig Miller, Jeffrey W Moses, E Murat Tuzcu, John G Webb, Pamela S Douglas, William N Anderson, and Eugene H Blackstone, "5-year outcomes of transcatheter aortic valve replacement or surgical aortic valve replacement for high surgical risk patients with aortic stenosis (PARTNER 1): a randomised controlled trial," The Lancet **385** (9986), 2477-2484 (2015).

110 Dhaval Kolte, Gus J Vlahakes, Igor F Palacios, Rahul Sakhuja, Jonathan J Passeri, Ignacio Inglessis, and Sammy Elmariah, "Transcatheter versus surgical aortic valve replacement in low-risk patients," Journal of the American College of Cardiology **74** (12), 1532-1540 (2019).

111 Cindy L Grines, Andrew J Klein, Holly Bauser-Heaton, Mohamad Alkhouli, Neelima Katukuri, Varun Aggarwal, S Elissa Altin, Wayne B Batchelor, James C Blankenship, and Foluso Fakorede, "Racial and ethnic disparities in coronary, vascular, structural, and congenital heart disease," Catheterization and Cardiovascular Interventions (2021).

112 Mohamad Alkhouli, David R Holmes, John D Carroll, Zhuokai Li, Taku Inohara, Andrzej S Kosinski, Molly Szerlip, Vinod H Thourani, Michael J Mack, and Sreekanth Vemulapalli, "Racial disparities in the utilization and outcomes of TAVR: TVT registry report," JACC: Cardiovascular Interventions **12** (10), 936-948 (2019); Anna Sleder, Shiloh Tackett, Matthew Cerasale, Chetan Mittal, Iyad Isseh, Ryhm Radjef, Andrew Taylor, Rashad Farha, Oleksandra Lupak, and Dana Larkin, "Socioeconomic and racial disparities: a case-control study of patients receiving transcatheter aortic valve replacement for severe aortic stenosis," Journal of racial and ethnic health disparities **4** (6), 1189-1194 (2017); Michael Yeung, Jimmy Kerrigan, Sandeep Sodhi, Pei-Hsiu Huang, Eric Novak, Hersh Maniar, and Alan Zajarias, "Racial differences in rates of aortic valve

replacement in patients with severe aortic stenosis," The American journal of cardiology **112** (7), 991-995 (2013).

113 Matthew C Henn and Marc R Moon, "Mechanical Prosthetic Valves", in *Cardiac Surgery* (Springer, 2020), pp. 291-298.

114 Yared Alemu and Danny Bluestein, "Flow-induced platelet activation and damage accumulation in a mechanical heart valve: numerical studies," Artificial organs **31** (9), 677-688 (2007); David M Wootton and David N Ku, "Fluid mechanics of vascular systems, diseases, and thrombosis," Annual review of biomedical engineering **1** (1), 299-329 (1999); B Min Yun, Jingshu Wu, Helene A Simon, Shiva Arjunon, Fotis Sotiropoulos, Cyrus K Aidun, and Ajit P Yoganathan, "A numerical investigation of blood damage in the hinge area of aortic bileaflet mechanical heart valves during the leakage phase," Annals of biomedical engineering **40** (7), 1468-1485 (2012); Liang Ge, Lakshmi P Dasi, Fotis Sotiropoulos, and Ajit P Yoganathan, "Characterization of hemodynamic forces induced by mechanical heart valves: Reynolds vs. viscous stresses," Annals of biomedical engineering **36** (2), 276-297 (2008).

115 George D Dangas, Jeffrey I Weitz, Gennaro Giustino, Raj Makkar, and Roxana Mehran, "Prosthetic heart valve thrombosis," Journal of the American College of Cardiology **68** (24), 2670-2689 (2016).

116 Alexander Kulik, Fraser D Rubens, Philip S Wells, Clive Kearon, Thierry G Mesana, Judith van Berkom, and B-Khanh Lam, "Early postoperative anticoagulation after mechanical valve replacement: a systematic review," The Annals of thoracic surgery **81** (2), 770-781 (2006).

117 Taolei Sun, Hong Tan, Dong Han, Qiang Fu, and Lei Jiang, "No platelet can adhere—largely improved blood compatibility on nanostructured superhydrophobic surfaces," Small **1** (10), 959-963 (2005); David L Bark, Hamed Vahabi, Hieu Bui, Sanli Movafaghi, Brandon Moore, Arun K Kota, Ketul Popat, and Lakshmi P Dasi, "Hemodynamic performance and thrombogenic properties of a superhydrophobic bileaflet mechanical heart valve," Annals of biomedical engineering **45** (2), 452-463 (2017); Daniel C Leslie, Anna Waterhouse, Julia B Berthet, Thomas M Valentin, Alexander L Watters, Abhishek Jain, Philseok Kim, Benjamin D Hatton, Arthur Nedder, and Kathryn Donovan, "A bioinspired omniphobic surface coating on medical devices prevents thrombosis and biofouling," Nature biotechnology **32** (11), 1134-1140 (2014); MT Khorasani and H Mirzadeh, "In vitro blood compatibility of modified PDMS surfaces as superhydrophobic and superhydrophilic materials," Journal of applied polymer science **91** (3), 2042-2047 (2004).

118 Douglas R Johnston, Edward G Soltesz, Nakul Vakil, Jeevanantham Rajeswaran, Eric E Roselli, Joseph F Sabik III, Nicholas G Smedira, Lars G Svensson, Bruce W Lytle, and Eugene H Blackstone, "Long-term durability of bioprosthetic aortic valves: implications from 12,569 implants," The Annals of thoracic surgery **99** (4), 1239-1247 (2015).

119 Lakshmi P Dasi, Hoda Hatoum, Arash Kheradvar, Ramin Zareian, S Hamed Alavi, Wei Sun, Caitlin Martin, Thuy Pham, Qian Wang, and Prem A Midha, "On the mechanics of transcatheter aortic valve replacement," Annals of biomedical engineering **45** (2), 310-331 (2017).

120 S Hamed Alavi, Elliott M Groves, and Arash Kheradvar, "The effects of transcatheter valve crimping on pericardial leaflets," The Annals of thoracic surgery **97** (4), 1260-1266 (2014).

121 María Del Carmen León Del Pino, Martín Ruíz Ortiz, Mónica Delgado Ortega, José Sánchez Fernández, Carlos Ferreiro Quero, Enrique Durán Jiménez, Miguel Romero Moreno, José Segura Saint-Gerons, Soledad Ojeda Pineda, and Manuel Pan Álvarez-Ossorio, "Prosthesis-patient mismatch after transcatheter aortic valve replacement: prevalence and medium term prognostic impact," The international journal of cardiovascular imaging **35** (5), 827-836 (2019).

122 Jean-Claude Laborde, Stephen JD Brecker, David Roy, and Marjan Jahangiri, "Complications at the time of transcatheter aortic valve implantation," Methodist DeBakey cardiovascular journal **8** (2), 38 (2012).

123 Raj R Makkar, Hasan Jilaihawi, Tarun Chakravarty, Gregory P Fontana, Samir Kapadia, Vasilis Babaliaros, Wen Cheng, Vinod H Thourani, Joseph Bavaria, and Lars Svensson, "Determinants and outcomes of acute transcatheter valve-in-valve therapy or embolization: a study of multiple valve implants in the US PARTNER trial (Placement of AoRTic TraNscathetER Valve Trial Edwards SAPIEN Transcatheter Heart Valve)," Journal of the American College of Cardiology **62** (5), 418-430 (2013).

124 Amir-Ali Fassa, Dominique Himbert, and Alec Vahanian, "Mechanisms and management of TAVR-related complications," Nature reviews Cardiology **10** (12), 685 (2013).

125 Marco Barbanti, Tae-Hyun Yang, Josep Rodès Cabau, Corrado Tamburino, David A Wood, Hasan Jilaihawi, Phillip Blanke, Raj R Makkar, Azeem Latib, and Antonio Colombo, "Anatomical and procedural features associated with aortic root rupture during balloon-expandable transcatheter aortic valve replacement," Circulation **128** (3), 244-253 (2013); Philipp Blanke, Jochen Reinöhl, Christian Schlensak, Matthias Siepe, Gregor Pache, Wulf Euringer, Annette Geibel-Zehender, Christopher Bode, Mathias

Langer, and Friedhelm Beyersdorf, "Prosthesis oversizing in balloon-expandable transcatheter aortic valve implantation is associated with contained rupture of the aortic root," Circulation: Cardiovascular Interventions **5** (4), 540-548 (2012); Alexander B Willson, John G Webb, Melanie Freeman, David A Wood, Ronen Gurvitch, Christopher R Thompson, Robert R Moss, Stefan Toggweiler, Ronnie K Binder, and Bradley Munt, "Computed tomography–based sizing recommendations for transcatheter aortic valve replacement with balloon-expandable valves: Comparison with transesophageal echocardiography and rationale for implementation in a prospective trial," Journal of cardiovascular computed tomography **6** (6), 406-414 (2012); Ronald K Binder, John G Webb, Alexander B Willson, Marina Urena, Nicolaj C Hansson, Bjarne L Norgaard, Philippe Pibarot, Marco Barbanti, Eric Larose, and Melanie Freeman, "The impact of integration of a multidetector computed tomography annulus area sizing algorithm on outcomes of transcatheter aortic valve replacement: a prospective, multicenter, controlled trial," Journal of the American College of Cardiology **62** (5), 431-438 (2013).

126 Samuel Bernard and Evin Yucel, "Paravalvular leaks—from diagnosis to management," Current treatment options in cardiovascular medicine **21** (11), 1-16 (2019).

127 Martine Gilard, Hélène Eltchaninoff, Bernard Iung, Patrick Donzeau-Gouge, Karine Chevreul, Jean Fajadet, Pascal Leprince, Alain Leguerrier, Michel Lievre, and Alain Prat, "Registry of transcatheter aortic-valve implantation in high-risk patients," New England Journal of Medicine **366** (18), 1705-1715 (2012); Neil E Moat, Peter Ludman, Mark A de Belder, Ben Bridgewater, Andrew D Cunningham, Christopher P Young, Martyn Thomas, Jan Kovac, Tom Spyt, and Philip A MacCarthy, "Long-term outcomes after

transcatheter aortic valve implantation in high-risk patients with severe aortic stenosis: the UK TAVI (United Kingdom Transcatheter Aortic Valve Implantation) Registry," Journal of the American College of Cardiology **58** (20), 2130-2138 (2011); Ganesh Athappan, Eshan Patvardhan, E Murat Tuzcu, Lars Georg Svensson, Pedro A Lemos, Chiara Fraccaro, Giuseppe Tarantini, Jan-Malte Sinning, Georg Nickenig, and Davide Capodanno, "Incidence, predictors, and outcomes of aortic regurgitation after transcatheter aortic valve replacement: meta-analysis and systematic review of literature," Journal of the American College of Cardiology **61** (15), 1585-1595 (2013).

128 Olivia N Gilbert, Charles H Choi, Jodie L Franzil, Melissa Caughey, Waqas Qureshi, R Brandon Stacey, Min Pu, Robert J Applegate, Sanjay K Gandhi, and David XM Zhao, "Comparison of paravalvular aortic leak characteristics in the Medtronic CoreValve versus Edwards Sapien Valve: Paravalvular aortic leak characteristics," Catheterization and Cardiovascular Interventions **92** (5), 972-980 (2018).

129 Irene Franzoni, Azeem Latib, Francesco Maisano, Charis Costopoulos, Luca Testa, Filippo Figini, Francesco Giannini, Sandeep Basavarajaiah, Marco Mussardo, and Massimo Slavich, "Comparison of incidence and predictors of left bundle branch block after transcatheter aortic valve implantation using the CoreValve versus the Edwards valve," The American journal of cardiology **112** (4), 554-559 (2013); George CM Siontis, Peter Jüni, Thomas Pilgrim, Stefan Stortecky, Lutz Büllesfeld, Bernhard Meier, Peter Wenaweser, and Stephan Windecker, "Predictors of permanent pacemaker implantation in patients with severe aortic stenosis undergoing TAVR: a meta-analysis," Journal of the American College of Cardiology **64** (2), 129-140 (2014); Prateek J Khatri, John G Webb, Josep Rodés-Cabau, Stephen E Fremes, Marc Ruel, Kelly Lau, Helen Guo, Harindra

C Wijeysundera, and Dennis T Ko, "Adverse effects associated with transcatheter aortic valve implantation: a meta-analysis of contemporary studies," Annals of internal medicine **158** (1), 35-46 (2013).

130 Panagiotis Karyofillis, Anna Kostopoulou, Sofia Thomopoulou, Martha Habibi, Efthimios Livanis, George Karavolias, and Vassilis Voudris, "Conduction abnormalities after transcatheter aortic valve implantation," Journal of geriatric cardiology: JGC **15** (1), 105 (2018).

131 MZ Khawaja, R Rajani, A Cook, A Khavandi, A Moynagh, S Chowdhary, MS Spence, S Brown, SQ Khan, and N Walker, "Permanent pacemaker insertion after CoreValve transcatheter aortic valve implantation: incidence and contributing factors (the UK CoreValve Collaborative)," Circulation **123** (9), 951-960 (2011).

132 Danny Dvir, John Webb, Stephen Brecker, Sabine Bleiziffer, David Hildick-Smith, Antonio Colombo, Fleur Descoutures, Christian Hengstenberg, Neil E Moat, and Raffi Bekeredjian, "Transcatheter aortic valve replacement for degenerative bioprosthetic surgical valves: results from the global valve-in-valve registry," Circulation **126** (19), 2335-2344 (2012).

133 Henrique B Ribeiro, Josep Rodés-Cabau, Philipp Blanke, Jonathon Leipsic, Jong Kwan Park, Vinayak Bapat, Raj Makkar, Matheus Simonato, Marco Barbanti, and Joachim Schofer, "Incidence, predictors, and clinical outcomes of coronary obstruction following transcatheter aortic valve replacement for degenerative bioprosthetic surgical valves: insights from the VIVID registry," European heart journal **39** (8), 687-695 (2018).

134 Ronen Gurvitch, Anson Cheung, Francesco Bedogni, and John G Webb, "Coronary obstruction following transcatheter aortic valve-in-valve implantation for failed surgical bioprostheses," Catheterization and Cardiovascular Interventions **77** (3), 439-444 (2011).

135 Ibrahim Sultan, Mary Siki, Tyler Wallen, Wilson Szeto, and Prashanth Vallabhajosyula, "Management of coronary obstruction following transcatheter aortic valve replacement," Journal of cardiac surgery **32** (12), 777-781 (2017).

136 Henrique B Ribeiro, John G Webb, Raj R Makkar, Mauricio G Cohen, Samir R Kapadia, Susheel Kodali, Corrado Tamburino, Marco Barbanti, Tarun Chakravarty, and Hasan Jilaihawi, "Predictive factors, management, and clinical outcomes of coronary obstruction following transcatheter aortic valve implantation: insights from a large multicenter registry," Journal of the American College of Cardiology **62** (17), 1552-1562 (2013).

137 Ashraf Hamdan, Israel Barbash, Ehud Schwammenthal, Amit Segev, Ran Kornowski, Abid Assali, Ella Shaviv, Paul Fefer, Orly Goitein, and Eli Konen, "Sex differences in aortic root and vascular anatomy in patients undergoing transcatheter aortic valve implantation: A computed-tomographic study," Journal of cardiovascular computed tomography **11** (2), 87-96 (2017).

138 Jaffar M Khan, Adam B Greenbaum, Vasilis C Babaliaros, Toby Rogers, Marvin H Eng, Gaetano Paone, Bradley G Leshnower, Mark Reisman, Lowell Satler, and Ron Waksman, "The BASILICA trial: prospective multicenter investigation of intentional leaflet laceration to prevent TAVR coronary obstruction," JACC: Cardiovascular Interventions **12** (13), 1240-1252 (2019).

139 Jaffar M Khan, Danny Dvir, Adam B Greenbaum, Vasilis C Babaliaros, Toby Rogers, Gabriel Aldea, Mark Reisman, G Burkhard Mackensen, Marvin HK Eng, and Gaetano

Paone, "Transcatheter laceration of aortic leaflets to prevent coronary obstruction during transcatheter aortic valve replacement: concept to first-in-human," JACC: Cardiovascular Interventions **11** (7), 677-689 (2018).

140 Ikki Komatsu, G Burkhard Mackensen, Gabriel S Aldea, Mark Reisman, and Danny Dvir, "Bioprosthetic or native aortic scallop intentional laceration to prevent iatrogenic coronary artery obstruction. Part 1: how to evaluate patients for BASILICA," EuroIntervention: journal of EuroPCR in collaboration with the Working Group on Interventional Cardiology of the European Society of Cardiology **15** (1), 47-54 (2019); Ikki Komatsu, G Burkhard Mackensen, Gabriel S Aldea, Mark Reisman, and Danny Dvir, "Bioprosthetic or native aortic scallop intentional laceration to prevent iatrogenic coronary artery obstruction. Part 2: how to perform BASILICA," EuroIntervention: journal of EuroPCR in collaboration with the Working Group on Interventional Cardiology of the European Society of Cardiology **15** (1), 55-66 (2019); Danny Dvir, Jaffar Khan, Ran Kornowski, Ikki Komatsu, Adnan Chatriwalla, G Burkhard Mackenson, Matheus Simonato, Henrique Ribeiro, David Wood, and Jonathon Leipsic, "Novel strategies in aortic valve-in-valve therapy including bioprosthetic valve fracture and BASILICA," EuroIntervention: journal of EuroPCR in collaboration with the Working Group on Interventional Cardiology of the European Society of Cardiology **14** (AB), AB74-AB82 (2018).

141 Romina Plitman Mayo, Halit Yaakobovich, Ariel Finkelstein, Shawn C Shadden, and Gil Marom, "Impact of BASILICA on the thrombogenicity potential of valve-in-valve implantations," Journal of Biomechanics **118**, 110309 (2021).

142 Farhan Khodaee, Dong Qiu, Danny Dvir, and Ali N Azadani, "Reducing the risk of leaflet thrombosis in transcatheter aortic valve-in-valve implantation by BASILICA: a

computational simulation study," EuroIntervention: journal of EuroPCR in collaboration with the Working Group on Interventional Cardiology of the European Society of Cardiology **15** (1), 67-70 (2019).

143 Hoda Hatoum, Pablo Maureira, Scott Lilly, and Lakshmi Prasad Dasi, "Impact of leaflet laceration on transcatheter aortic valve-in-valve washout: BASILICA to solve neosinus and sinus stasis," JACC: Cardiovascular Interventions **12** (13), 1229-1237 (2019).

144 VL Rayz, L Boussel, L Ge, JR Leach, AJ Martin, MT Lawton, C McCulloch, and D Saloner, "Flow residence time and regions of intraluminal thrombus deposition in intracranial aneurysms," Annals of biomedical engineering **38** (10), 3058-3069 (2010).

145 Maud B Gorbet and Michael V Sefton, "Biomaterial-associated thrombosis: roles of coagulation factors, complement, platelets and leukocytes," The Biomaterials: Silver Jubilee Compendium, 219-241 (2004).

146 Panagiota Kourkoveli, Konstantinos Spargias, and George Hahalis, "TAVR in 2017—What we know? What to expect?," Journal of geriatric cardiology: JGC **15** (1), 55 (2018).

147 Ole De Backer and Lars Søndergaard, "Is BASILICA the Standard for Preventing Coronary Obstruction in High-Risk Transcatheter Aortic Valve Replacement?", (American College of Cardiology Foundation Washington DC, 2021).

148 Robert J Lederman, Vasilis C Babaliaros, Toby Rogers, Jaffar M Khan, Norihiko Kamioka, Danny Dvir, and Adam B Greenbaum, "Preventing coronary obstruction during transcatheter aortic valve replacement: from computed tomography to BASILICA," JACC: Cardiovascular Interventions **12** (13), 1197-1216 (2019).

149 Hoda Hatoum, Jennifer Dollery, Scott M Lilly, Juan Crestanello, and Lakshmi Prasad Dasi, "Impact of patient-specific morphologies on sinus flow stasis in transcatheter aortic valve replacement: an in vitro study," The Journal of thoracic and cardiovascular surgery **157** (2), 540-549 (2019).

150 Brandon L Moore, Colorado State University.

151 Riccardo Toninato, Jacob Salmon, Francesca Maria Susin, Andrea Ducci, and Gaetano Burriesci, "Physiological vortices in the sinuses of Valsalva: an in vitro approach for bio-prosthetic valves," Journal of Biomechanics **49** (13), 2635-2643 (2016).

152 Prem A Midha, Vrishank Raghav, Rahul Sharma, Jose F Condado, Ikechukwu U Okafor, Tanya Rami, Gautam Kumar, Vinod H Thourani, Hasan Jilaihawi, and Vasilis Babaliaros, "The fluid mechanics of transcatheter heart valve leaflet thrombosis in the neosinus," Circulation **136** (17), 1598-1609 (2017).

153 Phillip M Trusty, Sanchita S Bhat, Vahid Sadri, Md Tausif Salim, Emelia Funnell, Norihiko Kamioka, Rahul Sharma, Raj Makkar, Vasilis Babaliaros, and Ajit P Yoganathan, "The role of flow stasis in transcatheter aortic valve leaflet thrombosis," The Journal of thoracic and cardiovascular surgery (2020); Gautam Kumar, Vrishank Raghav, Stamatios Lerakis, and Ajit P Yoganathan, "High transcatheter valve replacement may reduce washout in the aortic sinuses: an in-vitro study," The Journal of heart valve disease **24** (1), 22-29 (2015).

154 Prem A Midha, Vrishank Raghav, Ikechukwu Okafor, and Ajit P Yoganathan, "The effect of valve-in-valve implantation height on sinus flow," Annals of biomedical engineering **45** (2), 405-412 (2017).

155 Immanuel David Madukauwa-David, Vahid Sadri, Norihiko Kamioka, Prem A Midha, Vrishank Raghav, John N Oshinski, Rahul Sharma, Vasilis Babaliaros, and Ajit P Yoganathan, "Transcatheter aortic valve deployment influences neo-sinus thrombosis risk: An in vitro flow study," Catheterization and Cardiovascular Interventions **95** (5), 1009-1016 (2020).

156 Brandon L Moore and Lakshmi Prasad Dasi, "Coronary flow impacts aortic leaflet mechanics and aortic sinus hemodynamics," Annals of biomedical engineering **43** (9), 2231-2241 (2015).

157 Kazuaki Okuyama, Hasan Jilaihawi, and Raj R Makkar, "Leaflet length and left main coronary artery occlusion following transcatheter aortic valve replacement," Catheterization and Cardiovascular Interventions **82** (5), E754-E759 (2013).

158 Maria Bortot, Katrina Ashworth, Alireza Sharifi, Faye Walker, Nathan C Crawford, Keith B Neeves, David Bark Jr, and Jorge Di Paola, "Turbulent flow promotes cleavage of vWF (von Willebrand factor) by ADAMTS13 (a disintegrin and metalloproteinase with a thrombospondin type-1 motif, member 13)," Arteriosclerosis, thrombosis, and vascular biology **39** (9), 1831-1842 (2019).

159 Mirza Md Symon Reza and Amirhossein Arzani, "A critical comparison of different residence time measures in aneurysms," Journal of Biomechanics **88**, 122-129 (2019).

Appendix

Supplementary figures for chapter 3

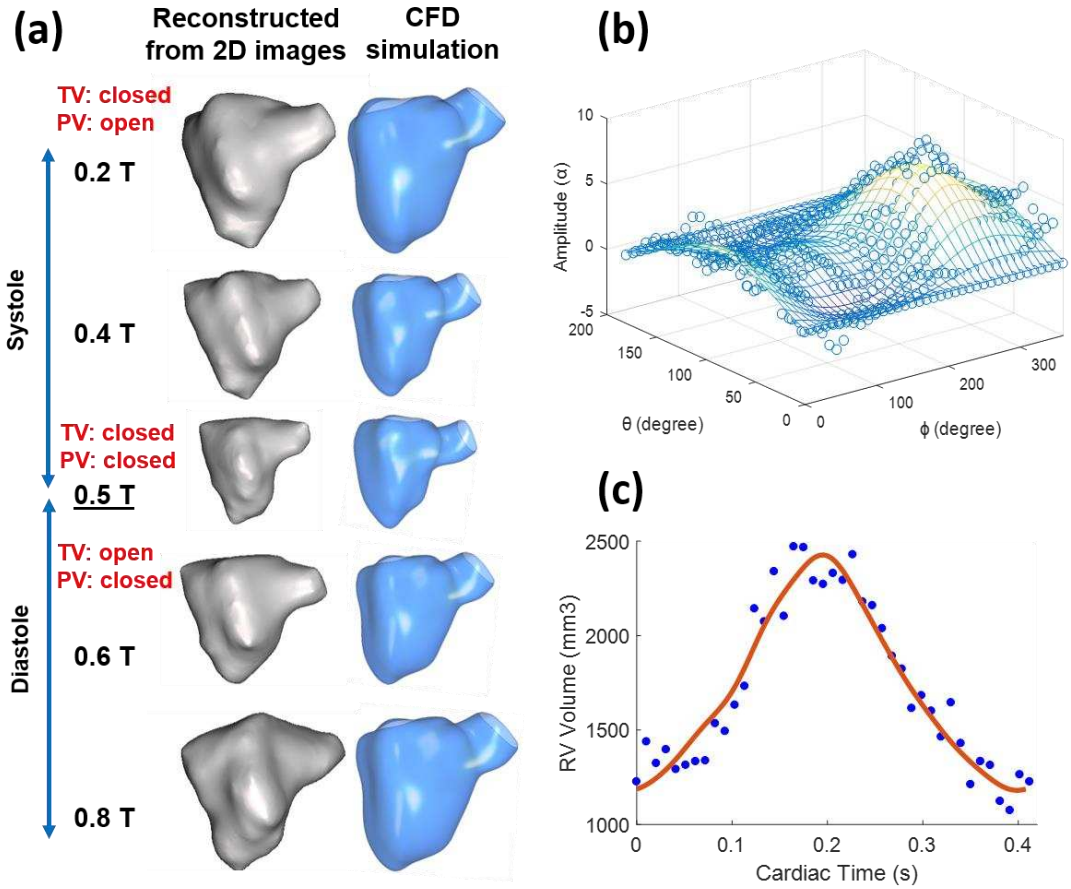

Figure 3S. 1. 3D reconstructed geometries (left) are in a good agreement with the CFD model (right). (b) Maximum amplitude of ventricular wall motion in θ and ϕ directions. (c) Estimation of right ventricle volume (red curve) using measured volumes at each time of the cardiac cycle (blue circles).

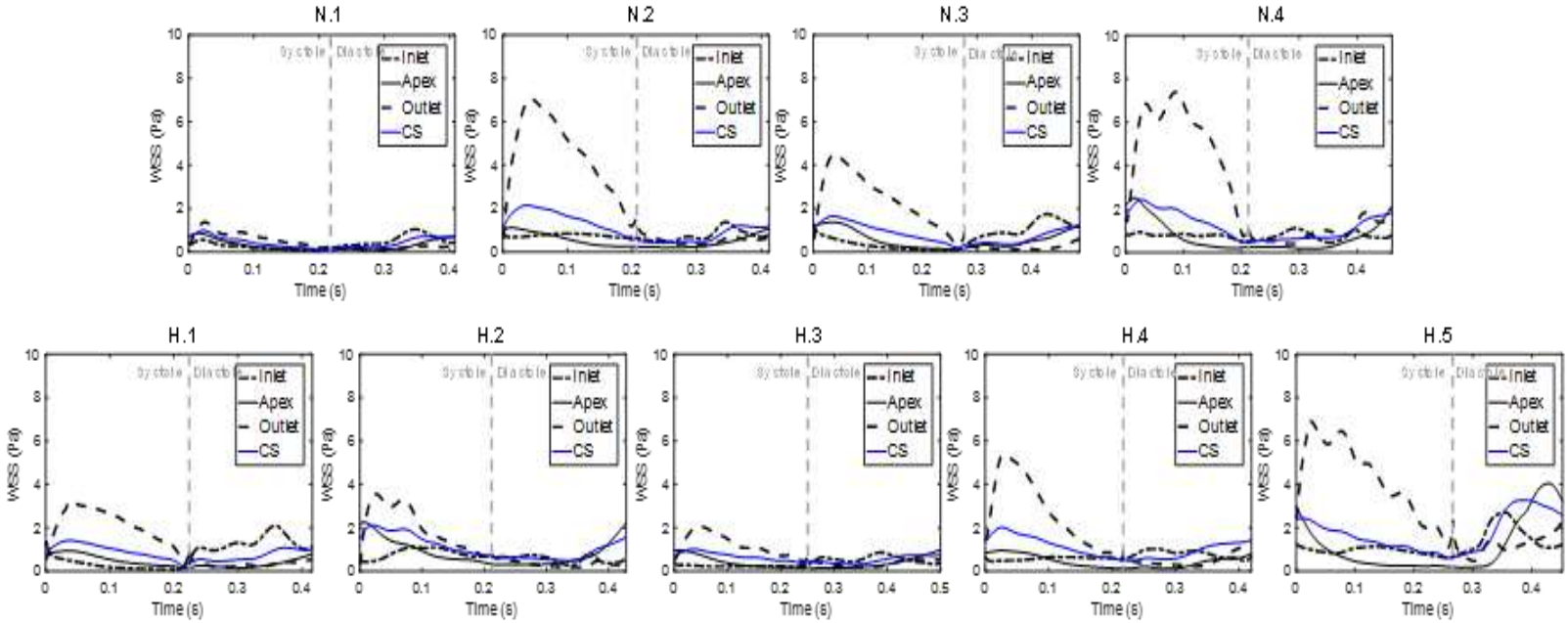

Figure 3S. 2. Area-averaged wall shear stress for normal and HLHS during systole and diastole at the inlet, outlet, apex, and the entire control surface (CS) of the right ventricle.